COMPARISON OF SINGLE-CELL SPIKE RATE AND TIMING IN RESPONSE TO COCHLEAR IMPLANT AND ACOUSTIC STIMULATION

Michaela Alisa Müller

Graduate School of
Systemic Neurosciences

LMU Munich

Dissertation der
Graduate School of Systemic Neurosciences
der Ludwig-Maximilians-Universität München

January 28, 2024

1st Supervisor
PD Dr. Michael Pecka
Department Biology II
Division of Neurobiology
Ludwig-Maximilians-University Munich

2nd Supervisor
PD Dr. Conny Kopp-Scheinpflug
Department Biology II
Division of Neurobiology
Ludwig-Maximilians-University Munich

First Reviewer: PD Dr. Michael Pecka
Second Reviewer: PD Dr. Conny Kopp-Scheinpflug
External Reviewer: Prof. R. Michael Burger Jr.

Date of Submission: 28.01.2024
Date of Defense: 20.06.2024

Abstract

Spatial hearing plays a crucial role in everyday communication and navigation. Sound localization in the horizontal plane relies on interaural level difference (ILD) as well as interaural time difference (ITD) cues. The lateral superior olive (LSO) and the medial superior olive (MSO) integrate excitatory and inhibitory synaptic inputs from both ears to generate our brain's sensitivity to these cues.

ITD is the dominant binaural cue for sound localization in noisy environments. However, individuals with hearing impairment or deafness, which are common sensory deficits, face challenges in interacting with their environment. Cochlear implants (CIs), electronic devices that bypass hair cells and directly stimulate the auditory nerve, offer a solution to restore spatial hearing in these individuals. Although CI patients are able to use ILDs, achieving good ITD processing remains a challenge. Understanding the underlying causes of poor ITD detection in CI patients and the effects of electrical stimulation on the binaural integration process for ITD detection is crucial.

This thesis focuses on investigating the differences between CI-based and acoustic stimulation of the auditory brainstem and their impact on fundamental principles of binaural integration. While low-frequency neurons in the MSO are primarily responsible for ITD processing in individuals with normal hearing, the envelope ITD information provided by CIs, combined with implantation techniques, is presumed to primarily stimulate higher frequency regions of the cochlea, thus activating the LSO pathway.

In this study, we conducted in vivo electrophysiological recordings from monaural inputs to the LSO, specifically the anterior ventral part of the cochlear nucleus (AVCN) and medial nucleus of the trapezoid body (MNTB). We used click-train stimuli with varying inter-click intervals (ICIs) to examine potential differences in the temporal precision of action potential (AP) firing between electrical and acoustic stimulation. Mongolian gerbils (Meriones unguiculatus) served as an animal model because of their closer resemblance than other rodents to the human low- and high-frequency hearing ranges.

Using this electrophysiological data, we employed a spike-count comparison model to predict ITD sensitivity in the LSO during CI-based stimulation. This model allowed us to compare our electrophysiological findings with model data and predict changes in ITD sensitivity during electric stimulation.

A significant aspect of this thesis was the establishment of two essential methods that laid the foundation for the new experimental paradigm in the laboratory. We developed a technique for acute CI implantation, deafening, and electrical stimulation of the auditory

brainstem to obtain in vivo electrophysiological recordings from single neurons during CI stimulation. Additionally, a histology protocol using Technovit® 9100 was implemented to verify the correct placement of the implant within the cochlea.

The acute CI implantation technique yielded stable and reproducible results, ensuring the feasibility of using this experimental design for future studies. The objective of the Technovit® 9100 histology protocol was not fully realized, as the CI was not evident in the histological sections of the Mongolian gerbil cochlea.

Analysis of the electrophysiological results revealed differences between electrical and acoustic stimulation in the auditory brainstem. We observed a tendency of higher spike probability for lower stimulation rates and significantly reduced jitter in electrically stimulated cells in both the AVCN and MNTB. Interestingly, the precise timing of electrical stimulation in the auditory nerve was maintained even with the involvement of more synapses in the AVCN and MNTB. This finding shows that the neural detection of ITDs must adeptly adjust to altered input statistics when exposed to CI stimulation, as opposed to the conditions observed in acoustic hearing.

The model indicates that the LSO is ITD-sensitive to electrical inputs and that the hyper-precision observed in our electrophysiological recordings from the AVCN and MNTB is transferred to the LSO. Importantly, the model suggests that the reduced jitter found in the electrical physiological data leads to a lateralization effect because of hyper-accurate ITD processing in the LSO. Furthermore, when we changed the electrically modeled jitter level to the one found in acoustic recordings, we exhibited a substantial recovery in the ITD coding capacity of the LSO model. Thus, this study highlights the critical role of input jitter as a key parameter in shaping ITD sensitivity in the LSO during CI-based sound localization.

Table of Contents

1 Introduction

Hearing constitutes one of the five mammalian senses, alongside vision, taste, touch, and smell. It plays a crucial role not only in communication but also in learning, forming meaningful relationships, and enjoying life to the fullest.

One important aspect of hearing is the ability to localize sound sources. Many animals rely on sound localization to avoid predators and ensure their survival. In the case of humans, for example, this ability allows us to identify approaching cars, bicycles, or other vehicles and to cross the street safely.

Sound localization in the horizontal plane depends on both interaural level difference (ILD) and interaural time difference (ITD) cues. The brain's sensitivity to these auditory cues is generated by the integration of excitatory and inhibitory synaptic inputs from both ears in the lateral superior olive (LSO) and the medial superior olive (MSO).

In environments with background noise, ITD becomes the primary binaural cue for sound localization. However, individuals with hearing impairment or deafness, common sensory deficits, encounter difficulties in navigating their surroundings. Cochlear implants (CIs), electronic devices circumventing hair cells to directly stimulate the auditory nerve (AN), present a solution to restore spatial hearing in such individuals. While CI users can utilize ILDs, achieving effective ITD processing remains a significant challenge. Therefore, comprehending the reasons behind poor ITD detection in CI patients and understanding the impact of electrical stimulation on the binaural integration process for ITD detection is crucial.

This thesis aims to explore the distinctions between CI-based and acoustic stimulation of the auditory brainstem and their effects on fundamental aspects of binaural integration.

The following chapter explains in detail how sound localization relies on binaural cues. I describe the anatomy and physiology involved in hearing and how the brain perceives and processes both binaural and spectral information. I also outline various hearing impairments and the potential treatment options available, such as CIs, which are electronic devices designed to restore hearing function. I then explore the challenges associated with sound source localization, specifically in individuals using CIs.

This background information supports the broader aim of the thesis, which is to provide a deeper understanding of the underlying neuronal mechanisms that contribute to these challenges.

1.1 General Overview of the Auditory Process

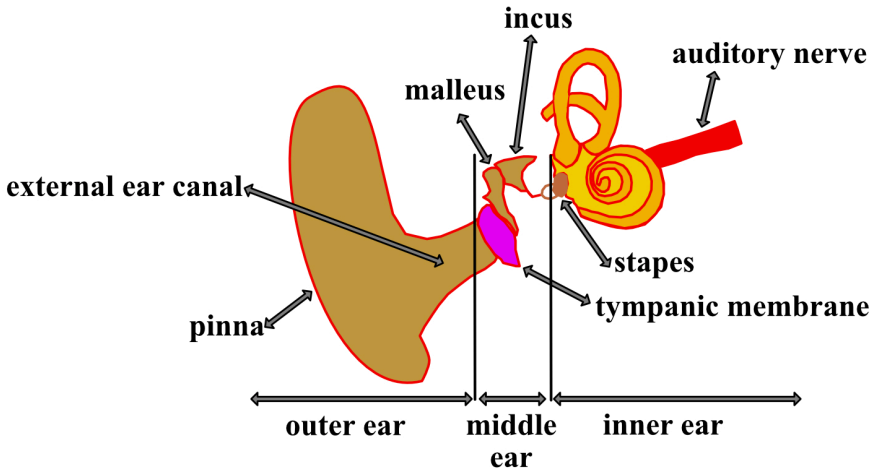

Figure 1: Illustration of the outer-, middle-, and inner ear.
The external ear comprises the pinna and the ear canal, which is separated from the middle ear by the tympanic membrane. The middle ear contains the three auditory ossicles: the malleus, incus, and stapes. Adapted from MEDEL Cochlear Implants Synchrony 2 (n.d).

Sound comprises waves that are created by vibrations and travel through space. It can be defined by a variety of attributes, including pressure, amplitude, and frequency. Frequency, expressed in hertz (Hz) or units per second (1/s), represents the quantity of vibrations occurring within a given time period. The hearing range of humans ranges from 20 Hz–16 kHz, but humans are most sensitive to sound at frequencies between 2–5 kHz (Geiger, 2019).

Sound pressure is quantified in pascals (1 Pa = 1 N/m²) (Geiger, 2019). Another way to quantify sound is by measuring its sound pressure level (SPL), in decibels (dB). This follows a ratio scale with an arbitrarily defined reference sound pressure, P_0, of 2×10^{-5} N/m^2. The equation that defines this pressure level is:

$$L = 20 \text{ x } {}_{10}\log \frac{Px}{P0} \text{ [dB] (Geiger, 2019).}$$

Thus, when sound pressure increases by a factor of 10, the sound pressure level would increase by 20 dB.

The initial stage of the auditory process involves the ear gathering this sound from the environment using its pinna, the soft, fleshy part of the outer ear. As sound waves travel through the auditory canal, they reach the tympanic membrane, causing it to vibrate. This vibration is then transferred to the ossicles and the oval window.

The outer, middle, and inner ear comprise the first part of the auditory pathway (Figure 1). The outer ear consists of the pinna and the external ear canal, which are separated from the middle ear by the tympanic membrane. Inside the middle ear are the three auditory ossicles:

the malleus, incus, and stapes (Figure 1). These amplify sound pressure at the oval window by a factor of 20 (Bear et al., 2007).

Located in the inner ear, the cochlea contains hair cells that convert sound into neural signals, subsequently transmitted as action potentials (APs) to the brain (Figure 2). APs play a crucial role in transmitting signals between cells and triggering the release of neurotransmitters, facilitating communication between neurons. These APs are initiated by signals from other neurons, altering the resting membrane potential of a cell. The resting membrane potential represents the voltage difference across the cell membranes, with the interior being negatively charged (typically -70 (mV)) relative to the exterior.

An action potential consists of distinct phases: depolarization, threshold, repolarization, hyperpolarization, and the refractory period (Draguhn, 2023).

1. Depolarization: A sufficiently strong stimulus induces the opening of ion channels, allowing positively charged ions (such as sodium) to enter the cell. This influx leads to depolarization, reducing the voltage difference across the membrane.
2. Threshold: As depolarization reaches the critical level of -50 (mV), voltage-gated sodium channels are activated, leading to a rapid influx of sodium ions. This event reverses the membrane potential (+30 (mV)), resulting in the generation of the action potential.
3. Repolarization: Following the peak of depolarization, the membrane potential starts to repolarize as sodium channels are inactivated and potassium ions exit the cell. This restores a negative membrane potential (typically -70 (mV).
4. Hyperpolarization: After repolarization but before returning to the resting membrane potential, the membrane occasionally exhibits a more negative state than the resting level.
5. Refractory Period: An action potential results in a refractory period, during which the neuron exhibits reduced responsiveness to additional stimuli.

Before delving into a detailed explanation of how an AP is generated in the auditory system in chapter 1.4, I first outline the anatomical components of the auditory system involved in this process.

1.2 Anatomy of the Cochlea

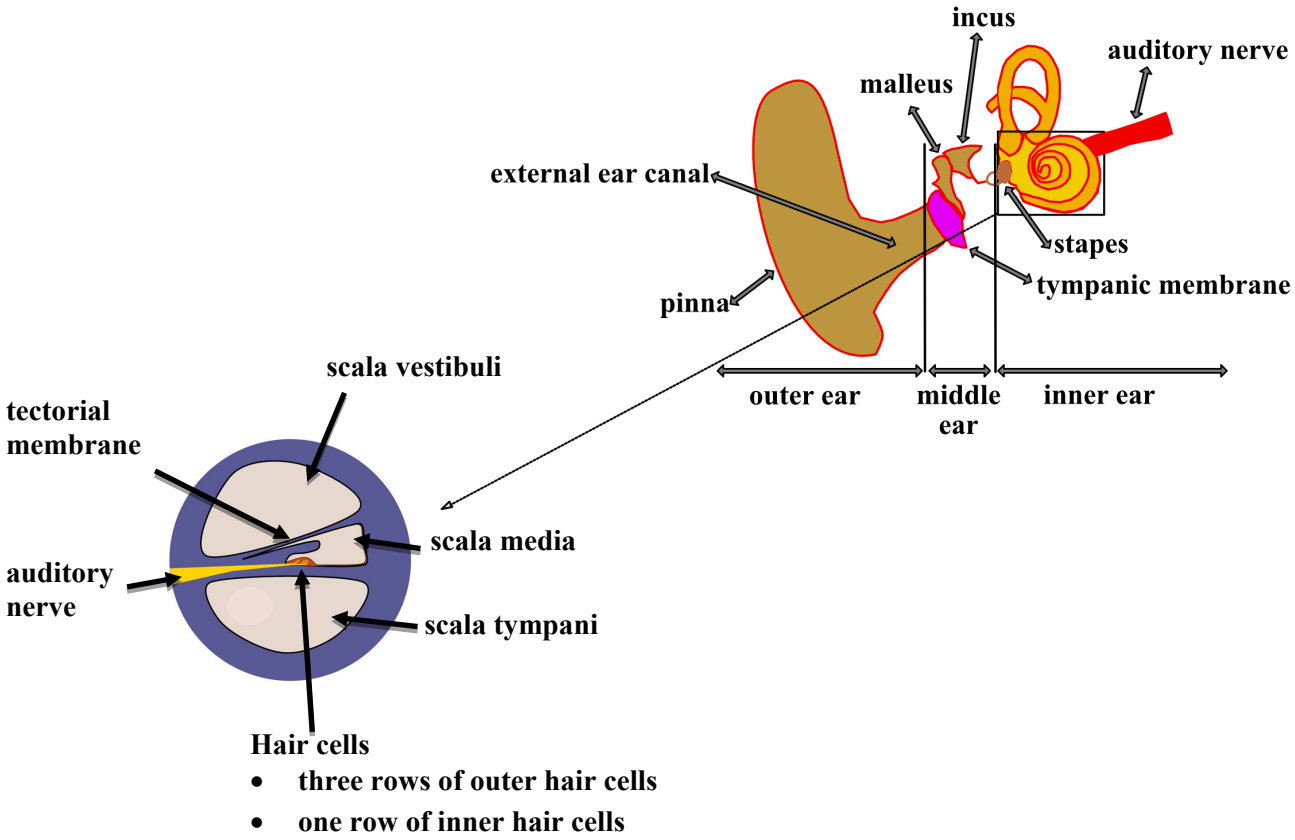

Figure 2: Illustration of the outer-, middle-, and inner ear, - along with a cross-section of the cochlea. The external ear comprises the pinna and the ear canal, which is separated from the middle ear by the tympanic membrane. The middle ear contains the three auditory ossicles: the malleus, incus, and stapes. Within the cochlea, there are three distinct compartments: the scala vestibuli, the scala media, and the scala tympani. The scala media contains the organ of Corti, which houses three rows of outer hair cells (OHCs), one row of inner hair cells (IHCs), and the tectorial membrane. The auditory nerve serves as the connection between the cochlea and the brain. Adapted from MEDEL Cochlear Implants Synchrony 2 (n.d) and Purves et al. (2001).

The cochlea contains two different fluids: the endolymph and the perilymph. The perilymph fills both the vestibular duct, or scala vestibuli, and the tympanic duct, or scala tympani (Figure 2). The endolymph fills the scala media, which is the third compartment of the cochlea.

At the apex of the cochlea, there is a connection point called the helicotrema, where the scala vestibuli and scala tympani merge. These fluids have distinct ionic compositions, which create an electrotonic gradient between the compartments. This so-called "endocochlear potential" comprises a voltage difference of +80 mV between the fluids, and is essential to producing neural activity (Geiger, 2019).

The three compartments are separated by two membranes. Reissner's membrane separates the scala vestibuli and the scala media, while the basilar membrane (BM) separates the scala media from the scala tympani (Geiger, 2019).

The scala media hosts the organ of Corti, which comprises three rows of outer hair cells (OHCs), one row of inner hair cells (IHCs), and the tectorial membrane (Bear et al., 2007) (Figure 2). On top of the hair cells are stereocilia, sensory receptors which extend into the endolymph. Both the stereocilia and the sensory inner hair cells are responsible for mechano-electric conduction.

The inner hair cells are connected to dendrites, which are extensions originating from the cell bodies of neurons—in this context, the spiral ganglion neurons (SGNs). These SGNs are a collection of cell bodies situated in the cochlea's spiral ganglion. Inner hair cells are innervated by the afferent dendrites of SGNs, which generate the first APs of the auditory pathway and transmit those to the brain (Johnson et al., 2019).

The axons of these SGNs collectively form the auditory nerve, also known as the eighth cranial nerve, establishing a neural connection that connects the cochlea to the cochlear nucleus in the central nervous system (Figure 3).

1.3 Anatomy of the Auditory Brainstem

The cochlear nucleus is the first auditory nucleus in the auditory brainstem, receiving direct input from the auditory nerve (Figure 3). Notably, the cochlea's tonotopy, where frequency is arranged in a topologically ordered manner (from high to low frequency), is also reflected in the cochlear nucleus. High-frequency fibers cover the dorsal and caudal parts of the nucleus, whereas the ventral and rostral regions receive low-frequency auditory input.

The cochlear nucleus can be further subdivided into three distinct regions (Held, 1893; Ramón y Cajal, 1909): the dorsal cochlear nucleus (DCN); the posterior ventral part of the cochlear nucleus (PVCN); and the anterior ventral part of the cochlear nucleus (AVCN) (Harrison & Irving, 1965, 1966).

The auditory nerve provides excitatory input to the large cells of the main ventral part of the cochlear nucleus (VCN) and the DCN. The AVCN, which is of most interest for this thesis, comprises globular bushy cells (GBCs), spherical bushy cells (SBC) (Figure 3), and multipolar stellate cells (Osen, 1969).

The two types of bushy cells, SBCs and GBCs, can be distinguished anatomically by their typical shape (Cant & Morest, 1979) and their location in the VCN. SBCs are located in the rostral part of the VCN, while GBCs embed in the caudal part of the VCN (Rubio, 2018). In addition to these bushy cells, two types of stellate cells, T- and D-stellate cells, can be found in the VCN (Doucet & Ryugo, 2006). Auditory nerve fibers form a connection with the

SBCs and GBCs via the endbulb of the Held synapse, one of the largest axonal terminals in the brain (Baker et al., 2010).

Regarding the ascending auditory pathway, the next section focuses on structures crucial to processing spatial information in the azimuthal plane. Specifically, GBCs project excitatory glutamatergic information onto contralateral neurons of the medial nucleus of the trapezoid body (MNTB) via the calyx of Held (Figure 3).

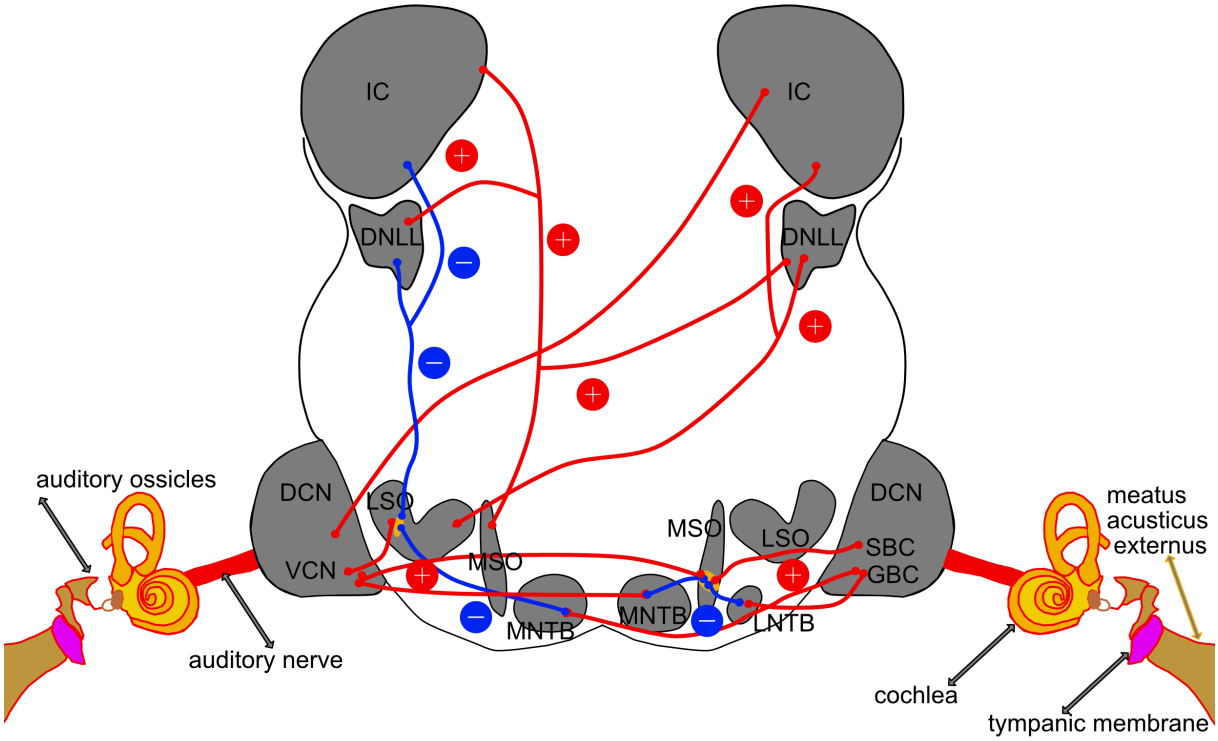

Figure 3: Illustration of the outer-, inner- and middle ear, the auditory brainstem, and its nuclei.
Red: excitatory input. Blue: inhibitory input. DCN: Dorsal cochlear nucleus. VCN: Ventral cochlear nucleus. SBC: Spherical bushy cells. GBC: Globular bushy cells. LSO: Lateral Superior Olive. MSO: Medial Superior Olive. MNTB: Medial nucleus of the trapezoid body. LNTB: Lateral nucleus of the trapezoid body. DNLL: dorsal nucleus of the lateral lemniscus. IC: inferior colliculus. See main text for further descriptions. Adapted from Grothe et al. (2010) and MEDEL Cochlear Implants Synchrony 2 (n.d.).

The calyx of Held is a giant synapse in the auditory system that transfers information from the presynaptic site (axonal endings of the GBCs) to the postsynaptic side (neurons of the MNTB) via neurotransmitters (Guinan & Li, 1990; Held, 1893). Glycinergic inhibitory neurons of the MNTB then project to the ipsilateral lateral superior olive (LSO), where they converge with ipsilateral excitatory glutamatergic SBCs (Figure 3).

Similarly, the medial superior olive (MSO), another nucleus essential for spatial processing, receives ipsilateral excitation via the SBCs as well as inhibition via the glycinergic cells of the MNTB (Figure 3). Besides these inputs, the contralateral

glutamatergic SBCs of the AVCN and the ipsilateral glycinergic neurons of the lateral nucleus of the trapezoid body (LNTB) also project onto the MSO.

The MSO and the LSO make up the primary nuclei of the superior olivary complex (SOC), which is where the inputs of both ears first come together and create binaural sensitivity. The specific functional roles of the MSO and LSO are described later in sections 1.9.2 and 1.9.3.

The excitatory projections of the MSO reach the ipsilateral and contralateral dorsal nucleus of the lateral lemniscus (DNLL) as well as the ipsilateral inferior colliculus (IC) (Henkel & Spangler, 1983). The LSO sends excitatory inputs to the contralateral DNLL and the IC (Figure 3). By contrast, the inhibitory projections of the LSO are forwarded to the ipsilateral DNLL and IC (Brunso-Bechtold et al., 1981; Glendenning et al., 1992). Glutamatergic excitatory input from the contralateral AVCN and binaural inhibitory input from the DNLL are sent to the IC (Pollak, 2012). The IC finally projects to the medial geniculate body (MGB), which transfers the information to the primary auditory cortex (A1) (Grothe et al., 2010).

1.4 Physiology of the Cochlea and the Auditory Pathway

In the auditory system, the initiation of an action potential (AP) commences with the initial phase of the auditory process. This phase entails capturing sound and transmitting the vibrations of the tympanic membrane through the ossicles to the oval window, initiating fluid movement within the cochlea.

The movement of the cochlear fluid, results in the displacement of the basilar membrane (BM), the tectorial membrane, and ultimately, the deflection of the stereocilia, sensory receptors, on top of the cochlea's hair cells.[1] The basilar membrane within the cochlea exhibits distinct deflection patterns at various locations in response to different frequencies, forming a tonotopic map. This tonotopic organization represents a topological arrangement, with higher frequencies predominantly causing maximum deflection at the basal region of the BM, while lower frequencies induce maximal deflection closer to the apex, near the helicotrema.

[1] The impedance of air is less than the impedance of the fluid. Usually, this would mean that the transduction of the sound waves to a liquid, i.e., the cochlear fluid, leads to considerable energy reduction. However, since the diameter of the stapes at the oval window is smaller than the diameter of the tympanic membrane, the ossicles amplify and move the cochlear fluid efficiently (Geiger, 2019).

The deflection of the stereocilia causes a bending of the tip links, initiating the opening of transduction channels. This allows a potassium influx from the positively charged endolymph (+80 mV) into the negatively charged cytoplasm of outer hair cells (-70 mV), resulting in depolarization (Bear et al., 2007). As the tip links return to their original position, transduction channels close, and the outer hair cells undergo repolarization. Due to periodic changes in membrane potential, the prestin molecules within the cell membrane of outer hair cells either shorten or lengthen. This causes the outer hair cells to oscillate in length, locally amplifying the traveling wave (Geiger, 2019).

Concerning the inner hair cells, the movement of the cochlear fluid results in the deflection of the stereocilia. This deflection, along with the influx of potassium from the positively charged endolymph (+80 mV) into the negatively charged cytoplasm of the inner hair cells (-40 mV), leads to depolarization. Consequently, the opening of voltage-gated calcium (Ca^{2+}) channels results in the influx of Ca^{2+} into the inner hair cells. The influx of Ca^{2+} into the inner hair cells induces the release of the transmitter glutamate from vesicles into the synaptic cleft. The binding of glutamate to the receptors of the SGNs initiates the generation of the first APs in the auditory pathway (Geiger, 2019; Johnson et al., 2019).

In summary, the BM's movement transduces changes of air pressure into neural activity. The auditory nerve then transmits these neural signals to the AVCN, in the form of APs.

The auditory nerve exhibits phase locking to low-frequency tones, i.e., the generation of APs at a specific part or phase of the stimulus waveform. This is essential for sound source localization (Grothe et al., 2010) and speech understanding (Verschooten et al., 2019). Phase-locking of the auditory nerve is species- and frequency-dependent and occurs in various mammals up to 5 kHz (Heil & Peterson, 2015). The response pattern of the auditory nerve to sustained pure tones exhibits a sharp onset with a steady decline to a more or less constant state (referred to as primary-like adaption) (Smith & Zwislocki, 1975). The SBCs and GBCs also express this response pattern.

1.5 Hearing Loss

The current number of people with some degree of hearing loss across the globe stands at 1.5 billion, a figure that is projected to increase to nearly 2.5 billion by 2050 (World Health Organization, 2021). In 2021, 430 million people required rehabilitation services for loss of hearing. This number is estimated to rise to 700 million by 2050 (World Health Organization, 2021).

The term “hearing loss” describes any decline or absence of hearing ability. Any alterations of the auditory pathway can cause hearing loss. These might be caused by infections, accidents, or hereditary factors. They may affect the inner ear (sensorineural hearing loss), or the outer or middle ear (conductive hearing loss). An occurrence of both types of hearing loss, sensorineural and conductive, is referred to as “mixed” hearing loss.

Other conditions to consider include central hearing loss, caused by central nervous system problems of the brain, and hidden hearing loss.

Hidden hearing loss is a type of hearing impairment that standard audiometric tests cannot easily detect. It can stem from various factors, including noise exposure, aging, peripheral neuropathy, and ototoxicity (Kohrman et al., 2020). The mechanisms underlying hidden hearing loss result from the degeneration of cochlear ribbon synapses, demyelination of the auditory nerve, and dysfunction of hair cells (Kohrman et al., 2020). Unlike sensorineural, conductive, or mixed forms of hearing loss, hidden hearing loss does not typically result in noticeable audiometric threshold shifts (Reiß et al., 2021).

Despite having normal thresholds for pure tones, individuals with central auditory processing disorder (CAPD), a special type of central hearing loss (Zahnert, 2011), may experience challenges in localizing sound and understanding language in noisy backgrounds. In addition, patients have longer response times in oral communication, as well as reading, spelling, and learning difficulties (Bellis & Bellis, 2015)

Physicians diagnose hearing loss by detecting a hearing threshold greater than 20 dB. People with disabling hearing loss, with a threshold greater than 35dB, may require rehabilitation services.

Cochlear implants are one possible treatment for individuals with deafness or severe to profound hearing loss (with a hearing threshold of 70 dB), who receive minimal benefit from traditional hearing aids. These implants are electronic devices that restore hearing by bypassing the hair cells and directly stimulating the auditory nerve with electric click trains. The initiation of the first action potential in the auditory pathway is elucidated in chapter 1.4, where the depolarization of the inner hair cells results in the release of glutamate, triggering the generation of an action potential in the auditory nerve. In the absence of functional inner hair cells, no action potentials are generated in the auditory nerve. Therefore, cochlear implants bypass the hair cells and directly stimulate the auditory nerve. Hence, CIs can provide a solution to restore hearing in patients with sensorineural and mixed hearing loss.

Such implants may not be very effective in cases of central hearing loss, where the problem derives from the brain’s processing of auditory information rather than an issue with

the cochlea itself (Dazert et al., 2020). However, people with central hearing loss may still qualify for CI implantation in certain cases, such as when they have co-existing sensorineural hearing loss: a CI may address peripheral hearing loss, enabling access to auditory information that can be processed by the brain. Individuals with central hearing loss must undergo a thorough evaluation by an experienced CI team to determine the potential benefits and limitations of CI implantation (Zahnert, 2011).

1.6 Cochlear Implants

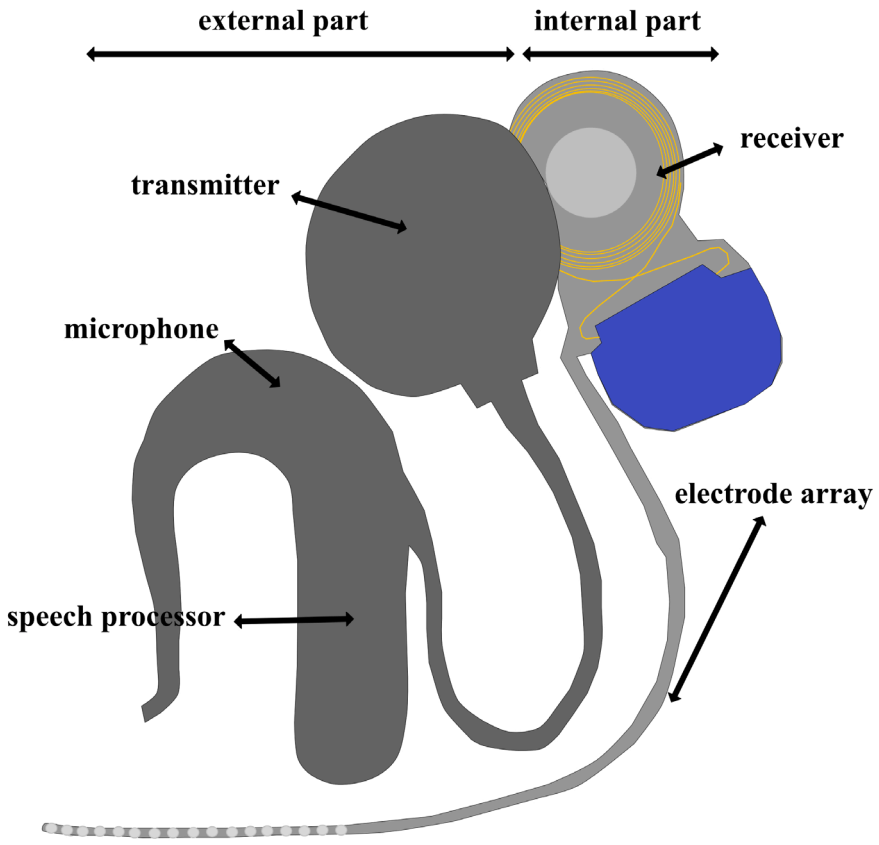

Figure 4: Components of the CI.
The external component comprises the speech processor, microphone, and transmitter. The internal component consists of the receiver and an electrode array. This array is implanted within the basal turn of the scala tympani. By delivering biphasic electronic pulses, the electrode array stimulates the auditory nerve, facilitating the perception of sound. Adapted from MEDEL Audio Processor SONNET 2 Cochlear Implant SYNCHRONY 2 (n.d.).

CIs are the most successful neuroprosthesis in use globally, with over 1 million implants placed worldwide by 2022 (Zeng, 2022).

The CI consists of two key components. The external part includes the speech processor, which is positioned near the outer ear, while the internal part is embedded in the bone above the ear (Figure 4). An external microphone senses incoming sounds and transmits them to the speech processor (Figure 4). The function of the processor is to turn acoustic signals into digital ones and to send these to the receiver via electromagnetic induction.

The receiver, in the internal part, transfers these electronic signals to the auditory nerve through an electrode array (Figure 4). This array is embedded within the basal turn of the scala tympani, a part of the cochlea. The electrode array delivers biphasic electronic pulses to stimulate the auditory nerve, enabling the perception of sound.

The objective of CIs is to simulate the experience of acoustic hearing by replicating the place of the stimulus using multichannel implants. These implants, which can have up to 24 electrodes (Croghan et al., 2017), mimic the tonotopic organization of the BM; that is, they stimulate the high-frequency regions near the base of the BM and the low-frequency regions near its apex. The processor extracts cues from speech and adjusts the stimulation rate to represent the frequency of the stimulus.

Limitations arising from the implantation process and the cochlear anatomy may result in the CI predominantly stimulating the higher frequency regions of the cochlea (Boyd, 2011; Canfarotta et al., 2021; Mehanna et al., 2019). CIs may also be limited in the range of sounds in speech that they are able to process.

The temporal structure of speech can be divided into three components: the temporal fine structure (TFS), the temporal envelope, and periodicity (Rosen, 1992). TFS refers to rapid oscillations near the center frequency, while the envelope represents slower amplitude modulations that are superimposed on the TFS (Figure 5). In a quiet setting, envelope cues can assist in speech recognition, whereas in noisy environments, TFS cues may help to distinguish speech from a competing background of sounds, as well as recognizing pitch and melody (Moon & Hong, 2014).

The continuous interleaved sampling (CIS) stimulation strategy most commonly used in CI speech processors focuses on encoding the envelope of the sound, resulting in the loss of the TFS and the fundamental frequency of the sound (Ricketts & Kan, 2021). Therefore, technicians have tried ways to incorporate TFS information into the sound-processing strategies of CIs, with mixed results. This approach is referred to as fine-structure (FS) temporal processing.

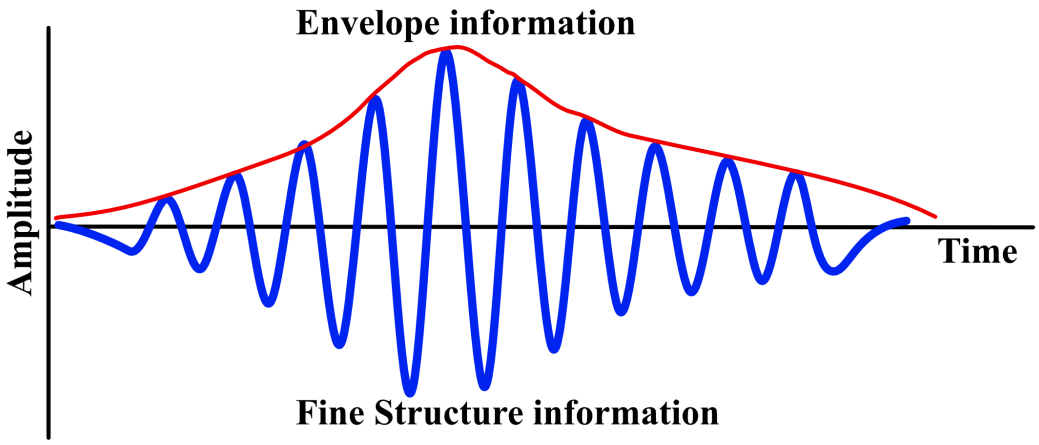

Figure 5: Envelope versus temporal fine structure.
The temporal structure of speech comprises two elements: temporal fine structure (TFS) in blue, and the envelope in red. Adapted from Dhanasingh and Hochmair (2021).

The CIS approach amplifies and passes the sound through band-pass filters (Wilson et al., 1991). It maps the amplitude of the sound and extracts the temporal envelope by rectifying and low-pass filtering of the sound with a cutoff frequency of 200–400 Hz (Laback et al., 2015). The resulting envelopes are then compressed to match the patient's dynamic range using nonlinear mapping, which accounts for the narrow dynamic range of electric hearing (Dhanasingh & Hochmair, 2021). The electrodes are activated in an interleaved fashion: in other words, the electrical pulses are not delivered simultaneously to more than one electrode.

Despite its various benefits, the performance of the CI for many patients (those receiving CIS stimulation) significantly deteriorates in complex environments where multiple sound sources are present. CI patients often encounter difficulties with sound source localization, for example. To discuss the specific localization challenges faced by CI patients, it is important to first understand the binaural cues used in this process.

1.7 Interaural Level Difference and Interaural Time Difference

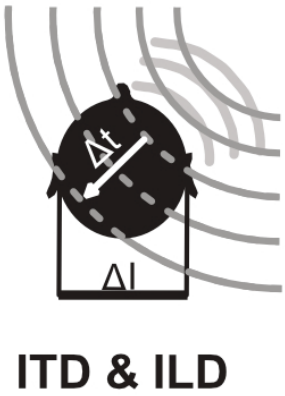

Figure 6: Binaural cues for sound source localization: the interaural level difference (ILD) and the interaural time difference (ITD).
ITD refers to the variation in the arrival time of a sound at each ear. ILD characterizes the dB level contrast between the ears, resulting from the head's shadow effect. Taken from Müller et al. (2023).

Two binaural cues are used for sound source localization: the interaural level difference (ILD) and the interaural time difference (ITD) (Figure 6). Depending on the angle from the sagittal plane, sound takes a different time to reach the left or right ear. The ITD measures the different arrival times of a sound at either ear, in the range of microseconds (µs). The human ITD threshold for pure tones is 11.5 µs (Laback et al., 2015), while maximum ITDs occur when the sound reaches the left or right ear at 90° from the sagittal plane (corresponding to values of 600–700 µs).

The ILD defines the difference in dB levels between the two ears. The "head shadow" effect creates ILDs when the head attenuates sound waves which are smaller than or equal to the diameter of the head. Hence, higher frequencies contribute predominantly to ILDs because the head attenuates these wavelengths more. In contrast, the wavelength of lower frequency sounds (approx. < 2 kHz) is larger than a human head and so they pass by without being significantly attenuated.

CI users mainly rely on ILDs for sound location (Aronoff et al., 2010; Grantham et al., 2008), unlike normal-hearing listeners who largely depend on ITDs for the localization of broadband sounds (Macpherson & Middlebrooks, 2002; Wightman & Kistler, 1998). ITD can be received as low-frequency fine structure ITD cues or as high-frequency envelope ITD cues. In both cases, the APs generated by a stimulus are phase-locked to either the fine structure stimulus (for low-frequency sounds) or the envelope (for high-frequency sounds), thereby providing highly precise information about the exact timing of specific stimulus waveforms at either ear.

Numerous studies have demonstrated that CI users are capable of detecting ITDs (van Hoesel et al., 2008); however, their performance in this regard is significantly inferior to that of individuals with normal hearing (Laback et al., 2015). In scenarios involving noise or multiple speakers, their performance is further degraded, and the benefits of bilateral CI implantation become less apparent.

The following chapter provides a more detailed description of the processes involved in ITD and ILD detection, including inputs from the brainstem's nuclei (the cochlear nucleus and MNTB) to the binaural processors (the MSO and LSO).

1.8 Cochlear Nucleus

The anatomy of the cochlear nucleus has already been outlined, with a particular focus on the AVCN (see chapter 1.3). To attain a more comprehensive understanding of this part of the anatomy, the functions of the DCN and PVCN will be outlined.

It is important to note that the DCN and PVCN are not strictly relevant to the central argument of this thesis, as they are not involved in binaural processing (by the MSO and LSO). However, it is crucial to have complete knowledge of all cell types to distinguish them during recording sessions and ensure the analytical process is precise.

Researchers are still trying to comprehend the full function of the DCN, which integrates numerous sensory inputs. The cells in the DCN are sensitive to spectral notches, which are cues present in the sound spectrum and represent frequency ranges characterized by a reduction in sound amplitude. These cues play a role in distinguishing the front from the back and to localize sounds monaurally (Nelken & Young, 1994).

The PVCN is populated by so-called octopus cells, which reside in the most caudal and dorsal parts of the PVCN (Oertel et al., 2000). Oertel et al. (2000) propose that octopus cells process and transfer information essential for speech understanding.

Each cell type in the AVCN, PVCN, and DCN has a specific spiking pattern. This pattern can be distinguished by a peri stimulus time histogram (PSTH). The PSTH represents the spiking of a neuron over time in response to acoustic stimulation. Each dot in a PSTH represents an AP. Pfeiffer (1966) has described the spiking pattern of these cells according to three categories: "primary-like," "chopper," and "onset." Through in vivo recordings and intracellular labeling of these different cell types, it has been possible to link these early electrophysiological recordings and spiking patterns with morphological findings (Friauf & Ostwald, 1988; Ostapoff et al., 1994; Rhode et al., 1983; Ryugo & May, 1993).

The spiking pattern of SBCs resembles the spiking pattern of the auditory nerve. In this respect, it can be considered primary-like: with a peak at the onset and then a decline to a steady level, exceeding 100 spikes per second (Blackburn & Sachs, 1989; Typlt et al., 2012). The spiking pattern of GBCs is like that of the SBCs, but they express an extra notch after the onset; therefore, the spiking pattern is called primary-like with notch (Blackburn & Sachs, 1989; Typlt et al., 2012).

Multipolar stellate cells create a different, "chopper" spiking pattern. These cells do not phase lock and have regularly spaced discharge peaks unrelated to the stimulus waveform (Blackburn & Sachs, 1989; Typlt et al., 2012). Octopus cells have fewer than 100 spikes per second and a sharp peak at stimulus onset. Afterward, there is little or no sustained activity (Blackburn & Sachs, 1989).

Apart from the spiking pattern described, the AP waveform can also serve as a distinguishing factor among different cell types in the AVCN. SBCs have a unique AP waveform during extracellular recordings. The waveform comprises: the AP of the presynaptic input of the endbulb of Held, referred to as pre-potential (PP) (Figure 11 b); the excitatory postsynaptic potential (EPSP); and the AP of the SBCs (Pfeiffer, 1966).

Despite these characteristics, numerous studies have questioned the conventional approach of distinguishing different cell types solely based on their physiological response patterns to acoustic stimulation and their morphological characteristics. These studies have reported instances where prevailing theories did not hold true, identifying certain cells that exhibit characteristics distinctive of other cell types.

Specifically, GBCs are recognized for displaying a variety of response patterns, not limited to the primary-like-with-notch pattern, but also including primary-like and various onset patterns, as evidenced in several studies (Rhode, 2008; Smith et al., 1991; Smith & Rhode, 1987; Spirou et al., 1990) Similarly, SBCs and stellate cells have been shown to exhibit a diverse array of PSTH patterns, as also discussed in previous research (Arnott et al., 2004; Spirou et al., 1990). Consequently, Typlt et al. (2012) propose that, "based on their physiological response properties, AVCN units can be better described as occupying specific areas within a coherent multidimensional parameter space, rather than forming clearly distinguishable groups of units."

Given the existing evidence suggesting a gradient between SBCs and GBCs, in our study we have integrated the PSTH, the distinct waveforms of BCs, and the spatial distribution of cell types as crucial components to differentiate between BCs and various other cell types within the cochlear nucleus.

The following chapter illustrates the auditory nuclei of the superior olivary complex that receive direct input from the SBCs or GBCs.

1.9 Superior Olivary Complex (SOC)

The primary nuclei of the superior olivary complex are the MNTB, the LSO, and the MSO. This chapter first gives an outline of the MNTB, which gives direct input to the LSO. It then describes the LSO and MSO, which are responsible for processing binaural cues for sound source localization in the brain.

1.9.1 Medial Nucleus of the Trapezoidal Body (MNTB)

As explained in chapter 1.3, the MNTB receives excitatory input from the GBCs. The anatomy and physiology of MNTB cells has been investigated in cats by Smith et al. (1998), who found some similarities to GBCs. MNTB cells reproduce the spiking pattern of GBCs: like the bushy cells, the MNTB cells have a PSTH that is primary-like with a notch. Given the extra synapse between the auditory nerve and the MNTB cells, the latency of these cells is slightly longer than that of the GBCs.

The synapse known as the calyx of Held forms the connection between the GBCs and MNTB neurons. This is supposed to be the largest synapse in the mammalian central nervous system. One AP triggers the release of glutamate from hundreds of transmitter release sites, leading to action potential with minimal jitter and short latency (Kopp-Scheinpflug & Forsythe, 2018). Therefore, the extracellularly recorded waveform of the MNTB exhibits, like the BCs, a compound waveform with a pre-potential and a postsynaptic AP (Guinan & Li, 1990; Kopp-Scheinpflug et al., 2003).

The inhibitory projections of the MNTB neurons are sent to the LSO, the MSO, and neighboring MNTB and VNTB neurons (Dondzillo et al., 2016; Kuwabara et al., 1991). These projections converge onto single neurons, with about 3–6 inputs onto each LSO neuron (Kim & Kandler, 2003), and about 2–4 inputs onto an MSO neuron (Couchman et al., 2010). Even though two synapses are involved in the connection between the auditory nerve and the MNTB, the MNTB provides fast and precise glycinergic inhibitory projections during ongoing stimulation (Kopp-Scheinpflug et al., 2008; Tolnai et al., 2008). MNTB neurons also follow the synaptic input from the cochlear nucleus with high temporal precision, even at high firing rates. Their capability to phase-lock to short tones exceeds even the capability of the auditory nerve (Smith et al., 1998).

1.9.2 Medial Superior Olive (MSO)

The MSO detects ITDs of low-frequency tones (< 3 kHz), with the cells in the MSO being primarily biased toward low frequencies (Grothe et al., 2010).

The MSO integrates the excitatory input from the ipsilateral and the contralateral SBCs of the AVCN with the inhibitor input from the ipsilateral LNTB and the contralateral inhibition input from the GBC via the MNTB (Grothe et al., 2010). Therefore, the ITD circuit of the MSO comprises two excitatory inputs and two inhibitory input types.

In his 1948 study, Jeffress postulated a model in which ITD processing with axonal delay lines compensate for the different latencies originating at the ipsilateral and contralateral sides (Jeffress, 1948). This model assumes binaural excitatory input. Although axonal delay lines have since been identified in certain bird species (Carr & Konishi, 1988), no such discoveries have been made in the superior olivary complex of mammals. Instead, recent studies strongly support the idea that glycinergic inhibition contributes to and refines ITD processing in the MSO by altering the internal delay (Grothe et al., 2010; Grothe & Pecka, 2014). Nevertheless, the MSO acts as a coincidence detector. The coincidence detection of excitatory inputs is sharply tuned by precise glycinergic inhibition.

Studies of the MSO have demonstrated that the MNTB's inhibitory information arrives before the cochlear nucleus's excitatory information (Roberts et al., 2013). Ford et al. (2015) have made some remarkable findings explaining this fast conductance. Depending on their characteristic frequency, the GBC axons which innervate the MNTB have differences in their internode length and diameter. The axons of low-frequency GBCs have a faster conduction velocity, shorter internode length, and thicker diameter toward the presynaptic terminal than high-frequency GBCs (Ford et al., 2015). These axons are tailored to provide highly precise temporal information to the MSO. However, there is a difference between high and low-frequency GBC axons and diversity between GBCs and SBCs. The GBC axons innervating the MNTB have a larger diameter and internode length than the SBC axons transmitting excitatory information to the MSO (Ford et al., 2015). These findings show that the inhibitory pathway from the MNTB to the MSO is tuned to compensate for the extra delay created by an additional synapse, the calyx of Held.

This myelination specialization is observable only in animals capable of ITD detection, such as gerbils, as shown by Stange-Marten et al. (2017). In addition to this myelination, when comparing low-frequency neurons with high frequency cells in gerbils, it becomes evident that low frequency cells have more stable synaptic delays than high frequency cells during ongoing stimulation (Stange-Marten et al., 2017). On the contrary, in mice, that

distinction between low and high frequencies has not been found, but synaptic delays are shown to be less variable overall. This observation underscores the finely tuned nature of ITD processing in the MSO, which is designed to deliver rapid and precisely timed information. Therefore, it is crucial to study ITD processing in a species that uses ITDs, e.g., the Mongolian gerbil, and not in mice or rats.

In summary, these findings indicate the importance of the precise interplay between the timing of excitatory and inhibitory inputs as well as the evolutionary specialization involved within the auditory system. Any alteration in this pathway will influence ITD detection in the MSO.

1.9.3 Lateral Superior Olive (LSO)

The LSO integrates and compares the excitatory postsynaptic potentials (EPSPs) from the ipsilateral side (SBCs of the AVCN) with the inhibitory postsynaptic potentials (IPSPs) from the MNTB. Thus, two synapses are involved in the inhibitory pathway to the LSO: the endbulb of Held at the cochlear nucleus level, and the calyx of Held at the level of the MNTB.

By contrast, for the ipsilateral excitatory pathway, there is a monosynaptic connection between SBCs and LSO. The ipsilateral excitation and contralateral inhibition foster a subtraction-like process. This subtraction-like process primarily works for ILDs and high frequencies. Even though the LSO has some low-frequency cells that detect ITDs, the primary ITD detector for low frequencies remains the MSO. Because of its principal high-frequency cells, the LSO has always been considered the primary ILD detector.

MSO and LSO share some common features, receiving excitatory input from the SBCs and inhibitory input from the MNTB. While the LSO receives two inputs, the ITD pathway of the MSO involves four inputs. Grothe and Pecka (2014) state that the ITD pathway of the MSO probably occurred later in its evolution. Two hundred million years ago, it is suggested the tympanic ear of our mammalian ancestors encoded higher frequencies, between 4 and 18 kHz (Rosowski & Graybeal, 1991), and mainly used ILD detection. Hence, Grothe and Pecka (2014) postulate that the relatively straightforward LSO pathway was inherited by the more complicated MSO pathway. Consequently, spatial hearing in the MSO and LSO is shaped by precisely timed inputs, generating ITD and ILD detection in the range of microseconds.

Besides its ILD sensitivity, the LSO also detects high-frequency envelope ITDs and low-frequency unmodulated ITDs (Finlayson & Caspary, 1991). Joris and Yin (1998) have demonstrated that cats can use envelope ITD in the LSO to lateralize complex sound sources. This envelope ITD sensitivity declines with increases in the modulation rate. Besides this

investigation, other studies have also found ITD sensitivity of LSO cells in other species (Finlayson & Caspary, 1991; Park et al., 1996; Shu Hui Wu & Kelly, 1992; Tollin & Yin, 2002). Beiderbeck et al. (2018) have demonstrated that the LSO of gerbils is sensitive to ITD click trains, also known as broadband noise. The click sequences, in Beiderbeck's investigation, comprised diverse inter-click intervals spanning from 5ms to 1ms, presented at a repetition rate of six clicks reiterated 20 times. As click trains are used for electrical stimulation in cochlear implants, these findings are highly relevant for our study, as explained in the following chapter.

1.10 Neuronal Processing of ITDs with Inputs from Cochlear Implants (CIs)

For individuals with normal hearing, the median ITD threshold of presented pure tones is 11.5 µs (Laback et al., 2015). Conversely, CI users achieve a median ITD threshold of 144 µs for low-rate electrical pulse trains (below 100 pulses per second (pps)). Their performance can also vary considerably: some CI users achieve thresholds comparable to those of individuals with normal hearing, while others exhibit results outside the range of natural ITDs (Laback et al., 2015). It should be noted that these ITD thresholds have been measured under controlled laboratory situations with perfect timing between the implants. Such controlled conditions are very unlikely to occur in real life; hence, researchers may overestimate the true thresholds involved in everyday hearing.

Even in defined laboratory conditions, some thresholds at stimulation rates ranging between 400–800 pps become unmeasurable. Yet studies have shown that speech perception is improved with higher stimulation rates, typically around 1,000 pps, which is why speech processors in implants tend to use sound coding strategies that stimulate at high rates (Kiefer et al., 2000; Loizou et al., 2000).

Nevertheless, while there is a discrepancy between the ITD thresholds for pure tones among normal-hearing listeners and CI users, research has shown that CI patients demonstrate comparable thresholds for envelope ITDs and similar rate limits to those observed in individuals with normal hearing. In normal-hearing patients, the rate limit for acoustic envelope ITDs ranges from 300 to 500 Hz, with an envelope ITD threshold of 100 µs (Bernstein & Trahiotis, 2002). Interestingly, CI patients exhibit envelope ITD thresholds of 100 µs and ITD rate limits (300–500 pps) that are coherent with the rate limits observed in high-frequency envelope ITDs of individuals with normal hearing (Laback et al., 2015). However, as previously noted, the envelope ITDs found in CI patients do not reflect the rate

limits of low-frequency pure tone ITDs of 1,400 Hz (Brughera et al., 2013) and the threshold of 20 µs for low-frequency pure tone ITDs (Thavam & Dietz, 2019).

Besides psychometric studies on humans, numerous studies on animals have shown neuronal ITD sensitivity to CIs. Several electrophysiological studies on cats and rabbits have focused on ITD detection with CIs in the auditory cortex (Tillein et al., 2010, 2016) and IC (Buck et al., 2021; Chung et al., 2016, 2019; Hancock et al., 2010, 2012; Rosskothen-Kuhl et al., 2021; Smith & Delgutte, 2007; Vollmer, 2018). Smith and Delgutte (2007) have found that cells in the IC of acutely deafened cats are sensitive to ITDs, although their sensitivity differs from that of animals with normal hearing, with some neurons exhibiting lower dynamic ranges of ITD sensitivity. Additionally, ITD sensitivity was shown to decrease with an increase in the pulse rate, achieving the best ITD sensitivity at pulse rates below 100 Hz. ITD sensitivity ranged from 10 to 200 pps (Hancock et al., 2010; Smith & Delgutte, 2007). Even though the rate limits in animal studies are lower than those observed in human studies, these results are still more closely comparable to envelope ITD sensitivity in CI patients and individuals with normal hearing than to those findings regarding low-frequency pure-tone ITDs.

Some studies of the auditory cortex and IC have focused on the influence of congenital deafness on ITD sensitivity to CI stimulation, discovering reduced ITD sensitivity compared with control subjects with experience of hearing (Hancock et al., 2010; Tillein et al., 2010, 2016). Nevertheless, Rosskothen-Kuhl et al. (2021) conclude that poor ITD detection in CI patients is more likely attributable to technical or treatment limitations rather than developmental auditory deprivation.

In summary, these studies do not provide a clear understanding of the actual computations that enable ITD processing during electric stimulation, or of the reason why CI users perform worse than individuals with normal hearing. We have yet to investigate how electrical ITDs are processed in the brainstem—the original site of ITD detection and encoding—with bilateral CIs and how this compares to acoustic ITD processing. This would allow us to determine to what extent differences in neural processing occur during the initial computation of ITDs in the brainstem or during downstream processing at higher areas (such as the IC and cortex).

1.11 Cue Reweighting

Plasticity can result in cue reweighting, whereby CI patients, due to the absence of available ITD cues, adapt and primarily depend on ILD cues for sound source localization.

This adaptation phenomenon is particularly evident in patients with unilateral hearing loss during adulthood (Agterberg et al., 2012; Kacelnik et al., 2006; Kumpik et al., 2010) or development (Keating et al., 2013; Newton, 1983). In such cases, individuals typically learn to rely on monaural spectral cues to localize sounds in the horizontal plane due to the absence of accessible binaural cues.

This recalibration of cues persists even after patients receive bilateral CIs, theoretically granting them access to binaural cues (Kral, 2017). However, because the neural pathways responsible for processing monaural spectral cues have become more prominent than those dedicated to detecting binaural cues (Keating et al., 2013), patients require training to overcome this neural remapping.

Binaural cues are present in individuals with bilateral CIs, and these cues can be transmitted to the brain. However, the selected stimulation approach for cochlear implants, specifically continuous interleaved sampling (CIS), primarily prioritizes the encoding of sound envelopes, which results in the omission of the TFS and the fundamental frequency of the auditory signal (Ricketts & Kan, 2021).

Additionally, it is worth noting that the current CIS stimulation strategy is constrained to high pulse rates of 1,000 pulses per second (pps) or greater, as reported by Laback et al. (2015). This limitation makes the prospect of detecting low-frequency, fine structure ITDs at the MSO level appear unlikely. Moreover, attempts to incorporate a fine structure coding strategy into the cochlear implant's speech processor have not yielded improvements in the processing of fine-structure ITDs in real-world situations (Fischer et al., 2021).

Considering these findings, and recognizing the limitations imposed by the technical aspects of CI surgery, which tend to predominantly activate the high-frequency area of the cochlea, we formulate a hypothesis suggesting that the low-frequency cells within the MSO, responsible for detecting low-frequency fine structure ITDs, may not receive significant stimulation from CIs.

An absence of TFS preservation in the stimulation has the potential to hinder the effective use of ITDs as a cue for sound localization among CI users. Furthermore, it may contribute to a gradual decline in ITD sensitivity among CI users over time, since the ITD information derived from temporal fine structure lacks the consistency necessary to serve as a reliable spatial location cue.

Given that the present CIS stimulation strategy and the limitations inherent to CI implantation are geared towards enhancing the perception of envelope-based ITDs, CI users adjust to these altered cues and primarily rely on envelope information for ITD detection.

As mentioned in section 1.9.3, research has shown that, in addition to their sensitivity to ILD, the cells within the LSO have the capability to detect interaural time differences arising from envelope ITDs in high-frequency stimuli (Finlayson & Caspary, 1991). Furthermore, studies involving gerbils have provided evidence that the LSO exhibits sensitivity to ITDs conveyed through click trains (Beiderbeck et al., 2018), further substantiating the notion that CIs predominantly activate the LSO.

As a result, we and other researchers (Dietz et al., 2016; Hu et al., 2022) put forward the proposition that CI users predominantly interpret envelope-based ITDs within the LSO rather than relying on the MSO.

1.12 Thesis Motivation

While the CI remains the most successful implantable electronic device, restoring hearing and enriching the lives of people who have hearing loss, it is still unable to provide a full range of solid ITD cues to all its patients. These cues are crucial for sound source localization and understanding speech in a noisy environment. Solving this deficit by understanding the neuronal processing of the electrical input to the auditory brainstem and then using this knowledge to enhance the speech processors is the next necessary step in CI research. In particular, we want to understand how the brain encodes the electrical inputs of the BCs in the AVCN and the cells of the MNTB and, by acquiring that knowledge, propose new ideas on how CI users can improve ITD detection.

This thesis concerns the differences between electrical and acoustic stimulation of the auditory brainstem, notably the inputs to the LSO and its influence on ITD processing in the LSO.

Preceding the investigation of the neuronal processing of electrical inputs, it was essential to establish two methods as a crucial goal of this thesis. First, we developed a surgical technique for CI implantation in gerbils. Second, we aimed to provide a histological verification of the location of the implant within the cochlea.

As such, the results of this thesis are organized into four parts. Each part is built on the results and outcome of the previous one. The first part corresponds to the establishment of CI implantation in gerbils, the second part focuses on the development of histological analyzes, the third part comprises physiological extracellular recordings in the auditory brainstem, and the fourth and final part aims at establishing an LSO model based on our in vivo recordings.

2 Methods and Materials

As explained in the previous chapter, two experimental methods were developed to pursue the central aims of this thesis. The first comprises a surgical technique for CI implantation in gerbils. The second experimental approach aimed to validate the implant's positioning within the cochlea through histological means, utilizing Technovit® 9100.

Throughout the experiment, the animal subjects were placed under anesthesia. Each experiment followed a specific protocol, which is outlined in Table 1.

The acoustic experiments involved six distinct steps and lasted approximately 8–9.5 hours. The electrical recordings comprised 11 steps, and consequently their duration was longer, approximately 11–13 hours. For detailed information about the duration of each step in the experiments, refer to the Table 1 "Scheme of the acoustic and electrical recordings".

The following section provides a step-by-step explanation of each experiment and provides insights into the animal model used.

Table 1: Scheme of the acoustic and electrical recordings.
The left section of the table presents the process and duration of the acoustic recordings, while the right section details the steps and duration of the electrical recordings. The acoustic recordings extended for a duration of 9.5 hours, whereas the electrical recordings persisted for 13 hours. In contrast to the 6 steps involved in the acoustic recordings, the electrical recordings comprised 11 steps.

Steps	acoustic recordings	Time (min)	electrical recordings	Time (min)
1	Anesthesia	45	Anesthesia	45
2	Placing of the headpin	15	ABR recording	30
3	Craniotomy	30	Placing of the headpin	15
4	Stereotaxis	90	Surgical preparation for the CI implantation	30
5	Recordings	360	Deafening of the animal	90
6	Euthanasia	30	ABR recording	30
7			CI implantation	30
8			Craniotomy	30
9			Stereotaxis	90
10			Recordings	360
11			Euthanasia	30
Total (hour)		**9,5**		**13**

2.1 Animals

All experiments complied with the German animal welfare law (55.2-1-54-2532-53-2015) and were performed on Mongolian gerbils (Meriones unguiculatus). The animals were housed in Tecniplast Type 4 cages measuring 610 x 435 x 215 mm, equipped with wooden chippings, wooden wool, and a shelter for retreat. Each cage accommodated a maximum of five animals. Environmental conditions were regulated at 23°C ± 2°C and 50% ± 10% humidity, and the animals were subjected to a 12-hour dark/light cycle.

For this study, it was essential to pick an animal model that reflects a human's low and high-frequency hearing range. Compared with other rodents, which mostly rely on high frequencies, Mongolian gerbils can process both low and high frequencies ranging between 0.1 and 60 kHz (Ryan, 1998). Mongolian gerbils are the only rodents that use low-frequency sounds to process ITDs and ILDs (Grothe & Pecka, 2014).

Additionally, it was essential to have convenient access to the cochlea. The bony bulla of the adult Mongolian gerbil is very prominent and makes an effortless CI implantation possible.

Adult animals (at least 3–7 months) of either sex weighing 60–100g were used for recording and implantation sessions. Choosing adult animals, we took into consideration that sound localization (Franzen et al., 2020; Seidl & Grothe, 2005), hearing ability (McFadden et al., 1996), and energy metabolism (Trattner et al., 2013) mature after the onset of hearing. In addition, other studies have proved that the cardiovascular system of these animals can endure prolonged anesthesia (Pecka et al., 2007, 2008, 2010).

It was also noted that animals older than two years can experience a decrease in hearing threshold and capacity (Mills et al., 1990). Accordingly, the age of the animals used in this study ranged from three months to two years.

2.2 Anesthesia

The anesthesia protocol used included general anesthesia and pain management both prior to and during the surgical procedure.

Thirty minutes before surgery, the animal was given a subcutaneous injection of a non-steroidal analgesic (pain relief) anti-inflammatory drug (Metacam® 1.5 mg/ml oral suspension, Boehringer Ingelheim Vetmedica GmbH, Ingelheim, 0.2 mg/kg) to substitute the analgesic effect of the ketamine used in the anesthesia. Ketamine is classified as a dissociative anesthetic, yet it has applications in pain management as well. Besides Metacam, local

anesthetics (Xylocain® Dental Pumpspray, 50ml, Astra Zeneca Gmbh, Wedel) were required to sedate the muscles and neighboring tissue prior to implanting the head pin and the CI.

To achieve anesthetization, the animal was injected intraperitoneally (0.5 ml/100 g body weight) with a solution of ketamine (20%) and xylazine (2%) diluted in 0.9% NaCl (Ketamin 10% Injektionslösung für Hunde und Katzen [injcection solution for dogs and cats], 100 mg/ml, MEDISTAR Arzneimittelvertrieb GmbH, Ascheberg, 50 mg/kg; Rompun® 2% Injektionslösung, 20 mg/ml, Bayer AG, Leverkusen, 2mg/kg). The combination of ketamine and xylazine is frequently employed as anesthetic agents for animals, commonly known as "Ketamine-Xylazine anesthesia." These two medications collaborate to bring about a state of unconsciousness and analgesia during medical procedures or surgical interventions in veterinary practice. Ketamine functions as a dissociative anesthetic, inducing a trance-like state, while xylazine serves as an alpha-2 adrenergic agonist, delivering sedation and muscle relaxation.

To sustain general anesthetic levels, the animal was regularly given the above-mentioned mixture of ketamine and xylazine via a micro-pump (Univentor 801 Syringe Pump, Univentor, France) with a flow rate of 1.7 µl per minute for every 70g of the animal's weight throughout the experiment. In the event of necessity, one-third of the original ketamine and xylazine dose was administered to the animal again.

The animal was considered anesthetized if it showed no eye-blink reflex, slight rotation of the bulbus oculi, positive corneal reflex, and lack of leg withdrawal reflex.

Throughout the implantation and recording sessions, anesthesia was supervised by monitoring parameters such as temperature (via a rectal probe), heart rate (EKG), breathing rate, pulse, and oxygen levels (using the Pulsoxymeter LifeSense® VET Portable Capnography and Pulse Oximetry Monitor, Nonin Medical, Inc., Plymouth, USA). The rectal probe and a heating pad were used to ensure the body temperature was maintained at 37°C. These parameters were monitored consistently to ensure that anesthesia levels were both secure and stable.

2.3 Placing of the Headpin

Upon confirming the correct level of anesthesia, the process began with the placing of the headpin. This step was necessary to assure a constant, secure head alignment in the electrophysiological recording setup for craniotomy, stereotaxy, and recordings.

First, a sterile surgical setting was created. An electric razor was used to shave the head and post-auricular implantation side of the animal and the area was then cleaned with

sodium chloride (NaCl). Subsequently, cuts were made bilaterally on either side of the tragus to ensure it could be folded. The folding of the tragus enabled visual control of the ear canal and the tympanum. Removing the tragus also allowed the headphones to be placed close to the eardrums, to ensure adequate acoustic hearing measurements. Exclusion of animals from the study was necessary if ear canals were plugged or eardrums were inflamed.

Afterward, the skin and tissue on top of the skull were removed and a local anesthetic was administered to sedate the bone. Following a five-minute period of local anesthesia, the tissue rostral to the bregma was removed using a raspatory. The bone tissue had to be eroded with phosphoric acid (Etch 35 gel) in order to enable a strong bond between the headpin and the skull. Restricting the exposure time of phosphoric acid to 30 seconds prevented further damage to the bone. After that, adhesive glue (Bond) was applied to the roughened portion of the skull and dried with ultraviolet light (UV).

The last part of the process involved attaching the UV-hardening plastic component (known as a charisma) above the adhesive glue, putting the pin in the charisma, and ensuring that the transverse bar of the pin was orthogonal to the skull. To complete the procedure, this construction was treated with UV light in three 40-second intervals. Following confirmation of the headpin's secure attachment, the animal was either deemed ready to undergo the CI implantation or taken to the acoustic chamber for additional preparatory steps.

The following chapters, 2.4–2.7, differ from the preparations for the acoustic experiments. They describe the preparatory steps taken for the electrical recordings, including the implantation of the CI.

2.4 Surgical Preparation for the Cochlear Implant

First, the postauricular area of the Mongolian gerbil was shaved and disinfected. Then the correct position of the surgical incision was identified by palpation of the tympanic bulla.

The initial curvilinear cutaneous incision, ranging from 2 to 3 cm, removed the superficial and deep skin layer. The correct position for the incision was 3 mm behind the pinna attachment; this was carried out with a disposable scalpel. Following this incision, the skin was retracted with a retractor, and the musculus auricularis superior and posterior (splenius capitis and cervicoauricularis) were incised with fine scissors (Risoud et al., 2016).

After the second incision, the retractor was repositioned to retract the muscles and the skin. The musculus temporalis was incised, after which the bony wall of bulla tympanica became visible. The retractor was then repositioned, and the rest of the muscles were removed from the bony wall of the bulla tympanica with a raspatory.

The bulla tympanica consists of a thin wall of bone and two thicker pillars. The septum superioris and the septum inferioris separate the bulla tympanica into three parts (epibullar, mediobullar, and hypobullar) (Risoud et al., 2016). The mediobullar part was opened with a drill, allowing it to impact the bony bulla wall with minor force. The tiny opening made it possible to identify the stapes, the stapedial artery, and the fenestra cochleae.

Since all the animals were deafened before the implantation (see following chapter 2.5), any noise damage created by the drill was considered acceptable. As the specific architecture of the dorsal part of the round window niche and the round window membrane prevent access to the round window, drilling needed to extract the dorsal section. Consequently, after accessing the bulla tympanica, sections of the round window niche were removed using the same drill. Careful attention was given to this process since the round window niche is situated near the stapedial artery.

The round window membrane was subsequently detached using a Bonn micro probe angled at 45 degrees. The final step supported the exact placement of the CI and the GELoader® tip (Eppendorf) needed for deafening.

2.5 Deafening

Most patients granted a CI are either deaf or suffer from severe to profound hearing loss. Our goal was to imitate the physiological state of deafness in the animal model. To guarantee there was no electrical stimulation of the hair cells, our animals were acutely deafened before the electrophysiological recordings. To meet this goal, the cochlea of the animal was treated with neomycin.

Neomycin belongs to the family of aminoglycoside antibiotics and has ototoxic effects, which are still not fully understood. Aminoglycoside combines with iron ions and membrane lipids to form complexes that generate oxidative radicals. These radicals enhance oxidative stress and may lead to apoptosis of the outer hair cells (Huth et al., 2011; Kranzer et al., 2015).

First, the perilymph of the scala tympani had to be replaced with neomycin. The successful completion of this task was enabled by inserting the GELoader® (20yl, Eppendorf) at the opening of the scala tympani through the round window and drawing off the fluid. The extraction of this perilymph and flushing of the scala tympani with neomycin sulfate (60mg/ml in NaCl) was done with great care and precision to avoid any harm to cochlea structures. The scala tympani was flushed for five minutes in total.

This process was iterated every 10 minutes over a span of 90 minutes. Subsequently, the neomycin was removed and the scala tympani was cleansed with a ringer solution to counter any neurotoxic effects on the spiral ganglia cells.

2.6 Auditory Brainstem Response Recordings

To evaluate the impact of the deafening technique on the animal's hearing sensitivity, an auditory brainstem response (ABR) was carried out (Figure 7). In this experiment, the ear was exposed to broadband clicks (Figure 7 a, 7 b) or high-frequency pure tones (Figure 7 c).

Our CIs were specifically designed to stimulate the basal high-frequency region of the cochlea, which means no low-frequency pure tones were used to determine if the animals were deaf. As click trains are frequently used for electrical stimulation in CIs, they were selected as our preferred approach for evaluating deafening, as well as for both electrical and acoustical stimulation in this study (refer to chapter 2.10).

ABR recordings capture the brainstem's auditory evoked potential, which generates waves corresponding to different auditory nuclei:

- Wave I and II originate from the auditory nerve;
- Wave III corresponds to the cochlear nucleus;
- Wave IV is associated with the superior olivary complex;
- Wave V correlates to the IC.

The loudness of the speaker determines the threshold in dB at which no wave is elicited anymore. To ensure good recording quality, the loudspeaker (MF1 Tucker Davis Technologies) was calibrated regularly with a microphone, type 4938, and a preamplifier, type 2670 (Bruel and Kjaer).

Prior to the recording, the animal was positioned on a heating pad regulated by the ATC 1000 DC Temperature Controller (World Precision Instruments) inside a double-walled sound-attenuated chamber (Industrial Acoustics, GmbH), which was lined with acoustic foam. The temperature was adjusted to 37°C in order to maintain a stable body temperature.

The recording electrodes were then placed on the animal as follows: The reference electrode was subdermally placed at the vertex, the active electrode was positioned over the bulla, and the ground electrode was inserted above the hindlimb. The placement of the loudspeakers accompanied this step. A short plastic tube extending from the loudspeaker was inserted into the outer ear. Finally, broadband clicks and pure tones were presented to the ear, and ABRs were detected.

Broadband clicks (0.1 ms duration, 0 ms rise/fall time) and pure tones of 28, 36, and 44 kHz (5 ms duration, 1 ms rise/fall time) were produced with Spike software (Brandon Warren, University of Washington, Seattle, WA; pre-amp gain: 20; additional gain: 0 dB) and played at a rate of 50/s. The auditory stimulus was transferred to the RZ6 Multi I/O Processor (TDT) and passed on to the loudspeakers. The RA16 PA 16 Channel Medusa preamplifier (TDT) and RZ6 Multi I/O Processor detected ABR waveforms.

After 1,000 repetitions for each frequency and intensity, the average of these ABR recordings was calculated. A hearing threshold above 70 dB, determined by ABR, indicated that the deafening procedure was successful (Figure 7 a).

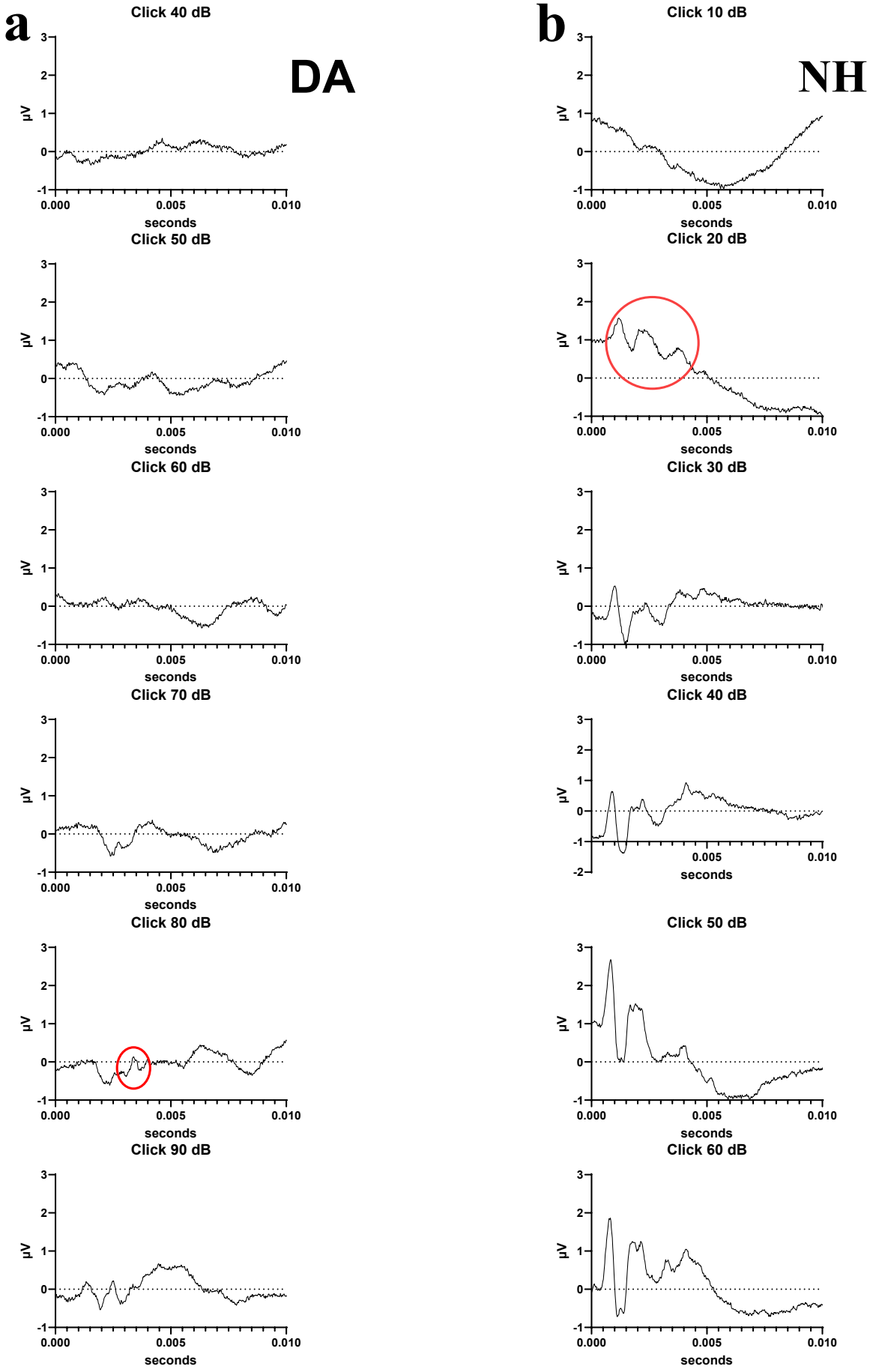
a
DA
Click 40 dB
Click 50 dB
Click 60 dB
Click 70 dB
Click 80 dB
Click 90 dB
b
NH
Click 10 dB
Click 20 dB
Click 30 dB
Click 40 dB
Click 50 dB
Click 60 dB
µV
seconds
0.000
0.005
0.010

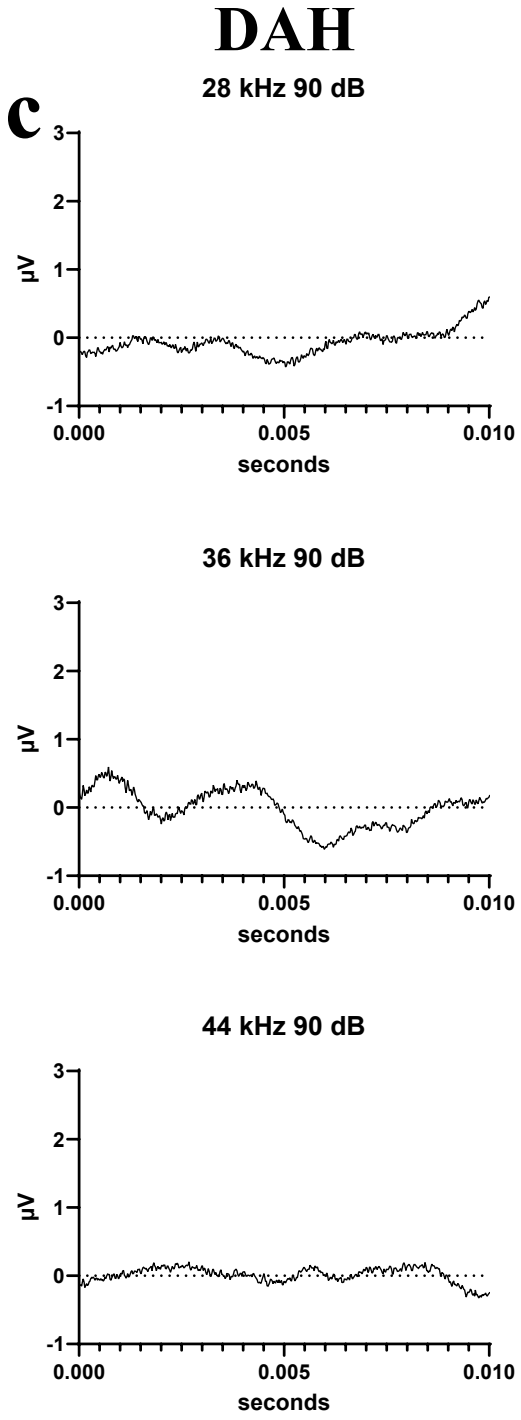

Figure 7: Example of ABR recordings used to verify deafening.
(a) Click-evoked ABR recordings ranging from 40 to 90 dB SPL in a deafened animal (DA) following the administration of the ototoxic drug neomycin; (b) ABR recordings in a normal-hearing animal (NH) from 10 to 60 dB SPL in response to click stimuli; (c) High-frequency pure tone ABR recordings at 90 dB in deafened animals (DAH). The red circle indicates the hearing threshold for both normal hearing and deafened animals. No threshold could be detected for high-frequency pure tones.

2.7 CI Implantation

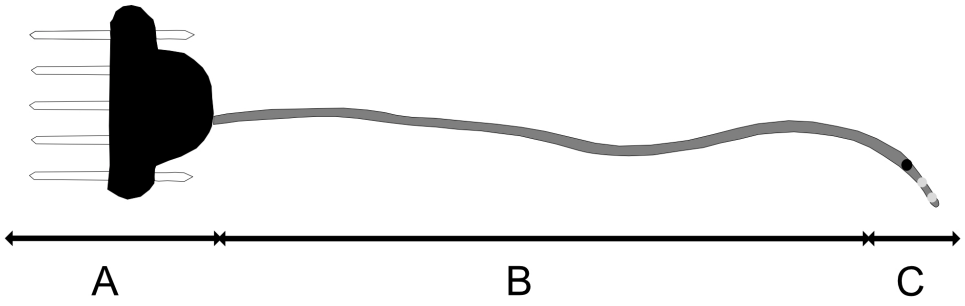

Figure 8: Cochlear implant
5-pin connector (A) and electrode array (B) with a black marker, an apical and basal electrode contact at the free end of the implant (C) (MED-EL Elektromedizinische Geräte GmbH, Innsbruck, S. Schilp).

The CIs used in this study, for either guinea pigs or Mongolian gerbils, were manufactured by MED-EL. Each implant consists of a connector, an electrode array, a black marker, and two electrodes at the end of the implant for stimulation (Figure 8).

Chapter 2.4 provides a detailed account of the initial procedural steps, which involve shaving, cleaning, making an incision in the skin and muscle, as well as accessing the bulla and removing the round window niche and membrane. In this chapter, the focus is on describing the insertion of the CI into the scala tympani of the cochlea (Figure 9), as well as its fixation.

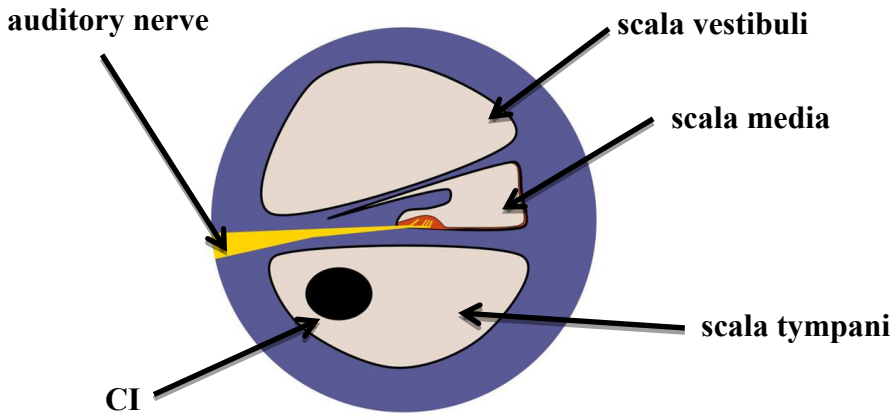

Figure 9: Cross-section of the cochlea illustration the placing of the CI within the scala tympani.
In the middle of the cross-section, the scala media becomes visible. This houses the organ of Corti, featuring three rows of outer hair cells (OHCs), one row of inner hair cells (IHCs), and the tectorial membrane. The yellow color represents the auditory nerve responsible for transmitting APs to the brain. Adapted from Purves et al. (2001).

In order to secure the implanted wire in the adjacent tissue, a peripheral venous catheter was employed to puncture the musculus auricularis posterior and musculus trapezius pars thoracica, guiding it towards the epibullar part of the bony bulla wall. Subsequently, the CI was fed through the peripheral venous catheter towards the round window. Once the peripheral venous catheter was removed, the CI was firmly anchored within the surrounding muscles. Finally, the device was inserted through the round window and carefully positioned within the scala tympani.

To avoid any displacement of the CI, the part of the wire that meets the septum superioris was securely bonded (using Histoacryl®) to the bony bully wall once the CI was fully inserted into the scala tympani and the desired position was achieved. Finally, the plug of the CI was placed on the back of the animal. To secure the remaining section of the wire between the muscle entry point and the plug, a skin suture was utilized to hold it in place. The knot of the suture was deliberately tied loosely to avoid damaging the metal wires.

2.8 Craniotomy and Stereotaxis

Recordings of the AVCN, MNTB, and LSO utilized the same hardware and were all conducted using an identical setup. For more information on the LSO recordings with acoustic stimuli, refer to the study by Beiderbeck et al. (2018).

Acoustic and electrical recordings had the following step in common. After the CI was implanted or the headpin placed (in the case of acoustic experiments), the animal was positioned on a custom-made stereotactic setup inside a sound-attenuated chamber. A thermostatically controlled heating pad (Fine Science Tools GmbH) maintained a temperature of 37.5°C to ensure comfort and stability during the procedure. Body temperature was monitored using a rectal probe, and the head was fixed with the headpin placed inside a metal rod.

Since reference and recording electrodes were placed inside the brain, we had to gain access to the tissue and perform a craniotomy and durotomy. The reference electrode was positioned within a small craniotomy located between bregma and lambda. The drilling for the recording electrode’s craniotomy and durotomy was carried out behind the sinus transversus, situated laterally to the midline. The specific lateral position depended on the auditory nuclei. Finally, the head of the animal had to be stereotactically aligned to lambda. The stereotactic alignment was essential to determine and reproduce the location of the auditory nuclei during every recording session.

Throughout the recording sessions, the surface of the brain was coated with a physiological NaCl solution (0.9%) to keep the superficial brain tissue healthy. Dry tissue would have led to necrosis and breaking of the tips of the recording electrodes.

2.9 In Vivo Electrophysiology

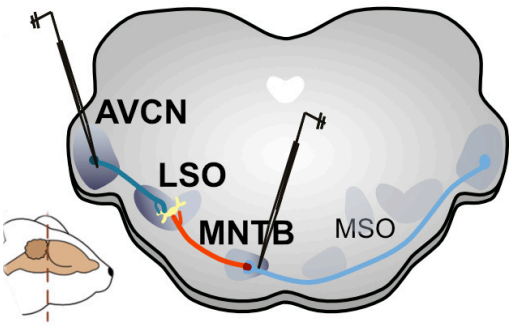

Figure 10: In vivo electrophysiology.
Sagittal plane representation of the Mongolian gerbil's auditory brainstem to illustrate the in vivo electrophysiological activity within specific auditory nuclei (the AVCN, MNTB, and LSO). The insertion of the tip of the glass electrode into the brain (specifically, the AVCN, the MNTB, or the LSO) allowed for the recording of APs. The glass electrode used for recording contained 5 units/µl of horseradish peroxidase. Taken from Müller et al. (2023).

APs were registered using a glass electrode containing horseradish peroxidase (Sigma-Aldrich Corp.) at a concentration of 5 units/µl, which was diluted in a 10% NaCl solution. As a result, the tip resistance ranged from 8 to 12 MOhm. The extracellular neuronal signal was recorded and underwent pre-amplification (Electro 705, World Precision Instruments), amplification (TOE 7607, Toellner Electronic), and filtering (Hum Bug Noise Eliminator, Quest Scientific Instruments Inc.).

Upon performing stereotaxis, the tip of the glass electrode was gently inserted into the brain at a 20-degree angle, facilitated by a motorized micromanipulator (Inchworm controller 8200, EXFO Burleigh Products Group) (Figure 10).

While employing Audiospike (HörTech GmbH), the extracellular neuronal signal was recorded, then subjected to pre-amplification (Electro 705, World Precision Instruments) and filtering using the Hum Bug Noise Eliminator from Quest Scientific Instruments Inc. After filtering, the recorded signal was transferred to a digital computer with a real-time processor (RP2, Tucker Davis Technologies Inc.) or via a sound card interface (Fireface UFX, RME-Audio).

Finally, Brain Ware (Jan Schnupp, Tucker Davis Technologies Inc.) or Audiospike (HörTech GmbH) were used to record and analyze the data. These software programs allow visual inspection of the recorded signal as well as online and offline spike sorting.

During the experimental phase, the initial recording and stimulation setup, consisting of Tucker Davis Technologies Inc. and Brainware, was replaced with a combination of Audiospike and an Audio Interface (RME fireface ufx II). Hence, from 2015 to 2018, Tucker Davis/Brainware was used; from the beginning of May 2018, Audiospike/Audio Interface was utilized.

2.10 Stimulus Generation

During the preparatory phase of the experiment, the stimuli applied during recording sessions differed between CI experiments and acoustic recordings. Electrical biphasic click stimuli were used during CI experiments, while acoustic recordings were performed using acoustic monophasic click stimuli.

Given that the LSO in gerbils can detect ITDs in click trains (Beiderbeck et al., 2018), and considering that CIs function by delivering electronic biphasic pulses resembling clicks to stimulate the auditory nerve, we opted to use acoustic clicks to imitate CI stimulation, rather than using pure tone stimulation. Additionally, the use of click trains enabled us to scrutinize the impact of each individual event within the ICIs. This approach allowed to explore how the LSO responses to changes in timing of the electrical click train.

To investigate this, we employed a model to assess the electrical ITD sensitivity of LSO cells. This approach aimed to test whether the activation of LSO cells was indicative of the primary source of ITD information for CI users, further shedding light on the role of the LSO versus that of the MSO in processing ITDs in this context.

During the experimental phase, both acoustic and electric stimulation were generated either using MATLAB and Tucker Davis Technologies Inc. or MATLAB and Audiospike (HörTech).

2.10.1 Acoustic Stimulation

Acoustic stimuli spanning the frequency range of 15 kHz to 90 kHz were digitally created using MATLAB (MathWorks) and then converted to an analog signal using an RX6 device from Tucker Davis Technologies Inc. The sampling rate used was 192 kHz. The signals were further attenuated using a PA5 device from the same company before being delivered to the headphones.

Utilizing Audiospike (HörTech), acoustic stimuli covering a range from 0.1 kHz to 90 kHz were generated digitally using MATLAB (MathWorks). Subsequently, these stimuli were converted to an analog signal through a sound card (Fireface UFX, RME, Audio AG) operating at a sampling rate of 192 kHz. Audiospike (HörTech) was employed to control stimulus presentation. The headphones used for both setups were the Etymotic er-4 micropro.

White noise bursts with a duration of 200 ms and rise/fall times of 5 ms were delivered through the headphones. These bursts were presented either to the ipsilateral ear, targeting the cochlear nucleus, or to the contralateral ear, targeting the MNTB. Once a neuron was detected, audio-visual methods were utilized to determine its characteristic frequency (CF) in response to pure tones, as well as its thresholds for pure tones and broadband stimuli. Neurons typically exhibit the highest sensitivity within a specific narrow frequency range. The CF represents the frequency to which the neuron responds with the lowest threshold, indicating its utmost sensitivity to that particular frequency.

Afterward, a series of six clicks, each with a duration of 50 µs, was presented in a pseudo-randomized order at five different ICIs of 5, 4, 3, 2, and 1 ms (Figure 11 a, c). The repetition rate for this click train was 20.

Apart from the click train and the audiovisual assessment of neurons, two additional recordings were taken, namely the frequency response area (FRA) and the PSTH. The FRA served to map the neuronal response to various frequencies and attenuations, graphically determining the neuron's CF and threshold. As described in chapter 1.8, the PSTH and the pre-potential together facilitate the differentiation of cell types in the cochlear nucleus (Figure 11 b) and the identification of cells in the MNTB (Figure 11 d).

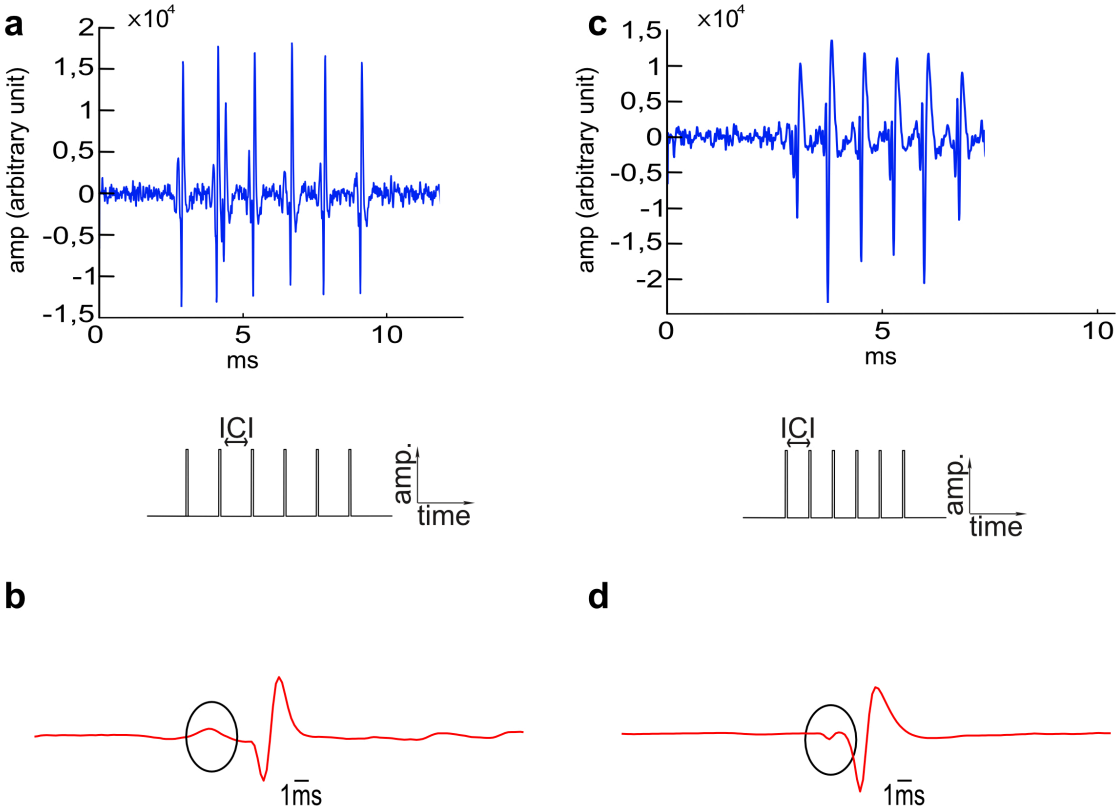

Figure 11: Examples of acoustic stimulated and recorded cells.
Figures (a) and (b) show raw data of one BC; (c) and (d) show raw data of one MNTB principal cell; (a) and (c) show raw recording trace of AP in response to the acoustic click train consisting of six clicks; (b) and (d) show average spike waveform of the recorded cells (a) and (c). The black circle indicates the pre-potential.

2.10.2 Electrical Stimulation

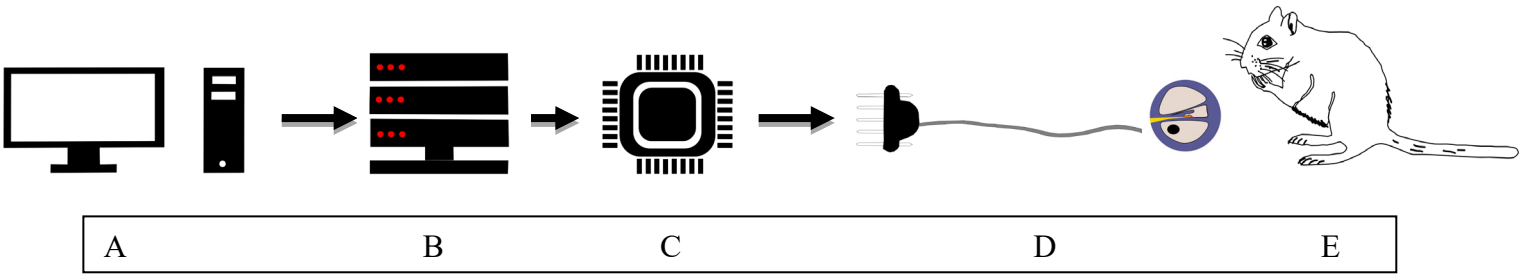

Figure 12: Electrical stimulation of the Mongolian Gerbil's Cochlea.
Digital electrical stimuli were initially produced (A) and then routed either to the RX6 (Tucker Davis Technologies Inc.) or an Audio Interface (RME Fireface UFX II) (B). Subsequently, these stimuli were channeled into a voltage-to-current converter (ICS5, Thomas Wulf Elektronik) (C) before being transmitted to a cochlear implant (CI), produced by MED-EL (D). This implant was surgically placed within the scala tympani of a Mongolian Gerbil (E).

Electrical stimuli were created using digital means—MATLAB (MathWorks) or Audiospike (HörTech GmbH)—and then either converted to an analog signal using an RX6 device from Tucker Davis Technologies Inc., or transferred to an audio interface, specifically the RME Fireface UFX II. Subsequently, these stimuli were directed to a voltage-to-current converter (ICS5, Thomas Wulf Elektronik) and delivered via a CI manufactured by MED-EL (Figure 12). The stimulation current varied from 0.11–0.49 milliampere.

To begin the experiment, a search stimulus was employed, consisting of a click train with a single click duration of 110 µs (with anodic and cathodic phases of 50 µs each and an interphase of 10 µs), presented at an ICI of 5 ms. When neuronal spikes were detected in response to this stimulus, the electrical threshold of the neuron was determined visually.

Subsequently, a sequence of six clicks, each lasting 110 µs (comprising anodic and cathodic phases of 50 µs each, and an interphase of 10 µs), was delivered in a pseudo-randomized manner, covering five distinct ICIs of 5, 4, 3, 2, and 1 ms. These click trains were delivered to either the ipsilateral or contralateral ear (Figure 13 a, c).

During electrical stimulation, strong electrical artefacts were observed (Figure 13 a, c). To focus solely on analyzing the spike waveforms and spike times resulting from the electrical stimulation, the artifacts were removed from the raw data traces. This was achieved by zeroing the amplitude values, typically within a range of +/-10 samples centered on the artifact peak, during the analysis process using MATLAB.

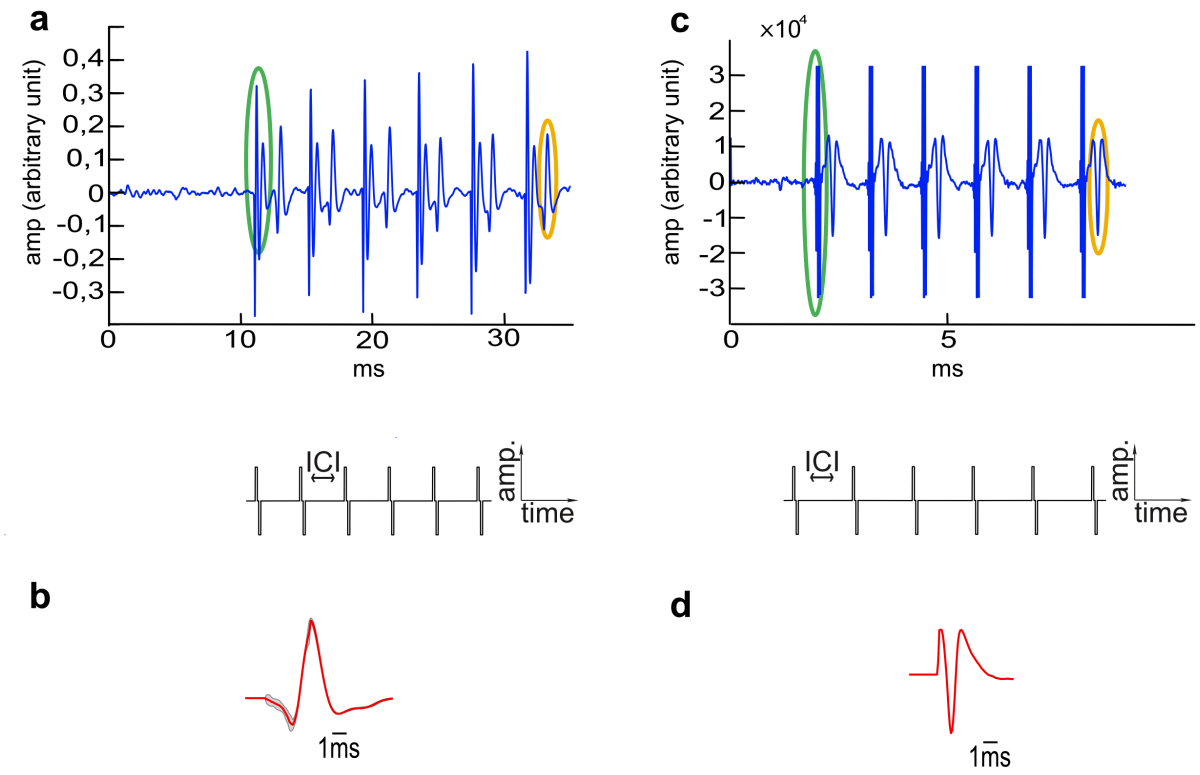

Figure 13: Examples of electrical stimulated and recorded cells.
Figures (a) and (b) show raw data of one BC; (c) and (d) show raw data of one MNTB principal cell; (a) and (c) show raw recording trace of AP in response to the electrical click train consisting of six clicks; (b) and (d) show the average spike waveform of the recorded cells (a) and (c). Green depicts the stimulation artifact; orange represents the AP.

2.11 Acoustic and Electrical Model

Technical limitations prevented us from conducting CI recordings in the LSO. As this thesis focuses on the electrical ITD sensitivity in the LSO and the influence of electrical stimulation on the inputs to the LSO, we employed a computational model. Dr. Hongmei Hu and Prof. Mathias Dietz from the University of Oldenburg produced the model's data.

The model framework was adapted from Klug et al. (2020). It displays, in principle, two combined models:

1. A coincidence-counting model of the LSO for binaural excitatory-inhibitory (EI) interaction.
2. An acoustic or electrical auditory periphery model of the auditory nerve.

The periphery model used by Bruce et al. (2018) functioned as the basis for the acoustically stimulated auditory nerve. This model replicates the middle ear, the cochlea, and the auditory nerve and receives input via a pressure waveform. The output is produced by a spike generator that transfers a series of auditory nerve spikes.

Most of the model parameters we adopted are analogous to Bruce et al. (2018) and Zilany et al. (2009, 2014). However, the intensity of the parameters of the auditory nerve was changed to 50/60 dB SPL to better mimic the excitatory input (50 dB SP) and inhibitory input (60 dB SPL) to the LSO.

The electrical auditory nerve model is based on the work of Hamacher (2004) and comprises four stages: cell membrane, membrane noise, refractory period, and latency and jitter. The model did not implement tonotopy and adaptation, and every auditory nerve had the same threshold input level. As for the acoustic periphery model, most of the parameters used by Fredelake and Hohmann (2012) and Hamacher (2004) were kept unchanged. Nevertheless, the auditory nerve mean and standard deviation of latency and jitter were modified to reflect the findings from the AVCN and MNTB physiological recordings. It is important to state that the acoustic and electrical periphery models do not include a cochlear nucleus or MNTB stage. As described above, we had to adapt the parameters of the auditory nerve to fit the output of the cochlear nucleus and MNTB.

The binaural integration stage incorporated the model framework from Klug et al. (2020), while retaining the original parameters of the coincidence-counting LSO model by Ashida et al. (2016). This model encompasses a wide array of stimulus classes and effectively replicates the characteristic response properties of LSO neurons (Hu et al., 2022; Klug et al., 2020).

Inhibitory inputs are provided by contralateral auditory nerve fibers, while excitatory synaptic inputs are provided by ipsilateral auditory nerve fibers. The rectangular inhibitory window (Winh) and the rectangular excitatory coincidence window were set to 1.6 ms and 0.8 ms, respectively, using the default settings of Ashida et al. (2016). Detailed parameter settings, as well as a description of the models, can be found in Bruce et al. (2018), Fredelake and Hohmann (2012), Hamacher (2004), Hu et al. (2022), Klug et al. (2020) and in Zilany et al. (2009, 2014).

A set of six digital rectangular clicks, each with a duration of 50 µs, was created at a sample rate of 100 kHz and employed as input for the acoustic auditory nerve model. Conversely, for the electrical auditory nerve model, six biphasic constant-amplitude pulse trains (with cathodic/anodic phases of 50 µs each) served as the input. Five different ICIs (5, 4, 3, 2, and 1 ms) were tested for each condition, at varying presentation levels, over 200 repetitions, and the results were recorded.

2.12 Histology with Diaminobenzidine

At the conclusion of the experiment, to confirm the recording site, iontophoretic administration of horseradish peroxidase (HRP) was carried out through the recording electrode by applying a current of 1 µA for a duration of 8 minutes. In some instances, no distinct HRP staining was found, and the identification of the recording site therefore depended on either tracing the path of the recording electrode or detecting a pre-potential (Figure 11 b, d) in the waveform of the recorded action potential.

After administering HRP, an intraperitoneal injection of a lethal dose of narcoren (Pentobarbital 500 mg/kg) was given. A needle was injected into the left ventricle when the heart stopped beating, while the right atrium was cut open. The animal underwent perfusion with a solution consisting of Ringer's solution containing NaCl (0.9%), heparin (100 µl), and five mM phosphate-buffered saline (PBS) in H_2O for a duration of 10 minutes. This was followed by perfusion with 4% paraformaldehyde (PFA in PBS pH 7.4) for an additional 10–25 minutes. Subsequently, the brain was extracted and put into 4% PFA for 1–2 days at 4°C. Afterward, the brain underwent three 10-minute washes in PBS (0.02 M) and was embedded in 4% agarose. Coronal brain slices of 50–80 µm thickness were produced using a vibratome.

Taking a diaminobenzidine (DAB) substrate kit (Vector Laboratories, Inc.), the brain was stained against HRP. Adding DAB leads to the oxidation of HRP, resulting in a brown precipitate at the administered location of HRP. The brown marking spot can be visualized using light microscopy (Figure 14).

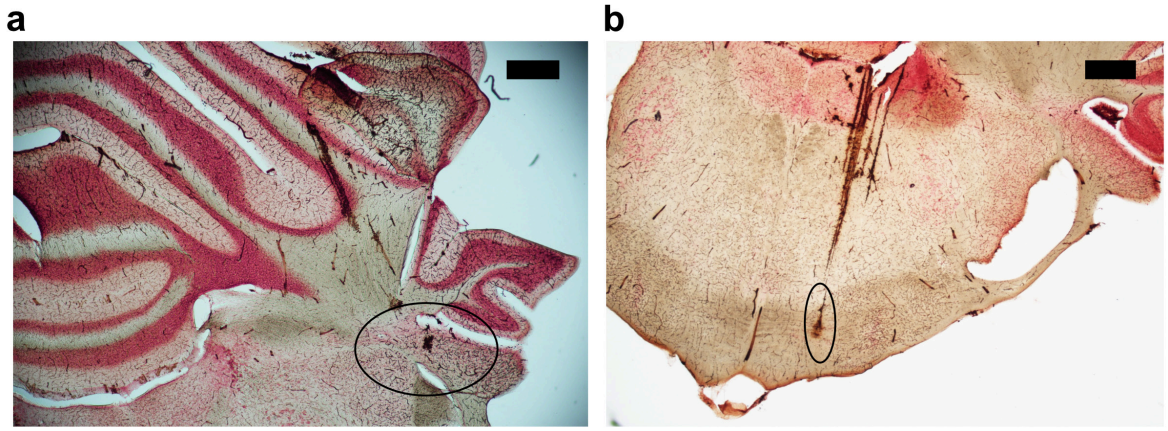

Figure 14: Example verification of the recording site.
In (a) the black circle demonstrates the HRP labeling of the recording site in the AVCN; with (b) showing the HRP labeling of the MNTB. Scale bar: 500 µm.

Initially, the brain was exposed to DAB for a duration of 8 minutes. Subsequently, the slices underwent three 10-minute washes with distilled water and PBS. Following the washes,

the slices were mounted onto glass slides and left to air-dry overnight. The subsequent day, the slices were counter-stained with neutral red according to the following protocol:

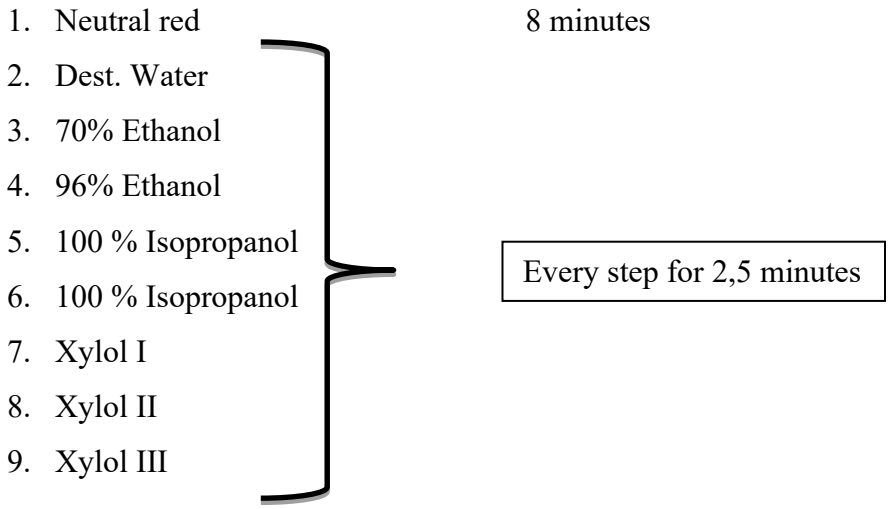

The solution of neutral red comprised 1 g neutral red, 4 ml acetate buffer (0,2 M) at a pH of 4,8 mixed with 100 ml distilled water. Ultimately, the slices were covered with glass objectives slides and DePeX (Serva Electrophoresis GmbH). Images of the slices were captured on a fluorescence microscope, and the correct recording site was verified.

2.13 Histology with Technovit® 9100

Our research aimed to evaluate both the positioning of the CI within the cochlea and the impact of the inserted CI on cochlear structures, specifically focusing on the density of the spiral ganglion. Consequently, we aimed to identify a material and accompanying technique that could accomplish both immunohistology and cochlea slicing without the need to remove the implant.

We finally settled on Technovit® 9100 as a promising material. However, four different methods were initially considered, using paraffin, celloidin, resin, and frozen sections.

Paraffin is widely used for embedding and slicing various tissues (Gillespie et al., 2003; Scheper et al., 2009). Paraffin is advantageous in that it can maintain high-quality morphology and immunogenicity. However, its high melting temperature can cause heat-induced trauma, which disrupts the morphology (Merchant et al., 2006).

By contrast, high-quality morphology can be achieved through celloidin (Hinojosa & Nelson, 2011); however, this material does not provide a stable immunohistology because celloidin is not completely removed from the tissue (Merchant et al., 2006).

Resin requires high temperatures for tissue polymerization and so is also unsuitable for immunohistology (Ruddell, 1967). In addition, like celloidin, resin also leads to incomplete removal from the tissue, which adds to poor antigenicity—numerous protocols have been devised to enhance low antigenicity, among them the high-temperature antigen retrieval technique (Yamashita & Okada, 2014). However, while this yields favorable results, the process is lengthy and complex.

Immunohistology commonly employs frozen sections, but their usage can cause morphology quality reduction due to the occurrence of freezing artifacts and crystal formation (Whitlon et al., 2001).

In addition, the metal components of the electrode array prevent traditional histology techniques (paraffin, celloidin, resin, frozen sections) being used to slice the cochlea while the implant is still in place. Therefore, other histology methods were taken into account.

Micro-grinding of the cochlea allows researchers to study the implant's effect on cochlea trauma and its position. However, disadvantages including the thickness of the slices (200–250 µm) and the loss of inner cochlea structures (Cisneros et al., 2017; Stöver et al., 2005) limits performance in immunohistology studies.

As a result, we finally focused on Technovit® 9100 as a promising material. Technovit® 9100 is a resin-based embedding material that hardens at cold temperatures between -8° C and -20° C, enabling the cutting of bones. The low temperatures of the Technovit® 9100 protocol result in the immunoreactivity of bone sections (Yang et al., 2003). A recently published paper by Bako et al. (2015) on Technovit® 9100 cochlea slices shows highly preserved cochlea morphology and immunogenicity. Hence, this study served as an orientation for our Technovit® 9100 experiment. We adopted the Technovit® 9100 protocol by adding the CI in the scala tympani. As Technovit® 9100 is able to slice bones, it should, generally speaking, be able to slice electrode arrays as well.

In the subsequent section, the methods utilized in Dick's (2017) bachelor thesis are detailed. The thesis primarily concentrated on developing a histology protocol for Technovit® 9100, with me serving as the project supervisor. Simon Dick conducted the majority of the practical tasks, such as staining, slicing, and analysis. I performed the CI insertion and bulla removal. Furthermore, I initiated and adjusted the protocols for slicing, staining, and analysis.

2.13.1 Technovit® 9100 Protocol

Technovit® 9100 was tested for slicing, preservation of morphology, and three different staining methods: (1) Giemsa, (2) hematoxylin-eosin, and (3) epoxy tissue stain. For this purpose, ten Mongolian gerbils were sedated with isoflurane and injected intraperitoneally with pentobarbital mixed with NaCl. After death confirmation, nine animals were unilaterally implanted with a CI, as described in chapter 2.7. Following this procedure, the bulla containing the cochlea subjected to implantation, as well as the bulla containing the non-implanted cochlea utilized as a control sample, were both extracted.

An incision was made, starting at the os foramen magnum, between the os interparietale and the os parietale. Using gentle force, the petrous bone was removed and placed in formalin (4%) at 4°C overnight. The following day, the petrous bone containing the cochlea was placed in an EDTA–citric-acid–PBS solution (0.35%) to decalcify. This process took between three to four days. After complete decalcification, the Technovit® 9100 protocol started. It consisted of four different steps: (1) dehydration, (2) preinflitration, (3) infiltration, and (4) polymerization (Table 2).

(1) Dehydration occurred in an ascending series of ethanol concentrations, ending in 100% ethanol, in which xylol served as an intermedium.

(2) Preinfiltration consisted of three steps. First, the cochlea was placed in a 1:1 mixture of Technovit® 9100 base solution and xylol overnight at room temperature. Then the cochlea was added to a mixture of Technovit® 9100 base solution and hardener and kept for eight hours at room temperature. Afterward, the same mixture was used to further preinfiltrate the tissue overnight at 4°C.

(3) Infiltration contained a 250 ml Technovit® 9100 base solution, 20 g PMMA powder, and 2 g hardener and lasted 24 hours at 4°C.

(4) Two different solutions were needed for the polymerization: stem solution A and stem solution B. First, the cochlea was placed in midmodiolar orientation in the histoform N. Then both solutions were poured onto the histoform. Afterward, an exicator that produces a vacuum removed unwanted bubbles. This was necessary because remaining oxygen prevents polymerization. Next, the tissue was placed at either -16°C for 2 days or at -4°C for 4–14 days in a freezer. Some cochleae exhibited incomplete polymerization and needed extra time to harden at room temperature. At the end of this part of the procedure, the cochleae were blocked onto the histobloc N by pouring Technovit® 3040 onto the histoform and dried overnight at room temperature.

After complete polymerization, the histobloc was sliced with a microtome at 10 µm. Then, the slices were straightened with 60% Ethanol, covered with foil, put into a press, and left in an incubator at 37°–60° degrees overnight. During the squeezing process, we observed a phenomenon where sections were lost from the slices. As a result, not all of the slices could be assessed at first. However, upon identifying this issue, the pressure was adjusted, resulting in an improvement. Following these modifications, nearly all the slices could be evaluated.

The sections were finally stained with one of the following: Giemsa, hematoxylin-eosin (HE), or epoxy tissue stain (ETS).

Table 2: Technovit® 9100 protocol.
The process involved four specific phases: (1) dehydration, (2) preinfiltration, (3) infiltration, and (4) polymerization, for a total duration ranging from 8 to 18 days.

Step	Solution	Temperature	Time
Dehydration	30% Ethanol	RT	1 h
	40% Ethanol	RT	1 h
	50% Ethanol	RT	1 h
	60% Ethanol	RT	1 h
	70% Ethanol	RT	Overnight
	80% Ethanol	RT	2 x 1 h
	90% Ethanol	RT	2 x 1 h
	96% Ethanol	RT	2 x 1 h
	100% Ethanol	RT	2 x 1 h
	Xylol	RT	3 x 1 h
Preinfiltration	Technovit Base solution + Xylol (1:1)	RT	Overnight
	Technovit Base solution + hardener 1	RT	8 h
	Technovit Base solution + hardener 1	4°C	Overnight
Infiltration	Technovit Base solution + hardener 1 + PMMA Powder	4°C	24 h
Polymerization	Stem solution A + Stem solution B (9:1)	-4°C – -16°C	4-14 days

2.13.2 Staining

The Giemsa and HE staining protocols were executed according to the manufacturer's protocols (Table 3,Table 4). Before every staining, the use of Giemsa required producing a new base solution (1 ml of Giemsa + 50 ml Aqua dest.). The first four steps of the Giemsa and HE protocol served for deplastification.

Table 3: Giemsa staining protocol
The staining procedures followed the specified guidelines outlined in the manufacturer's Technovit 9100® protocols.

Solution	Time [min]
Xylol	2 x 20
2-Methoxyethylacetat	20
Aceton	2 x 5
Aqua dest.	2 x 5
Giemsa-solution	30 - 40
Aqua dest.	1
Aceton/Xylol 95:5	10
Aceton/Xylol 70:30	10
Aceton/Xylol 30:70	10
Xylol	10

Table 4: Hematoxylin eosin staining protocol.
The staining methods adhered to the prescribed instructions detailed within the manufacturer's Technovit 9100® protocols.

Solution	Time [min]
Xylol	2 x 20
2-Methoxyethylacetat	20
Aceton	2 x 5
Aqua dest.	2 x 5
Hematoxylin	10
Water	2
Eosin	5
Aqua dest.	1
70% Ethanol	5
80% Ethanol	5
96% Ethanol	5
100% Ethanol	5
100% Isopropanol	5
Xylol	3x5

The epoxy tissue stain (ETS) staining protocol was based on (Aescht et al., 2010) (Table 5). The ETS was diluted in water at a 1:5 concentration. In contrast with the other staining methods, the incubation of the slides took place on a heater at 42° degrees.

Table 5: ETS staining protocol.
The procedure for an epoxy tissue stain (ETS) was derived from the method described by Aescht et al. (2010).

Solution	Time [min]
ETS-solution	6
Aqua dest.	2
70 % Ethanol	0,25
Water	2
Xylol	3 x 10

2.13.3 Modification of the Staining Protocols

During the initial stages of staining, we encountered certain challenges associated with the adherence of tissue slices to the slides and their deterioration during deplastification. In addition, in some cases we needed to adjust the intensity of the staining, to gain either a milder or a stronger effect. Consequently, we decided to implement several modifications to the staining protocols:

1. Elimination of specific steps, including the deplastification process.
2. Incorporation of an additional coating on the slides using a mixture consisting of 2% ponal classic and 0.01% poly-l-lysine, in a 2:1 ratio.
3. Alteration of the staining concentrations.
4. Reduction or extension of the incubation times.

A comprehensive description of the modifications implemented in the three staining protocols are provided below. The outcomes resulting from these modifications are presented afterward in Chapter 3, which provides the results of our research.

Giemsa modifications:

We shortened the incubation time in the Giemsa solution from 50 to 35 minutes and omitted the first four steps (deplastification) of the original protocol (Table 6).

Table 6: Modified Giemsa staining protocol.

Solution	Time [min]
Giemsa-solution	35
Aqua dest.	1
Aceton/Xylol 95:5	10
Aceton/Xylol 70:30	10
Aceton/Xylol 30:70	10
Xylol	10

Hematoxylin-eosin modifications:

The first four steps (deplastification) were withdrawn. Secondly, ethanol (70%, 96%) and isopropanol were removed from the protocol. Additionally, the incubation time for hematoxylin was increased to 15 minutes, and the incubation time for eosin was reduced to 4 minutes (Table 7).

Table 7: Modified hematoxylin eosin staining protocol.

Solution	Time [min]
Hematoxylin	15
Water	2
Eosin	4
Aqua dest.	1
96% Ethanol	5
100% Ethanol	5
Xylol	5

Epoxy tissue stain (ETS) modifications:

The modification of ETS included slight modifications. The incubation time of distilled water and ethanol was modified, and the ratio of the ETS solution was changed to 1:10 (Table 8).

Table 8: Modified ETS staining protocol.

Solution	Time [min]
ETS-solution	6
Aqua dest.	2x5
70% Ethanol	0,25
Water	2
Xylol	3 x 10

2.14 Programs and Analysis

We utilized custom-made MATLAB programs (The MathWorks Inc.) for data analysis in this study. The physiological data for AVCN and MNTB were assessed by computing the median spike probability and jitter for every inter-click interval (ICI). Additionally, the LSO was examined to determine its dynamic ITD range and delta slope per dB ILD. The spike probability for each neuron was determined by dividing the median spike rate per trial by 6, corresponding to the number of pulses per trial. Jitter was calculated based on the standard deviation of the AP latency in relation to the eliciting click. The range between the ITDs which caused the maximum and minimum spike rates was termed the dynamic ITD range.

By computing the delta slope, which is the normalized maximal and minimal spike rates' difference divided by the dynamic ITD range, we evaluated the effect of ILDs on ITD sensitivity. We calculated the difference between the values obtained at the most positive and negative ILD conditions tested for each LSO neuron and then divided this difference by the respective ILDs. To analyze the significance across groups, we employed a non-parametric ANOVA test. Additionally, for assessing the statistical significance of individual ICIs, we used the Mann-Whitney U-test. As previously mentioned (Sakitt, 1973), the standard separation D is calculated as follows:

$$Dn = |mu_{n+1} - mu_n| / (sqrt(sigma_{n+1} * sigma_n))$$

where mu_{n+1} and mu_n represent the mean values of the hemispheric rate differences to two ITD values, and $sigma_{n+1}$ and $sigma_n$ are their respective standard deviations. We applied a 5-

sample moving average filter to smooth Dn. The sigma of the model responses follows a Poisson noise assumption.

MATLAB programs (The MathWorks Inc.) were employed to visualize the data. Figures were generated using Affinity Designer (Version 1, Serif). Statistical analysis was conducted using SPSS (IBM Corp. Released 2022. IBM SPSS Statistics for Windows, Version 29.0. Armonk, NY: IBM Corp).

The process of reviewing the text for grammatical and spelling errors included the utilization of ProWritingAid. ChatGPT was employed to rephrase my originally authored and formulated text, without altering the core content of the dissertation.

3 Results

The research at the heart of this thesis was focused on three goals: the first was to establish a successful CI implantation method, while the second was to develop a successful electrical stimulation technique. Our third aim, to establish a histology protocol with Technovit® 9100, had limited success, as will be explained in the succeeding chapters.

The analysis of the acoustic and electrical recordings, as well as the modeling results, will be presented in the concluding chapter.

3.1 Establishment of a CI Implantation and Stimulation Process

CI implantation is a complicated process that requires the surgeon to be highly precise and knowledgeable of the right order of steps. Before performing surgery on living creatures, experience with the CI was gained through training on the removed inner ear of Mongolian gerbil corpses. The surgeon adhered to the following training routine:

1. Identifying the gerbil anatomical inner ear structures on 10 isolated Mongolian gerbil corpse's inner ear
2. Implanting CIs
    a. on 10 isolated gerbil Mongolian corpse's inner ear,
    b. on 10 cochleae of Mongolian gerbil corpses,
    c. on living Mongolian gerbils.

3.1.1 CI Implantation

Step 1: Identifying the main anatomical inner- and middle ear structures using the isolated inner ear of ten gerbil corpses.

Determining the structures of the inner- and middle ear was the first step in utilizing the CI implantation technique in Mongolian gerbils. Consequently, the tympanic bulla of 10 Mongolian gerbil corpses were extracted and decalcified with ethylenediaminetetraacetic-acid (EDTA)-PBS solution (0.35%). The amount of time necessary to decalcify the bone is determined by its size. Since the bony bulla wall of the Mongolian gerbil is a very thin structure, this was generally 3–4 days. After this time, the bony wall was removed with scissors, and the round and oval window, together with the stapedial artery, were identified. A prominent feature of the Mongolian gerbil cochlea was then detected at the entry of the round window: the so-called round window niche. It became evident that the presence of the round window niche could pose a potential obstacle to the successful implantation of a CI.

Step 2 a: CI implantation on 10 isolated cochleae from Mongolian gerbil corpses

Following the structure identification, the implantation of the CI was performed on the removed inner ear (Figure 15). Forceps were used to push the CI slowly into the scala tympani. It was determined that the prominent round window niche hindered the implantation process and obscured the sight of the implant's black implantation spots. Therefore, the second implantation attempt involved using a drill to remove parts of the round window niche, resulting in satisfactory results. Upon surgically removing portions of the round window niche, we were able to uncover the black implantation spots of the CI, enabling us to insert the implant seamlessly into the scala tympani.

A microscope was then employed to provide images of the structures of the decalcified inner ear. Once these structures were identified, the next step was implanting a CI into a Mongolian gerbil corpses cochlea.

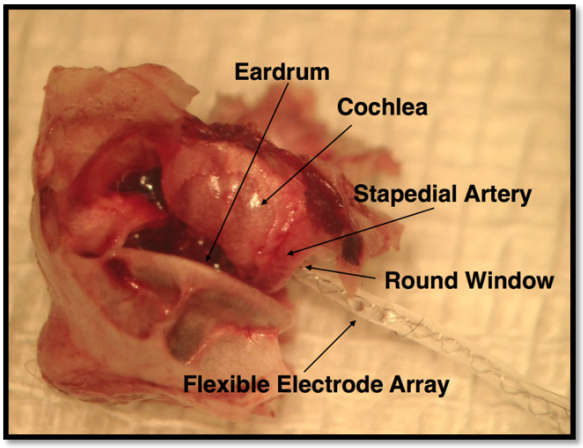

Figure 15: Anatomical specimen depicting the anatomical structures of the inner- and middle ear and the structures of the implanted CI.
Illustration of the CI placed within the scala tympani of the cochlea. The anatomical sample clearly demonstrates the proximity of the stapedial artery to the round window, highlighting the need for meticulous care to avoid any damage to this artery during CI implantation.

Step 2 b: CI implantation on 10 whole Mongolian gerbil corpses

During the implantation process, we faced several challenges or obstacles. As a result of manufacturing issues, we were compelled to reuse the CIs following the initial implantation. This necessitated the development of novel strategies to ensure a secure and stable implantation while allowing for subsequent removal of the CI after recording, in order to perform additional implantations on other animals.

After resolving these challenges, the implantation procedure on gerbil corpses closely mirrored that of live animals. For more information on the implantation process, please refer to Chapter 2 on “Material and Methods.”

In the subsequent section, the difficulties we encountered will be outlined and the innovative approaches we developed to overcome them will be elaborated upon.

Reuse of CIs:

In our acute CI experiment, careful consideration was given to every step of the implantation process in order to facilitate the reuse of the CIs without causing any damage to the implant. While chronic animal CI experiments typically utilize acrylic Paladur® by Hereus Kulzer to secure the CI to the animal’s skull (Fischer, 2015; Wiegner, 2016), this approach was not suitable for our acute experiment. Heraeus Kulzer is a company dedicated to dental products and solutions, recognized for delivering materials and technologies tailored for dental professionals. Paladur® represents an effective denture repair plastic utilized in the rehabilitation of oral functions, including chewing, speaking, and enhancing aesthetics. It serves to restoratively or prosthetically stabilize the remaining dentition and/or the alveolar ridge. Paladur® is specifically designed for long-term dental prostheses and its hardening properties render CI reuse impossible. As an alternative, we devised a solution involving the use of tissue adhesive.

Using this adhesive, we implemented three fixation points. First, the neck muscles served as a temporary placeholder; secondly, the wire of the implants was bonded to the bony wall using Histoacryl®; and finally, a skin suture on the back provided a secure grip for the wire.

However, employing tissue adhesive, such as Histoacryl®, used by Fischer (2015), and VetbondTM, utilized by Wiegner (2016) to attach the CI onto the bony bulla wall presented us with new challenges and difficulties. As we applied Histoacryl® to the bony bulla wall and the CI, we encountered complications when attempting to remove the adhesive from the implants. Histoacryl® adhered strongly to the implant, causing an increase in its diameter and making reimplantation initially difficult. To mitigate this effect, we used a different size of venous catheter during the operation and carefully removed the adhesive from the wire.

CI implantation:

During the insertion of the CI into the scala tympani, additional challenges were identified. The flexible nature of the CI's tip necessitated precise placement in front of the round window to ensure smooth passage through this window without any obstructions. The bending of the electrode array, induced by contact with adjacent cochlea structures further complicated the precise positioning of the CI's tip and the overall implantation process. Additionally, great care had to be taken while handling the CI wire with forceps to prevent damage to the wires connected to the electrodes concealed beneath the silicone layer.

Step 2 c: CI implantation on living Mongolian gerbils.

After conducting experiments on deceased Mongolian gerbils and analyzing the errors made during surgical procedures on their corpses, we proceeded to implant CIs into live animals. During the recordings, we observed that the CI remained within the scala tympani, and there were no instances of injury to the stapedial artery during the surgery. None of the animals were excluded from the study due to mishaps during the implantation process. The implantation model we employed proved successful in obtaining acute CI recordings in the Mongolian gerbils.

3.1.2 Stimulation of the Cochlear Implant

The stimulation process initially involved stimulating electrodes using voltage, but this was found to have limitations. Because of the high non-linearity discovered during the analysis of voltage stimulation produced by an interconnecting tool, Prof. Dr. Hemmert and Dr. Obando provided us with support. They manufactured a voltage-to-current converter to get a well-defined current output (Figure 16). Unfortunately, this attempt resulted in low saturation thresholds and this approach was again unusable in the experiment.

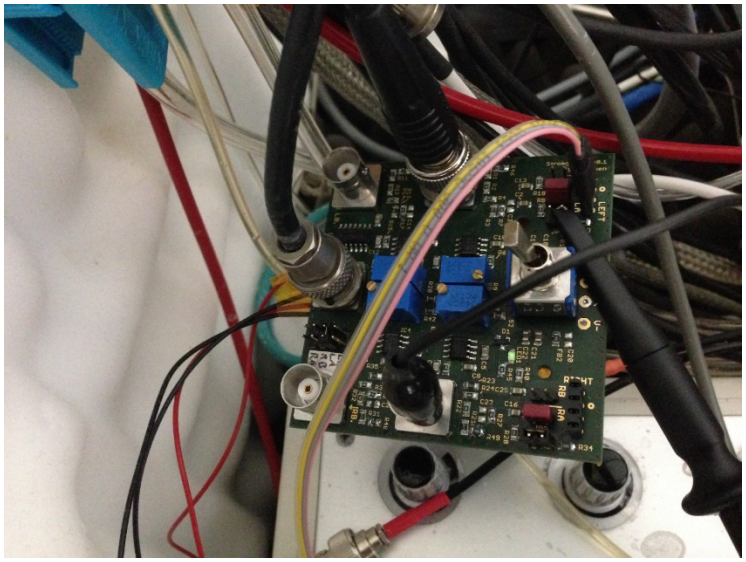

Figure 16: Self-made voltage to current converter resulted in a low saturation threshold.

Ultimately, the decision was made to invest in a customized CI voltage-to-current converter (ICS5, Thomas Wulf Elektronik) to allow stable current steps and well-defined currents that were applied. This allowed recording data to be obtained from electrically stimulated cells at 2 dB above the threshold.

To establish the capability of the customized CI voltage-to-current converter (ICS5, Thomas Wulf Elektronik) to generate stable current steps, we conducted measurements of the applied current at different voltage levels before conducting the initial experiment. Throughout the experiments, the applied current ranged from 0.11–0.49 milliampere, depending on the threshold of the electrically recorded cell that was identified visually. Bipolar stimulation was employed, with an active electrode located in the most apical part of the cochlea, and another electrode in the adjacent, basal part of the cochlea serving as a reference.

3.2 Histology with Technovit® 9100

This chapter presents the outcomes of Dick's (2017) bachelor thesis, conducted in the Pecka lab under my supervision. Please refer to Chapter 2.13 for an account of my participation and contribution to the thesis.

A grading system was employed to evaluate the level of detection, with assigned values representing different grades. The grading system used in this analysis was as follows: "--" indicated not detectable, "-" represented poor detection, "+" denoted good detection, and

"++" signified very good detection. The assessment included evaluation of (1) the staining quality, (2) the morphology, and (3) the slicing of the implant. These are described as follows:

1. The original staining protocol revealed decent results regarding the Giemsa staining process (Figure 18). The removal of the deplastification steps depended on the loss of slices during the process and was not involved in the staining quality. The first results of the ETS staining produced intense staining, which did not allow for cell differentiation (Figure 19 A, B). On the contrary, HE staining was mainly too weak to evaluate the (Figure 17 A, B). After modifying the protocol and removing specific steps, the quality of the Giemsa staining remained the same. The modification of the HE staining led to better results, while the detection of SGNs improved compared with the older protocol (Figure 17 C). Changes in the ETS protocol produced better cell differentiation and the unwanted violet staining tone vanished (Figure 19 C). In the end, the best staining results were achieved with Giemsa (Figure 18).

2. All membranes (Reissner's, tectorial, and basilar membranes) were mostly detectable in good quality (Table 11, Figure 20, Figure 21). The CI did not interfere with the slicing process, and the cochlea structures stayed intact (Figure 20).

3. The primary objective is yet to be accomplished. While the knife sliced the implant without damaging structures, the CI was not detected on the slides (Table 9, Table 10, Figure 20).

Table 9: Preliminary evaluation of staining quality and detectability of the CI.
The evaluation was carried out using a grading system that involved assigning values to indicate the level of detection. The grades used in the system were as follows: "--" for not detectable, "-" for poor detection, "+" for good detection, and "++" for very good detection.

Staining	Detection of implant	Detection of SGNs
Giemsa	--	++
HE	--	-
ETS	--	+

Table 10: Evaluation of staining quality and detectability of the CI following protocol modification.
The analysis was conducted to assess the staining quality and detectability of the CI after implementing protocol modifications.

Staining	Detection of implant	Detection of SGNs
HE	--	+
ETS	--	++

Table 11: Evaluation of cutting quality for cochlea embedded in Technovit without implant.
The assessment utilized a +/- system to rate the criteria as follows: (--) not detectable at all, (-) poorly detectable, (+) well detectable, (++) very well detectable.

Staining	Mid-modiolar orientation	Reissner's membrane	Tectorial membrane	Basilar membrane
Giemsa	+	--	++	++
HE	+	+	+	+
ETS	+	--	+	+

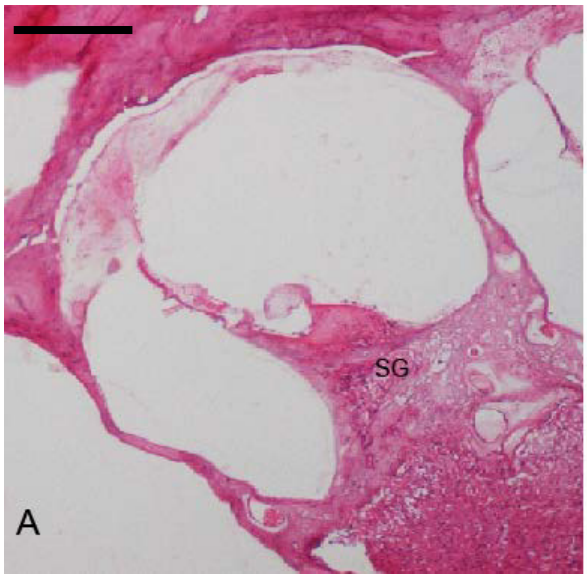

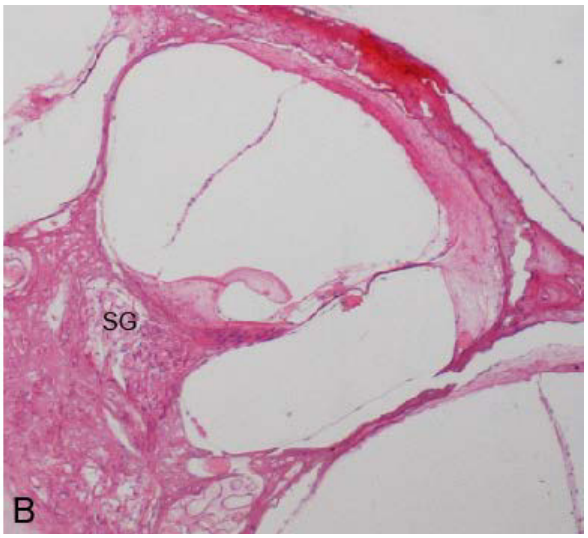

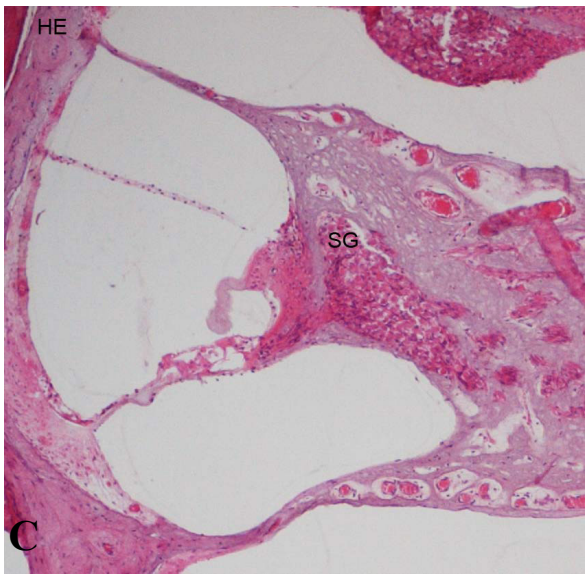

Figure 17: Comparison of individual turns in Technovit sections stained with hematoxylin-eosin. Image C displays the staining after modifying the staining protocol, while images A and B represent the staining prior to the protocol adjustment. The spiral ganglion cells are clearly visible in image C, whereas in images A and B the spiral ganglion cells are barely discernible. The black scale bar depicts 200 micrometers (µm). Taken from Dick (2017).

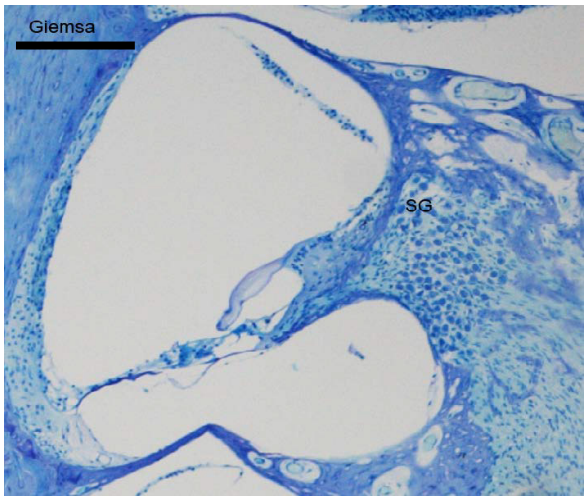

Figure 18: Section of a cochlear turn stained with Giemsa.
The initial staining method showed satisfactory outcomes in Giemsa staining. Ultimately, the most optimal staining results were obtained using Giemsa. The black scale bar depicts 200 micrometers (µm). Taken from Dick (2017).

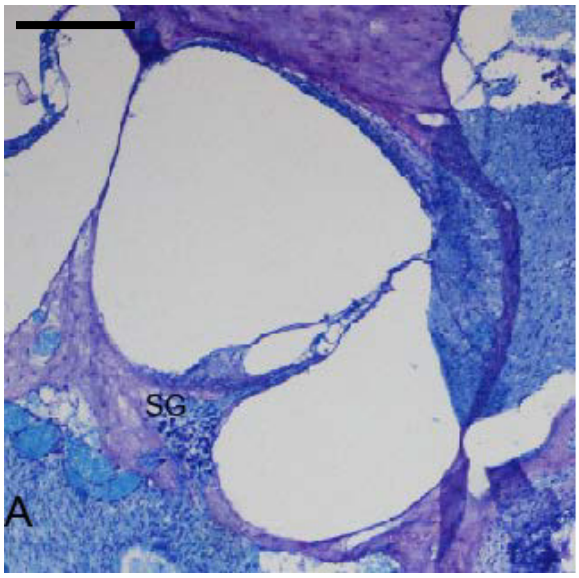

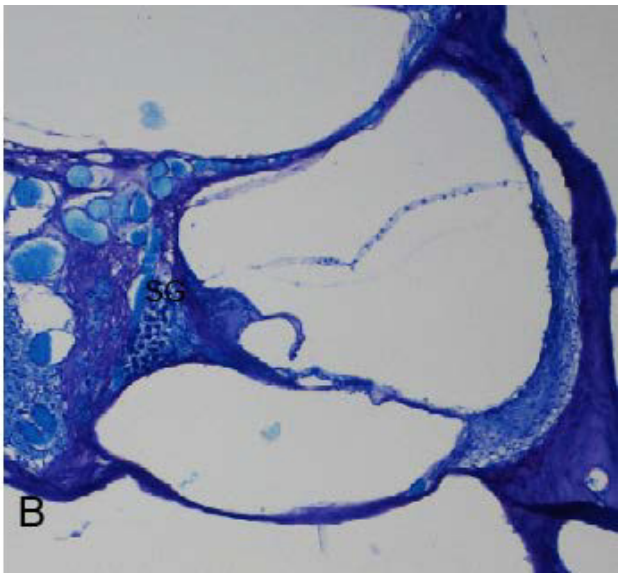

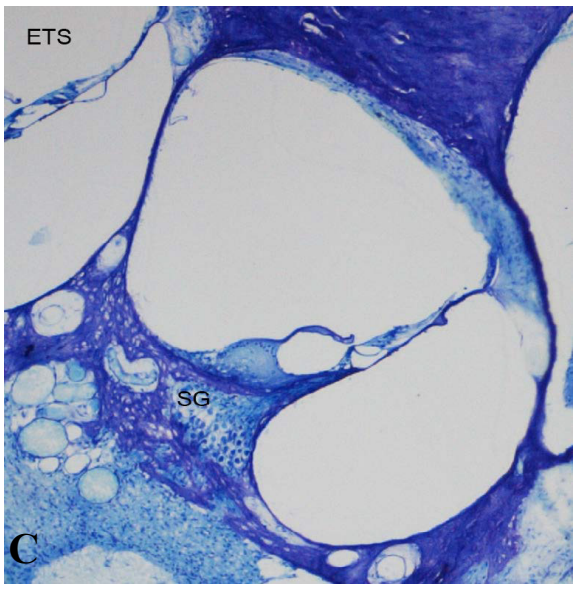

Figure 19: Comparison of individual turns in Technovit sections stained with ETS.
Image C illustrates a section after adjusting the incubation times. The spiral ganglion cells are clearly visible, as well as other tissues. Image A depicts the undesired violet staining tone. Image B demonstrates a dark staining with ETS. Nevertheless, in both images A and B the spiral ganglion cells are still distinguishable. The black scale bar depicts 200 micrometers (µm). Taken from Dick (2017).

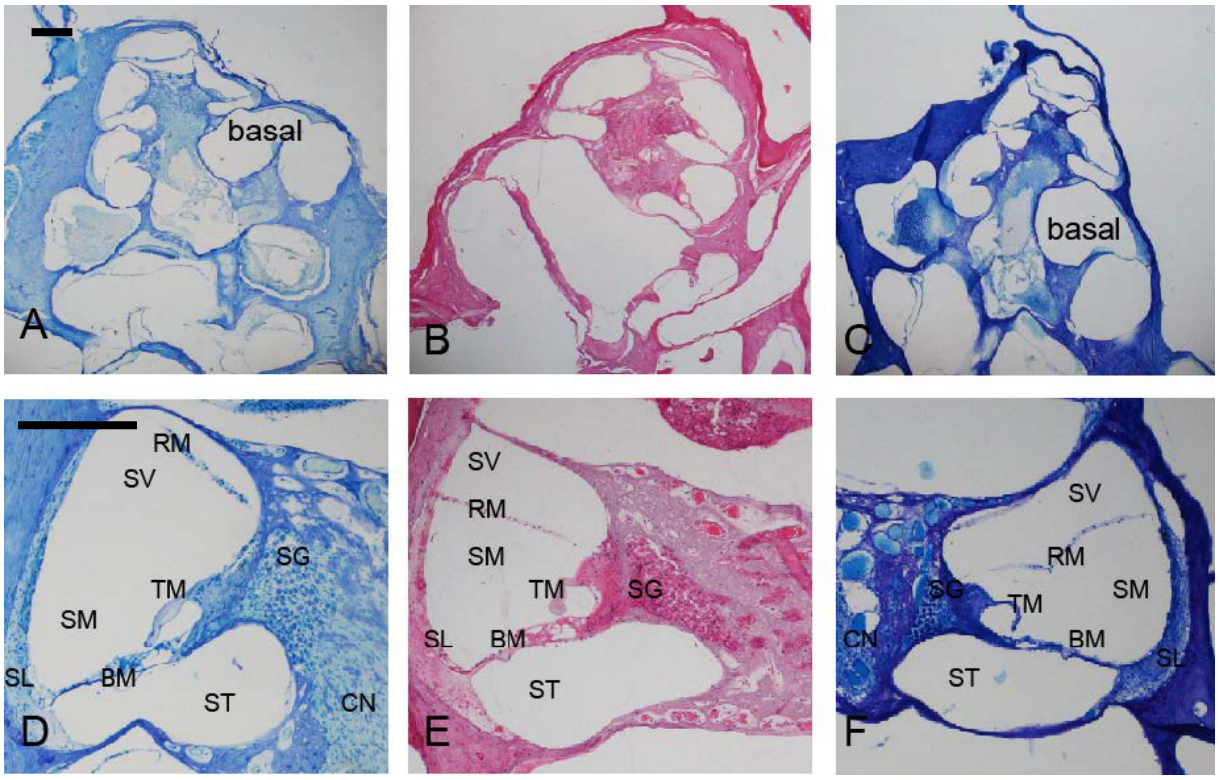

Figure 20: Comparative analysis of sections from implanted samples.
Images A–C present the complete cochlea, while images D–F focus on individual turns of the cochlea. Giemsa staining was applied to produce images A and D, hematoxylin-eosin staining to produce images B and E, and ETS staining for images C and F. The scales and membranes of the respective turns were labeled as follows: (SV) scala vestibuli, (SM) scala media, (ST) scala tympani, (RM) Reissner's membrane, (TM) tectorial membrane, (BM) basilar membrane, (SG) spiral ganglion, (SL) spiral ligament, (CN) cochlear nerve. The black scale bar on the left lower row depicts 200 micrometers (µm), that on the left upper row 500 micrometers (µm). Taken from Dick (2017).

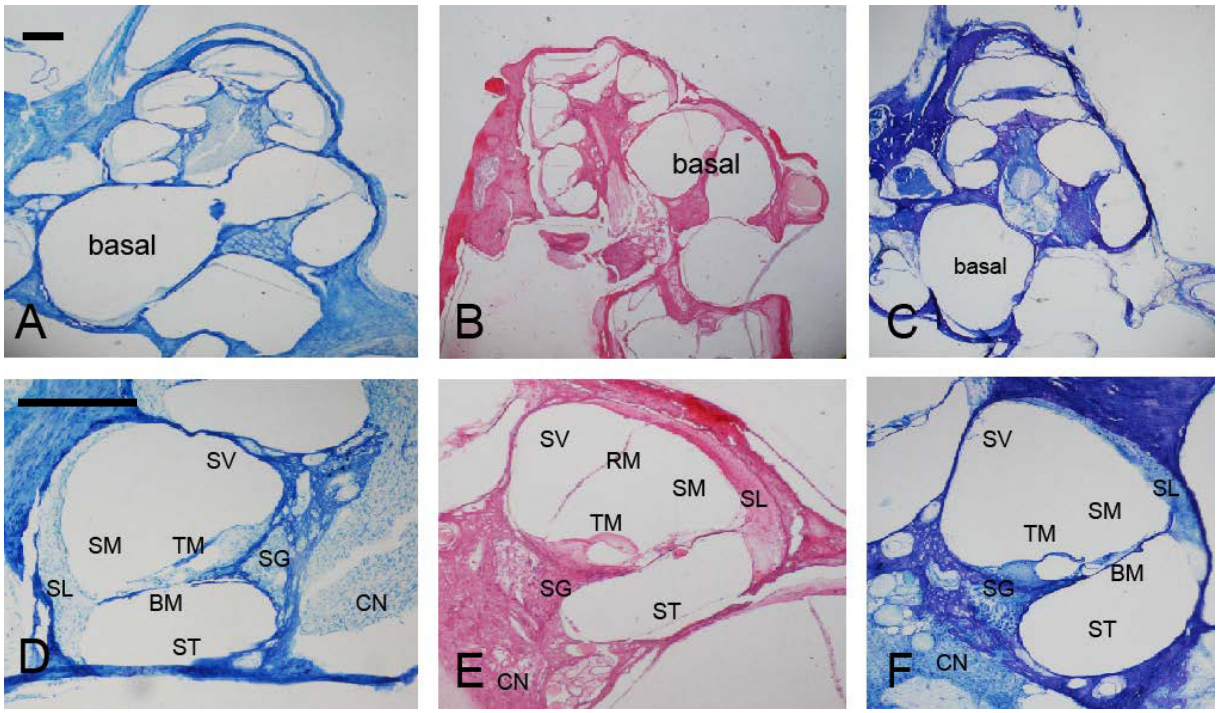

Figure 21: Comparative analysis of sections from control samples.
Images A–C provide an overview of the entire cochlea, while those labelled D–F focus on individual turns. Image A corresponds to a Giemsa-stained sample, images B and E to samples stained with hematoxylin-eosin, and images C and F to samples stained with ETS. The respective scales and membranes of the turns were identified as follows: (SV) scala vestibuli, (SM) scala media, (ST) scala tympani, (RM) Reissner's membrane, (TM) tectorial membrane, (BM) basilar membrane, (SG) spiral ganglion, (SL) spiral ligament, (CN) cochlear nerve. The black scale bar on the left lower row depicts 200 micrometers (µm), that on the left upper row 500 micrometers (µm). Taken from Dick (2017).

3.3 Acoustic and Electrical Stimulation of the AVCN and the MNTB

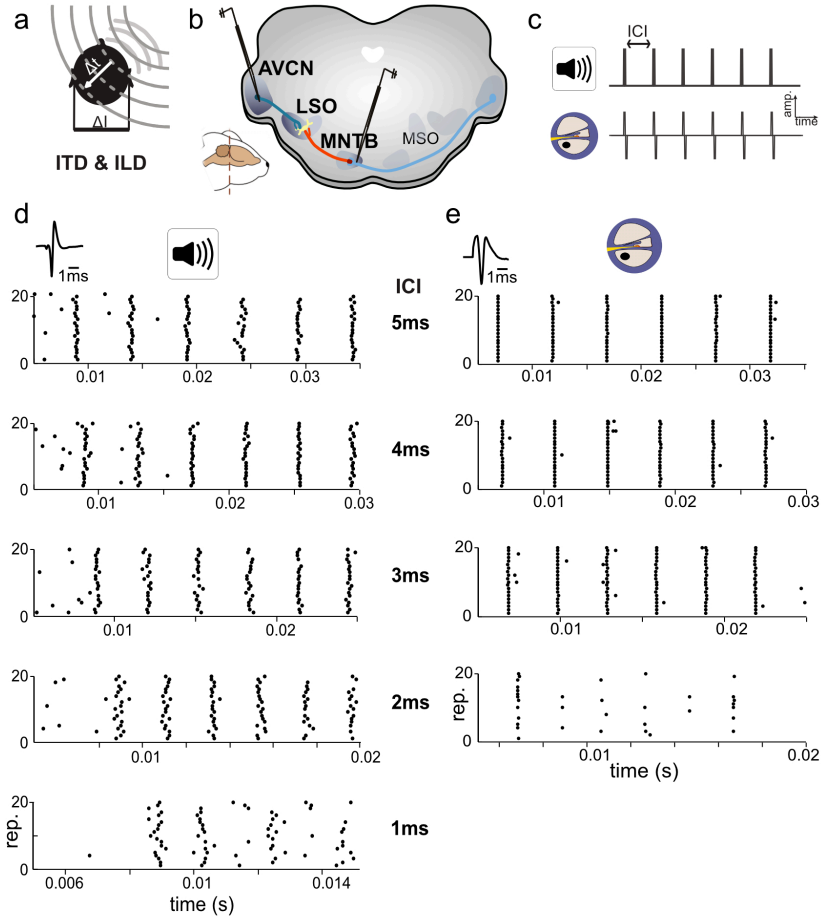

Figure 22: Responses in auditory brainstem neurons differ between acoustic and electrical stimulation. (a) The egocentric location of a sound source in the horizontal plane generates specific interaural time differences (ITDs) and interaural level differences (ILDs). (b) Extracellular single cell recordings with glass pipettes were conducted in either the antero-ventral cochlear nucleus (AVCN), medial nucleus of the trapezoid body (MNTB), or lateral superior olive (LSO). (c) Acoustic and electrical [i.e., cochlear implant (CI)-based] stimulation consisted of a train of six clicks with varying inter-click intervals (ICIs) from 5 to 1 ms. (d) Exemplary dot-raster displays of single cell recordings from MNTB [action potential (AP) waveforms shown on top] during acoustic in response to different ICIs. (e) Same as panel (d) but for electrical stimulation. Each ICI was repeated 20 times. Responses to the individual clicks are readily identifiable, particularly at larger ICIs and overall spike probability decreased with smaller ICIs. Note the difference in spike timing variability (jitter) for each click at all ICIs between acoustic and electrical stimulation. Data from ICI = 1 ms for electrical stimulation was not analyzed due to a strong overlap of APs and electrical artifacts. Taken from Müller et al. (2023).

In order to examine potential differences in the response properties of the AVCN and MNTB during acoustic and electrical stimulation, we conducted extracellular single-cell recordings in both parts (Figure 22 b).

To establish a baseline dataset for acoustic stimulation, we presented a sequence of six clicks lasting 50 µs each at 30 dB above the threshold. The clicks were randomly ordered and delivered at five different ICIs of 5 ms, 4 ms, 3 ms, 2 ms, and 1 ms (Figure 22 c). Depending on the specific nuclei, the clicks were directed either to the ipsilateral ear (AVCN) or the contralateral ear (MNTB). Each ICI was repeated twenty times (Figure 22 d, e).

Conversely, the electrical dataset was obtained by stimulating the cells in the AVCN and MNTB using an electrical mean 2 dB above the threshold. We generated a digital voltage that was converted into a current for stimulation (see chapter 2 Methods and Materials section 2.10.2 Electrical Stimulation for more details). The current was then delivered to the auditory nerve through an implanted CI. The electrical stimulus consisted of a train of six clicks, with each click lasting 110 μs (anodic phase 50 μs; cathodic phase 50 μs; interphase 10 μs). Similar to the acoustic click train, the electrical click train was presented in a random order at five different ICIs (5 ms, 4 ms, 3 ms, 2 ms, 1 ms) and was repeated 20 times. However, due to strong interference caused by the stimulation artifact, data analysis for the 1-ms ICI was not possible in the electrical dataset.

During the extracellular recordings, the animals were anesthetized using ketamine and xylazine, and their condition was carefully monitored by the researcher. At the conclusion of the recording session, horseradish peroxidase (HRP) was used to mark the recording location, and the animals were euthanized using pentobarbital. Subsequently, the brain was collected for histological verification of the recording site.

The acoustic dataset comprised recordings from 18 cells in the MNTB, obtained from a total of 10 animals. These MNTB cells had a median CF of 15 kHz, with a CF range spanning from 7 kHz to 35 kHz. Additionally, recordings were made from 22 BCs in the AVCN, collected from 13 animals. The BCs in the AVCN had a median CF of 16.4 kHz, ranging from 1.2 kHz to 35.1 kHz.

Regarding the electrical recordings, the AVCN dataset consisted of recordings from 11 cells, which were acquired from animals with severe hearing loss (n = 8). The MNTB dataset included recordings from nine cells, obtained from animals with either moderate hearing loss (animals: n = 1, recorded cells: n = 1) to severe hearing loss (animals: n = 2, recorded cells: n = 2), as well as animals that underwent deafening procedures without obtaining ABR recordings (animals: n = 4, recorded cells: n = 6) (Figure 23).

The data analysis focused on two key aspects: spike probability, which represents the average percentage of clicks in the train that generated APs, and response jitter, which measures the standard deviation of spike timing. Jitter is essential for assessing the temporal precision of neuronal responses, particularly in relation to ITD processing.

Drawing from previous studies on the auditory nerve, we hypothesized that electrical responses in the auditory system might exhibit greater precision than acoustic responses (Hartmann et al., 1984; van den Honert & Stypulkowski, 1987).

3.3.1 Spike Probability

We observed that the acoustic stimulation of the BCs in the AVCN and the MNTB principal cells resulted in similar responsiveness patterns (Figure 23 a, Table 12, $p = 0.098$ Kruskal–Wallis H-test). The spike probability was relatively high for larger ICIs, approaching 100% (one spike per click and repetition) and decreased significantly with smaller ICIs (Table 12).

With acoustic stimulation, the MNTB cells showed a slight tendency towards higher responsiveness compared with the BCs for ICIs of 4 ms, 3 ms, 2 ms and 1 ms. However, this tendency shifted at an ICI of 5ms, where the BCs exhibited a greater tendency to spike at each click.

Regarding the neuronal response to electrical pulse-trains, the spike probability of BCs dropped at ICI of 2ms (Figure 23 b). Notably, the MNTB data at an ICI of 2 ms displayed a large variability with strong bimodality, where some cells did not respond while others exhibited spike rates close to six spikes per repetition. These findings suggest that at least a subset of MNTB neurons keep their ability to encode information even at a pulse rate of 500 pulses per second (pps).

Overall, we found a tendency for higher response rates in the electrically stimulated MNTB and BCs (Figure 23 b). However, it is important to note that the median values of the acoustic and electrical MNTB data were quite similar (Figure 23 and Table 12; $p = 0.949$ Kruskal-Wallis H-test). The electrical MNTB data exhibited a considerable amount of variability.

3.3.2 Jitter

We observed that the spike timing of the cells in the MNTB and the AVCN in response to the acoustic click train was similar (Table 12 and Figure 23; $p = 0.949$ Kruskal–Wallis H-test). Interestingly, we found that the spike timing jitter during electrical stimulation was nearly identical in both the MNTB and AVCN across all ICIs (Figure 23 b). When comparing the electrical and acoustic datasets for the MNTB and AVCN, we found statistically significant differences for all ICIs, with the electrical data displaying drastically lower values (approx. 10-fold smaller) than the acoustic data (Figure 23 and Table 12; all ICIs for MNTB and BCs resulted in $p < 0.001$, Mann–Whitney-U-test). Based on these observations, we can conclude that electrical stimulation yields higher precision in the AVCN and MNTB in comparison with acoustic stimulation.

This data shows that the high precision observed in AN response to electrical stimulation, as previously reported by Hartmann and Klinke (1990) and Dynes and Delgutte (1992) persists and may even be enhanced in subsequent brainstem nuclei.

These findings suggest that this hyper-precision is likely to affect the processing of binaural spatial information in the MSO and LSO. We therefore compared acoustic click-train data from the LSO with the responses of a published auditory brainstem model.

Table 12: Median values for spike probability and jitter shown in Figure 23.

		ICI 5 ms	ICI 4 ms	ICI 3 ms	ICI 2 ms	ICI 1 ms
Acoustic medians	MNTB (probability)	84.58%	85.42%	76.67%	64.95%	35.88%
	BCs (probability)	90.83%	81.25%	70.00%	57.08%	27.92%
	MNTB (jitter)	0.14 ms	0.15 ms	0.14 ms	0.14 ms	0.11 ms
	BCs (jitter)	0.18 ms	0.14 ms	0.13 ms	0.14 ms	0.10 ms
Electrical medians	MNTB (probability)	95.83%	95.00%	93.33%	95.93%	
	BCs (probability)	100.00%	91.67%	83.33%	42.11%	
	MNTB (jitter)	0.021 ms	0.019 ms	0.023 ms	0.020 ms	
	BCs (jitter)	0.031 ms	0.025 ms	0.020 ms	0.017 ms	

ICI 5 ms: MNTB p = 0.27, BC p = 0.058; ICI 4 ms: MNTB p = 0.21, BC p = 0.089; ICI 3 ms: MNTB p = 0.14, BC p = 0.61; ICI 2 ms: MNTB p = 0.2, BC p = 0.017; Mann–Whitney U-test.

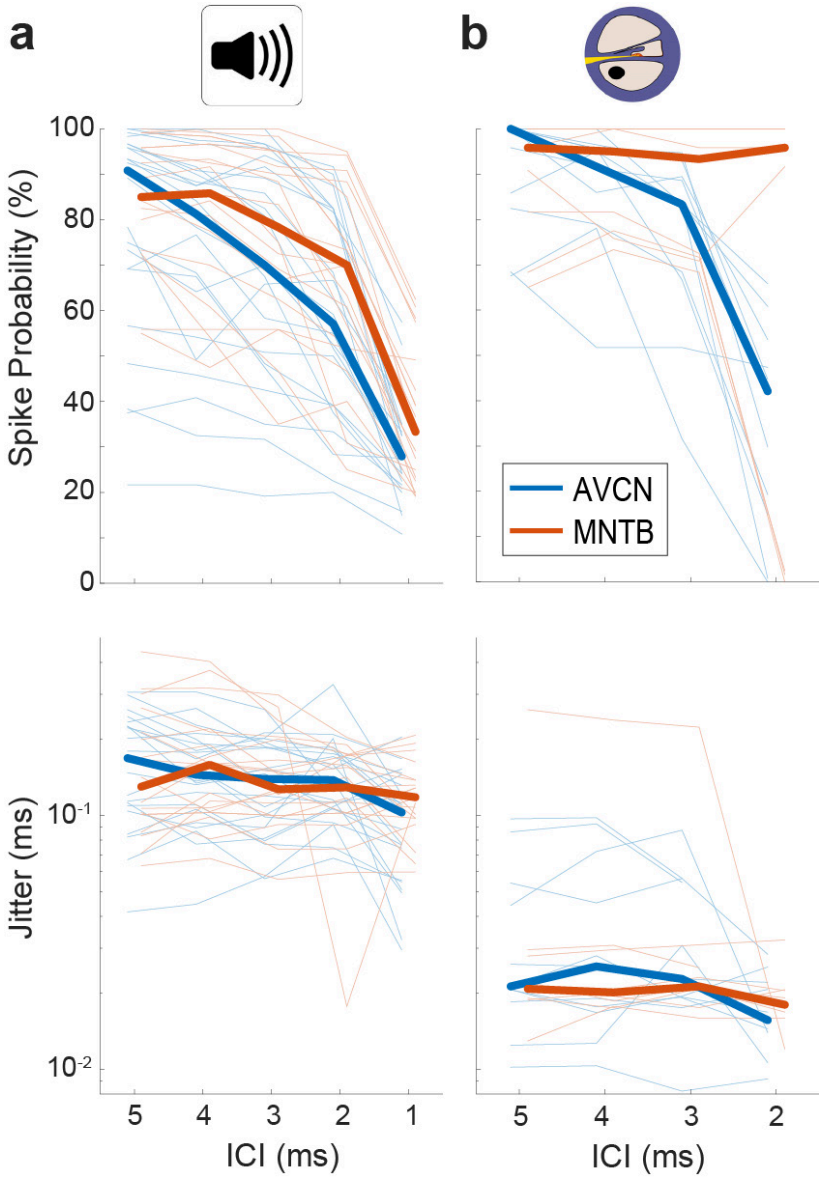

Figure 23: Quantification of spiking probability (upper row) and precision (lower row) in gerbil antero-ventral cochlear nucleus (AVCN) and medial nucleus of the trapezoid body (MNTB) in response to acoustic (a) and electrical (b) click train stimulation.
Plotted are average values for each recorded neuron (thin lines) and the sample medians (bold lines). Taken from Müller et al. (2023).

3.3.3 Summary

In summary, the response properties of cells in the AVCN and MNTB during electrical stimulation exhibit distinct differences compared with their responses to acoustic stimulation, particularly in terms of timing. The question arises as to how these differences in response properties affect spatial processing. In the auditory system, the MSO and LSO integrate excitatory and inhibitory inputs from both ears individually. Beiderbeck et al. (2018) showed that LSO neurons display high sensitivity to ITDs for each individual click in a series of

acoustic click trains. This sensitivity was found to be shaped by the precise timing of inhibitory signals. We therefore propose that the temporal integration process in the LSO may be influenced by the altered precision observed during electrical stimulation of the AVCN and MNTB cells. Moreover, we speculate that this changed integration process might account for the diminished sound localization ability observed in individuals with bilateral CIs.

However, the impact of these differences on the integration process of the LSO remains unknown, as there is a lack of physiological data. Understanding how this altered neuronal responsiveness affects ITD detection in the LSO is crucial.

3.4 Acoustic Stimulation of the LSO

Our goal was to assess ITD sensitivity in the LSO under both electrical and acoustic stimulation. Dr. Beiderbeck performed binaural recordings from 15 LSO neurons, utilizing the identical acoustic click train stimuli employed for the AVCN and MNTB (Figure 24 a; Beiderbeck et al. (2018), unpublished subset of data). Based on these recordings, we assessed the rate-ITD functions at an ILD of 0 dB, drawing conclusions regarding the dynamic ITD range. This dynamic ITD range is characterized as the range between the ITDs that induce the highest and lowest response rates. The results showed that the dynamic ITD range consistently encompassed or surpassed the physiological range of ITDs observed in gerbils (approximately 300 µs; Maki and Furukawa (2005)) for all ICIs (Figure 24 b). The median dynamic ITD ranges for ICIs of 5, 4, 3, 2, and 1 ms were 400, 400, 400, 400, and 600 µs, respectively (Figure 24 b).

Subsequently, we examined how different ILDs influenced the steepness of the slope in the rate-ITD functions, which represents the change in normalized AP rate over the dynamic ITD range. This analysis was conducted due to previous research (e.g., Beiderbeck et al., 2018; Park et al., 1995) indicating that differences in sound intensity can impact ITD sensitivity in the LSO. When different ILDs were applied, we observed only minor to moderate effects across all ICIs (Figure 24 c; norm. spikes/rep/µs/dB∗ 10−5): ICI 5 ms: 6.0, 2.3, 7.1; ICI 4 ms: 6.0, 3.0, 7.1; ICI 3 ms: 2.0, 1.5, 8.4; ICI 2 ms: 4.2, 2.0, 9.4, ICI 1 ms: 3.2, 2.0, 6.6. These findings suggest that the LSO can maintain its ITD sensitivity across various binaural conditions (Figure 24 c).

To understand how the altered input statistics for the AVCN and MNTB to LSO during CI stimulation affect ITD processing in the LSO, ideally electrical ITD response functions from the LSO would be obtained. Nevertheless, the task of recording individual LSO neurons with bilateral CI stimulation posed significant challenges and, ultimately, was

not successful. As an alternative, we constructed a model based on the physiological data obtained from the AVCN, the MNTB and the LSO, and then simulated both acoustic (Figure 24 d) and electrical inputs to the LSO, as the primary aim of this modeling approach was to predict any changes in ITD sensitivity during electrical stimulation.

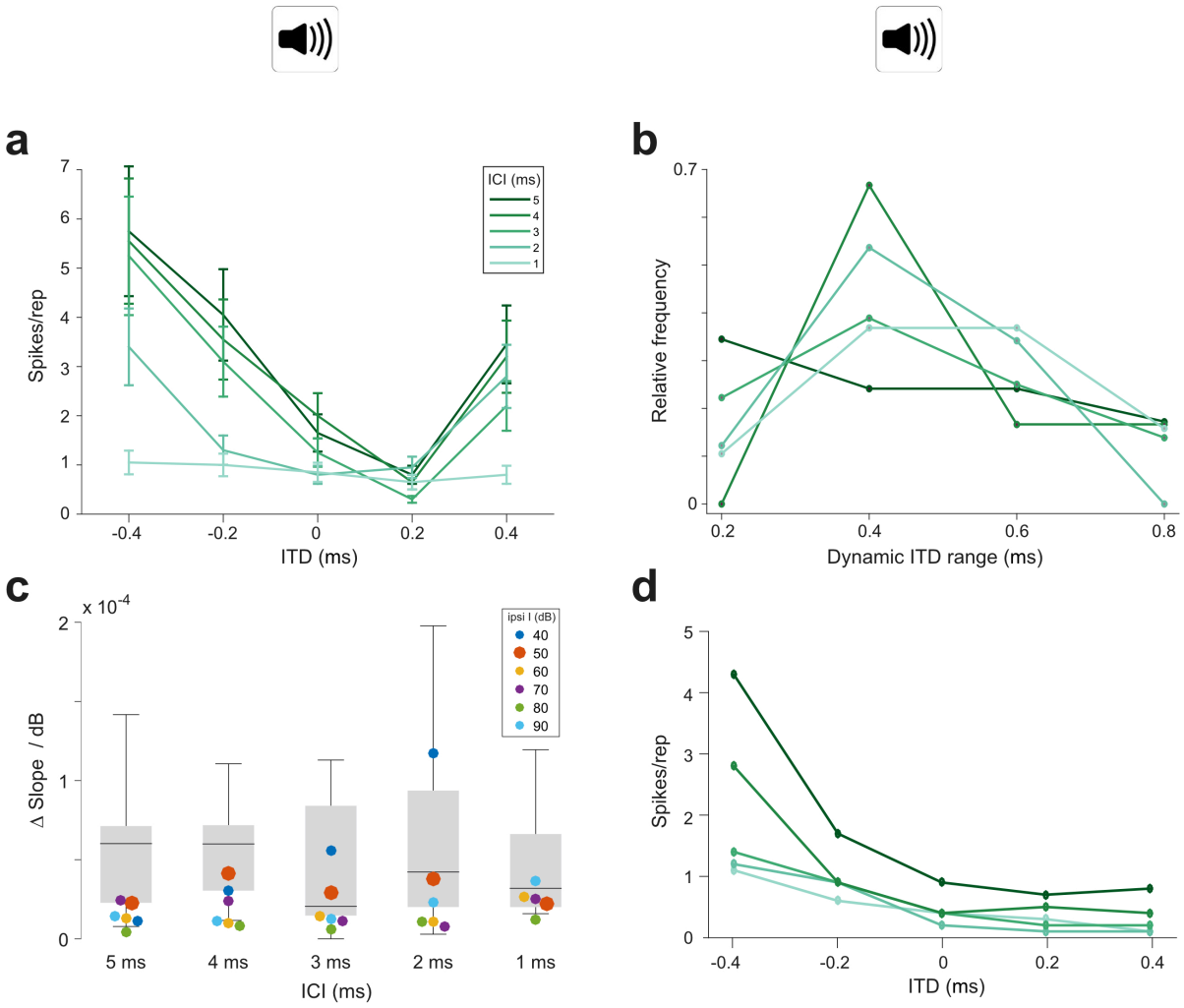

Figure 24: Interaural time differences (ITD) sensitivity of lateral superior olive (LSO) neurons to click trains is maintained over a large range of interaural level differences (ILDs).
(a) Example rate-ITD function from a gerbil LSO neuron. Plotted are mean rates and the standard errors. (b) Histogram of dynamic ITD ranges at ILD = 0 dB across all 15 recorded LSO neurons. (c) Quantification of magnitude of changes in the slope steepness of rate-ITD functions with changes in ILD for gerbil LSO (boxplots) and model (at various intensities of the excitatory input, colored dots). The slope/dB was calculated by first determining the slope of rate-ITD functions (difference in the normalized maximal and minimal spike rates divided by the respective ITD range), and then subtracting these values between the most positive and negative ILD that each LSO neuron was tested for and dividing this difference by the respective difference in ILD. (d) Model rate-ITD function during acoustic stimulation (ipsi intensity = 50 dB; ILD = 0 dB). Taken from Müller et al. (2023).

3.5 Modeling of the Electrical and Acoustic Stimulation of the AVCN and MNTB

We applied a functional count-comparison model of the LSO as described by Ashida et al. (2016). This model enabled us to extract response properties for both acoustic and electrical stimulation at different stages of the LSO pathway (Hu et al., 2022). The model demonstrates a high degree of accuracy in replicating both the response characteristics of the LSO and its characteristic spatial perceptions. This level of precision is consistently maintained across a diverse set of stimulus categories (Klug et al., 2020; Hu et al., 2022).

By incorporating this model with a pre-existing auditory nerve model capable of both acoustic and electrical stimulation, we facilitated the comparison of the model's performance with our physiologically recorded data from the AVCN and MNTB.

To predict changes in the ITD sensitivity during both electrical and acoustic stimulation, it was crucial for the model's responsiveness to closely align with the physiological data obtained from the AVCN and MNTB. Initially, it was essential to establish an acoustic stimulus intensity at the input stage of the model (auditory nerve) that would lead to similar responsiveness as found in the extracellular recorded AVCN and MNTB neurons. It is important to note that the model does not have an AVCN or MNTB stage, and that the auditory nerve directly leads to the LSO count comparison model. Therefore, the parameter settings of the auditory nerve were adapted to replicate the physiological responsiveness of the AVCN and MNTB.

By employing previously published parameter settings (Ashida et al., 2016), we observed that at model levels of 50dB and 60dB the model displayed comparable responsiveness (Figure 25 a) to what we had determined during extracellular recordings in the AVCN and MNTB of the gerbil (at 30db above threshold) (Figure 23 a).

Subsequently, we sought to assess the extent to which the responses from the electrical model align with the physiological recordings. Similar to the acoustic model, the electrical model displays comparable spike probability to the physiological data gathered from gerbils (Figure 23 b and Figure 25 b). After all, in both models, the values decrease with decreasing ICIs. As found in the physiological data, the modeled jitter decreased by a similar factor (10x) between acoustic and electrical stimulation (Figure 23 b and Figure 25 b). Thus, we concluded that the inputs to the LSO in the model do an adequate job of replicating the jitter of the cells in the AVCN and MNTB.

Based on these findings, this model may be utilized to replicate the acoustic and electrical stimuli to the LSO, allowing for a deeper understanding of the LSO's electrical ITD detection capabilities.

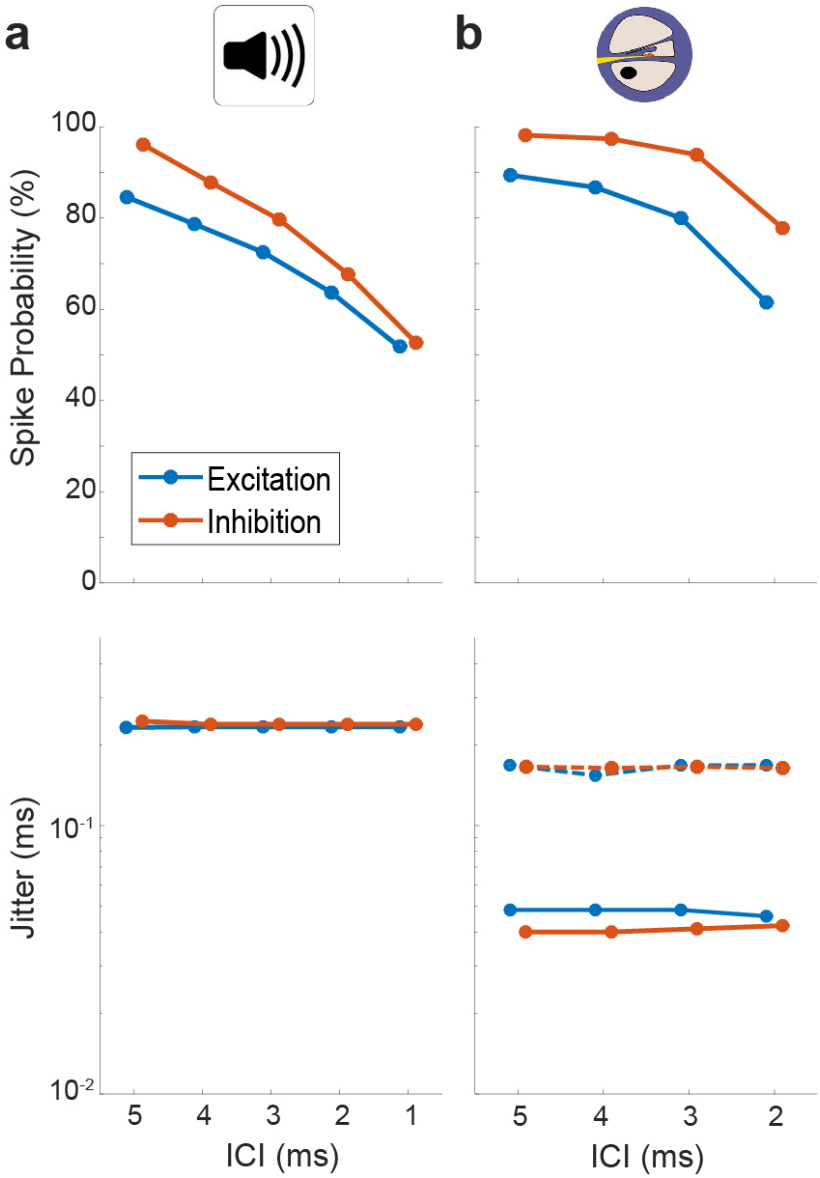

Figure 25: Quantification of spiking probability (upper row) and precision (lower row) of model excitatory and inhibitory inputs to lateral superior olive (LSO) [corresponding to antero-ventral cochlear nucleus (AVCN) and medial nucleus of the trapezoid body (MNTB), respectively] in response to acoustic (a) and electrical (b) click train stimulation.
Plotted are medians and 95% confidence intervals. Dotted lines represent model condition with auditory nerve (AN) jitter levels during electrical stimulation that resemble physiological acoustic jitter levels. Taken from Müller et al. (2023).

3.6 Modeling of the Electrical and Acoustic Stimulation of the LSO

As an initial step, we conducted a test to assess how well the LSO stage of the model captures the characteristic ITD features observed in the LSO at 0 dB ILDs. The results revealed that the model quantitatively resembles the physiological data from the LSO. At ipsilateral intensities of 50 dB SPL, which had previously been identified as the best fit for the electrical response behavior of the AVCN, the model exhibited qualitatively similar ITD sensitivity as found in the gerbil LSO at all ICIs.

Next, we quantified the effects of changing the ILD on the slope of the rate-ITD functions (the steepness of this slope representing the change in AP rate per unit ITD) at various ICIs. This analysis was performed across different ICIs and shows that the model approximates the physiological acoustic and electrical recordings from the LSO qualitatively and even quantitatively, with a high degree of accuracy. This indicates that the model can effectively predict the LSO ITD sensitivity.

Our objective was to assess the model's ability to distinguish adjacent ITDs with 20 µs increments. This evaluation covered the entire range of ITDs produced by the human head, with the goal of delivering a precise assessment of the model's informational content.

To quantify the distinguishability of adjacent ITDs, we calculated the standard separation "D" (Sakitt, 1973). For the computation of D, we utilized the hemispheric rate-difference model of spatial coding (Gleiss et al., 2019; Grothe et al., 2010). The hemispheric rate-difference model compares the rate difference between the LSOs in each hemisphere. The assumption was made that the responses in one hemisphere were reflected by the corresponding LSO in the other hemisphere, and subsequently, these responses were subtracted from each other at each ITD. This computation involved calculating the ratio between differences in mean rate and response variability, assuming conservative Poisson noise due to the high determinism of the LSO model.

The findings indicated that the rate-ITD functions exhibited a distribution of D in response to acoustic stimulation (Figure 26 a) that covered a significant portion of the human physiological ITD range. The peak values of D were observed at midline or slightly lateralized ITDs (Figure 26 b). During bilateral electrical stimulation, we conducted further testing using the LSO model and obtained new measurements of D. The LSO model displayed a steep rate modulation in response to ITDs for all ICIs, indicating that the sensitivity to electrical ITDs was maintained (Figure 26 c).

Although lateralized ITDs to either hemisphere yielded response rates that were nearly indistinguishable, the modulation (reflected in the slope of the function) was restricted to a

narrower range of ITDs, approximately ±100 µs and 0 µs ITD, in comparison with the acoustic ITDs. This “hemispheric binarization” led to a notably reduced distribution of D (Figure 26 d), with high distinguishability near the midline but no distinguishability at more lateral positions on either side.

For human listeners, the ability to perceive left versus right with small ITDs around the midline can be interpreted as a lateralization effect, while resolution is nearly absent for larger ITDs within each hemisphere. By contrast, the distribution of D during acoustic stimulation displayed a more gradual pattern, enabling the differentiation of ITDs within each hemisphere (Figure 26 b).

Given our earlier findings that the increased response precision (jitter) during electrical recordings was the primary difference when compared with acoustic stimulation, we were curious whether this effect might contribute to the heightened lateralization observed. Consequently, we conducted tests to investigate whether altering the electrical jitter level of excitatory and inhibitory LSO inputs to a level more closely resembling that of acoustic recordings (approximately 20 µs to approximately 180 µs) would influence the ITD sensitivity of the model LSO. Interestingly, this adjustment in jitter level (Figure 25 b) led to the reinstatement of a broader dynamic range of ITD (Figure 26 e) and an accompanying expansion of the range of distinguishable ITDs (Figure 26 f).

These results from the model suggest that the coding capacity of the LSO is influenced by artificial electrical stimulation, with the jitter level being a critical factor in shaping the ITD sensitivity during CI-based sound localization.

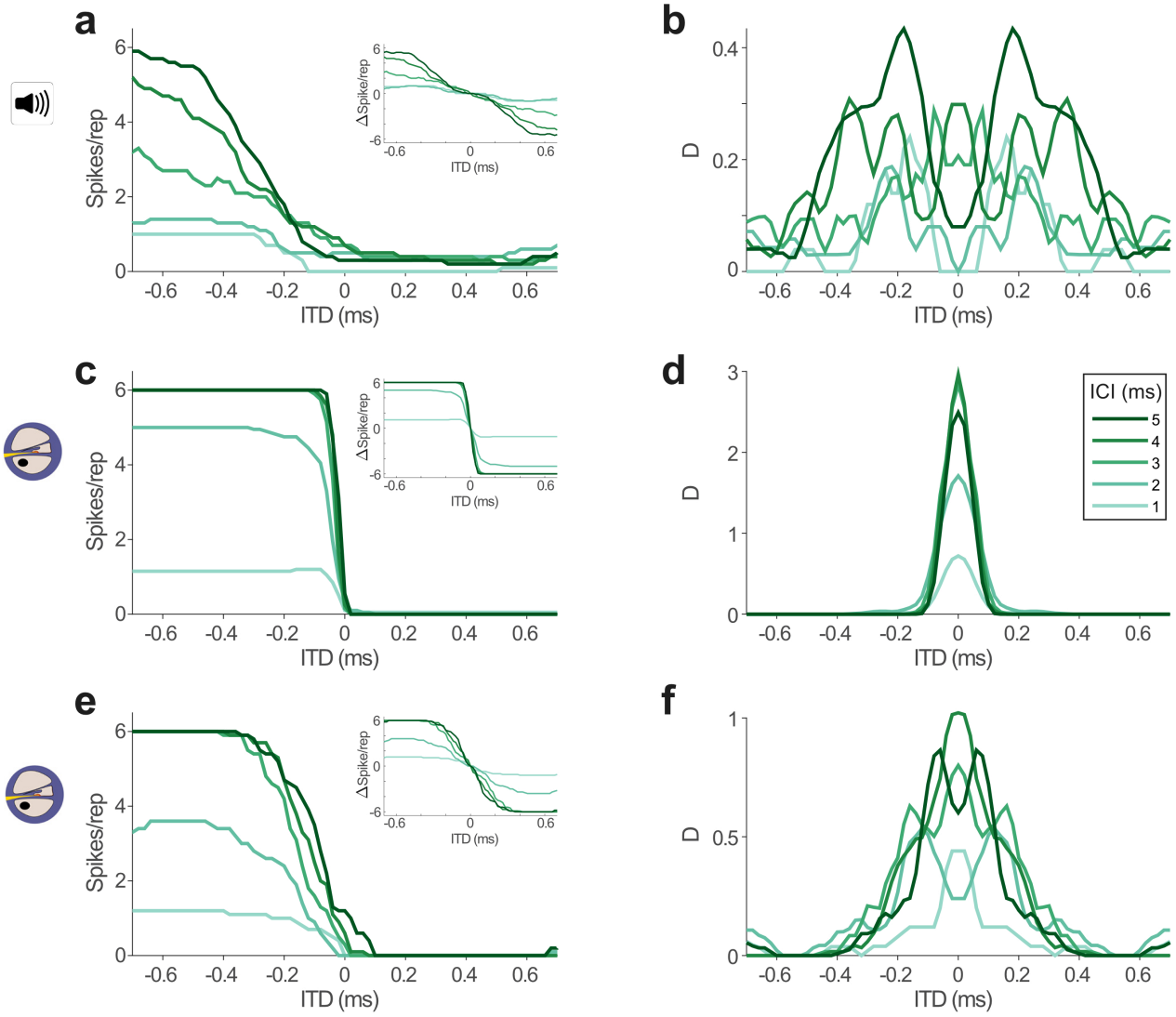

Figure 26: Interaural time differences (ITD) sensitivity in model lateral superior olive (LSO) is maintained during electrical stimulation, but altered by jitter level.
(a) Model rate-ITD functions during acoustic stimulation. Inset shows hemispheric rate differences for all inter-click intervals (ICIs) (assuming mirrored rate-ITD functions in the LSO on the other brain hemisphere). (b) Standard separability D of the hemispheric rate differences for the data shown in panel (a). (c,d) Same as in panels (a,b), but for electric stimulation. (e,f) Same as in panels (a,b), but for electric stimulation with jitter levels of the model inputs increased to resemble acoustic conditions. Taken from Müller et al. (2023).

4 Discussion

The study established crucial methods for acute cochlear implant (CI) procedures, including implantation, deafening, and electrical stimulation, enabling the recording of neuronal activity during CI stimulation. Additionally, a histological protocol using Technovit® 9100 was established. Electrophysiological analysis of the recorded cells uncovered distinctions between electrical and acoustic stimulation in the auditory brainstem. Cells stimulated electrically exhibited higher spike probability at lower rates and reduced jitter. Despite the involvement of more synapses, precise timing of electrical stimulation in the auditory nerve was maintained at the level of the AVCN and MNTB, suggesting adaptive neuronal ITD detection in response to altered input statistics during CI stimulation, as opposed to conditions in acoustic hearing.

The model proposed that the LSO is responsive to electrical inputs, and the hyper-precision observed in electrophysiological recordings from AVCN and MNTB extends to the LSO. The reduced jitter in electrical data resulted in a lateralization effect, indicating hyper-accurate ITD processing in the LSO. When the modeled jitter level was adjusted to that found in acoustic recordings, there was a substantial recovery in the ITD coding capacity of the LSO model.

This discussion encompasses the unique challenges arising from altered input statistics, the significance of precise timing (jitter) in neuronal ITD detection, and the potential implications for sound localization in individuals with CIs. Furthermore, the methods employed in this study are examined, and the hypothesis suggesting that CI users primarily rely on the LSO for ITD detection is discussed. By addressing these aspects, the discussion sets the stage for a comprehensive consideration of the study's impact and the broader implications it carries for advancing our understanding of auditory processing in both normal and CI-based hearing.

4.1 Methods

To translate findings from animal research to humans, it is essential to research both organisms and organs that are very similar to humans. Hence, for our study, it was necessary to conduct experiments on animals with a similar hearing range to humans (0.2–16 kHz) and on animals expressing MSO and a similar ITD sensitivity.

The Mongolian gerbil is specialized in ITD detection and differs from the mouse in both myelination and synaptic delay patterns. The gerbil illustrates differences between GBCs and SBCs and between low- and high-frequency GBCs in terms of diameter and internode

length to guarantee fast conductance and stable synaptic delays from GBCs to the MSO (Ford et al., 2015; Stange-Marten et al., 2017).

This specialization in myelination and synaptic delay has not been found in mice (Stange-Marten et al., 2017). Because of the high-frequency hearing range of mice, they barely experience fine-structure ITDs. Mice still express the MSO, but apart from a few features, their MSO differs in anatomy and physiology from the typical MSO found in other mammals (Fischl et al., 2016). Even though mice lack low-frequency hearing, they are still sensitive to envelope ITDs in the IC (Ono et al., 2020); however, they miss the ITD specialization found in the Mongolian gerbil.

The hearing range of many mammals is centered above 5 kHz in the high-frequency hearing range (Grothe & Pecka, 2014). As mentioned in 1.7, ILDs are the most prominent cue for high-frequency sound localization, while ITDs are mainly used for low frequencies. The hearing range of Mongolian gerbils expands from low to high frequencies between 0.1 and 60 kHz (Ryan, 1998). By comparison, the frequency range of mice ranges from 2 to 90 kHz (Masterton & Heffner, 1998), while it ranges from 1 to 80 kHz in rats, from 0.2 to 50 kHz in guinea pigs, and from 0.125 to 60 kHz in cats (Malmierca & Ryugo, 2012).

According to these hearing ranges, guinea pigs and cats would also represent an excellent model to study the effect of electrical stimulation on envelope ITD processing in the LSO. These animal models are also widely used in hearing research. Nonetheless, German law requires conducting experiments according to the 3R principles (replacement, refinement, reduction). Consequently, higher-developed animals (rats, guinea pigs, cats) can only serve in experiments if other animals cannot deliver the research answer.

Besides these considerations regarding animal hearing ranges and German animal welfare law, the implantability of the animal model was also considered. Both mice and Mongolian gerbils are suitable models for CI implantation. Because of their head size, mice are more challenging, but recent studies confirmed good outcomes (Claussen et al., 2019; Soken et al., 2013). Even so, the positive aspects of the Mongolian gerbil as an animal model, especially its exquisite ITD sensitivity, outweighed these considerations of mice. Hence, experiments were conducted on the Mongolian gerbil.

4.1.1 Anesthesia

The main components of the anesthesia were ketamine and xylazine. Ketamine has hypnotic, analgesic, and amnesic effects (Gao et al., 2016). Combined with xylazine, it is widely used as an anesthetic in veterinary medicine and animal research.

Ketamine binds as a noncompetitive antagonist to the *N*-methyl-*D*-aspartate receptors (NMDA receptors) (Chizh, 2007), which are widely presented in the lower auditory pathways (Sanchez et al., 2015). Stahl (2013) has demonstrated that it also binds to AMPA receptors. Hence, ketamine might affect neuronal transmission in the auditory pathway and interfere with the experimental results.

The second component, xylazine, is an α_2 adrenoceptor agonist with sedative, analgesic, and muscle-relaxant effects. Xylazine influences the parasympathetic and non-parasympathetic systems on receptors activated through adrenalin or noradrenalin. Therefore, it does not directly affect the neurons of the auditory system.

Ketamine is, compared with other anesthetics such as isoflurane, or the combination of medetomidine, midazolam, and fentanyl (MMF), less controllable and only partly antagonizable. Isoflurane is the best controllable anesthetic but has been proven to be less than ideal for hearing research (Ruebhausen et al., 2012). An advantage of MMF is the reversibility of its general anesthesia effect, which can be repealed by the administration of antagonists. However, midazolam binds to the benzodiazepine site of gamma-aminobutyric acid (GABA) receptors and enhances its effects (Olkkola & Ahonen, 2008). GABA, in turn influences sound localization in the LSO and MSO, so any enhancing effects are unwanted (Magnusson et al., 2008; Stange et al., 2013). In addition, neuroimaging studies using midazolam-induced sedation have resulted in contradictory findings of either a reduction of brain activation (Frölich et al., 2017) or preserved activation (Tian et al., 2010) in the auditory cortex.

Most of the studies conducted on the effect of ketamine on the auditory system agree that it only mildly affects the results of hearing research. A study on the effects of ketamine and pentobarbital on the IC and A1 has demonstrated that IC neurons are only mildly affected; A1 neurons, however, were profoundly influenced by anesthetics that improved temporal precision (Ter-Mikaelian et al., 2007). Smith and Mills (1989) have proved that ketamine does not affect gerbil ABR recordings. Another study, comparing the effect of isoflurane and ketamine on the sensitivity of ABR thresholds, concluded that isoflurane leads to a decreased sensitivity of the ABR threshold. The threshold recorded with ketamine was 27 dB lower than with isoflurane (Ruebhausen et al., 2012). In agreement with these studies, Cederholm et al. (2012) has similarly determined that isoflurane increases the hearing threshold while also showing that ketamine produces stable ABR thresholds (Cederholm et al., 2012).

These findings are surprising, because both anesthetics are NMDA antagonists and should induce the same effects. One plausible explanation for the different effects of ketamine and isoflurane might be that ketamine reduces blood flow to the IC (Lo et al., 1991), which induces an increase in the excitatory neurotransmitter release of glutamate (Yao et al., 1993). This effect could temper the antagonistic effect of ketamine on the NMDA receptor.

Following from these findings, our anesthesia comprising ketamine and xylazine seems superior to isoflurane and MMF, even though it is less controllable. However, it is suggested that future studies should be conducted on awake animals to avoid any anesthetic effects and make the findings more comparable to humans.

4.1.2 Deafening

To replicate the state of deafness or profound hearing loss in humans, animals were deafened by the ototoxic neomycin drug through the round window, 1–2 hours before the electrophysiological recordings took place. Preceding the recordings, the animals' normal hearing was verified with ABR recordings. To impede any possible ototoxic effects on SGNs, neomycin was extracted after the deafening process, and the cochlea was washed with a ringer solution.

Even though chronic or congenital deafening would be more comparable to human studies, we aimed to study the electrical influence on ITD detection in animals with fully developed binaural hearing. Long-term deafening effects lead to changes in circuit formation and anatomy of the auditory brainstem and therefore influence ITD detection. The long-term deafening effects would impede investigations into the impact of electrical stimulation on short-term variations. To solely test the electrical stimulus on intact spatial hearing, all the other parameters were excluded, and acute deafening was favored.

Considering the extended period between deafening and recordings, we opted against systemic administration of ototoxic drugs, as the effect on SGNs would be uncertain. Moreover, the effect would not be as manageable as local administration.

As opposed to chronic deafening, our acute local deafening did not have an effect on the animals' hearing prior to the experiment. Thus, we were able to exclude any long-term effects of hearing loss. Wiegner (2016) has demonstrated that acute local administration of neomycin does not affect auditory nerve fibers. However, chronic administration of ototoxic drugs can have long-term effects on the auditory system: Ryugo et al. (2010)have demonstrated that neonatal administration of neomycin expanded postsynaptic densities, decreased synaptic vesicle (SV) density by 35.4%, and reduced the somatic size of SBCs.

Furthermore, Sanes and Bao (2009) have found that hearing loss changes excitatory and inhibitory gain, which leads to an over-excitability of the central nervous system.

For a detailed review of deafness-induced changes in the auditory pathway, I refer the reader to research by Shepherd and Hardie (2001).

Hearing experience is essential for developing localization skills. Refinement of inhibitory inputs in the MSO is activity-dependent and happens shortly after hearing onset (Franzen et al., 2020; Kapfer et al., 2002). In a study by Franzen et al. (2020), Mongolian gerbils were exposed to omnidirectional white noise without binaural cues, resulting in a faster refinement of excitatory inputs and calcium signaling. In addition, those gerbils that were exposed to omnidirectional noise after hearing onset failed to develop normal ITD tuning, while older animals did not exhibit changes (Seidl & Grothe, 2005). Thus, it can be concluded that the development of sound source localization is shaped by binaural cues.

Given these various effects, my thesis deliberately did not include developmental aspects and effects of prolonged deafening, to allow for better interpretability of the results concerning responsiveness and binaural processing.

Our acute deafening resulted in moderate (animals n = 1, cells n = 1) to severe (animals n = 10, cells n = 13) hearing loss. Even though we tested prolonged deafening times and tried to apply different concentrations of neomycin and other ototoxic drugs, such as kanamycin, we could not find a reason for incomplete deafening with neomycin for click tones. After these findings, deafening was tested for pure tones at high frequencies (28–44 kHz, as shown in Figure 7 c) and found to be successful. No ABR waveforms could be elicited at these high frequencies. Since our CI was inserted at the base of the BM and intended to stimulate high-frequency cells, our deafening can be regarded as successful, even though click stimuli produced ABR waves at 70–90 dB (Figure 7 a). The incomplete deafening results for click tones may be due to residual intact low-frequency hair cells, which would still respond to noise stimulation.

In addition, the deafening noise exposure caused by drilling during the implantation may have resulted in additional damage to the hair cells. This could be verified by trying to stimulate the auditory cells during our CI experiments; none of the cells reacted to acoustic stimulation. Despite the lack of confirmation regarding the success of the deafening procedure for four animals (n= 6 cells) within the dataset, their deafness status remains plausible as they underwent identical deafening protocols and were also subjected to noise exposure during the implantation process.

Furthermore, it is worth noting that there was no observable spontaneous activity detected during the electrophysiological recordings conducted during CI-based stimulation. This serves as additional evidence of successful deafening, even though the click ABR recordings conducted before the experiment indicated predominantly severe hearing loss. Although indications suggest the animals were deaf during the recording sessions, future research should implement a deafening protocol with thresholds exceeding 90 dB, to entirely eliminate the possibility of any electrophonic stimulation.

4.1.3 Possible Electrophonic Stimulation

As described earlier, the deafening resulted in moderate (animals n = 1, cells n = 1) to severe (animals n = 10, cells n = 13) hearing loss. Even though we could never acoustically stimulate cells after the CI implantation, and deafened animals demonstrated complete deafening in the high-frequency range, we cannot completely rule out that electrophonic stimulation of residual hair cells was carried out during our recordings.

Electrophonic stimulation differs from electro-neural stimulation (stimulation of the SGNs) in terms of its lower threshold, more extensive dynamic range, and more extended response rate latency (~1 ms) (Sato et al., 2017). However, these differences are not disadvantageous for our study, since we are interested in the basic principles (spike timing, spikes per repetition) of electrical stimulation of the auditory pathway.

The fact that the firing rate is higher in the deafened condition than in the hearing condition (Sato et al., 2016) could interfere with our analysis of the MNTB cells. This is due to the inclusion of animal recordings (n = 4) in which confirmation of deafness was not conducted before the experiment. Nonetheless, we detected a similar responsiveness and response timing of the cells in the MNTB and the cells of the AVCN. Furthermore, as detailed in section 4.1.2, our acoustic stimulation of the AVCN and MNTB was not successful after deafening. During the cochlea implantation, additional noise damage was applied to the hair cells via drilling, and spontaneous activity was not detected during our electrical recordings post-deafening. Therefore, the research results do not indicate that electrophonic stimulation occurred during CI-based stimulation.

4.2 Results

This thesis has been divided into four sequential parts:

1. Establishing a CI implantation technique;
2. Establishing the Technovit® 9100 histology;
3. In vivo extracellular recording of the cells in the AVCN and MNTB;
4. Setting out an LSO model.

Accordingly, the discussion of the results is organized into four corresponding parts.

4.2.1 CI Implantation and Stimulation

The CI implantation procedure for gerbils described in this thesis was based on research by Wiegner (2016) and Fischer (2015). Wiegner established a multichannel CI for chronic use in the Mongolian gerbil, whereas Fischer conducted chronic implantation in guinea pigs, performing ABR and impedance measurements over a 16-week period. Given that our implantation method was initially designed for acute experiments spanning several hours rather than weeks, adjustments had to be made to align with the experimental design. The subsequent points highlight both differences and similarities in the approach between our method and those employed by Fischer and Wiegner.

4.2.1.1 Reference electrode

In experimental animal designs, researchers can either place the reference of the implant externally or use one of the implanted electrodes as a point of reference. However, evidence has suggested a significant decrease in magnitude and electrical resistance when a reference electrode is placed closer to the stimulation electrode (Ramos-Miguel et al., 2015).

Thus, we tested both systems but did not detect notable differences during electrical stimulation between the reference positions. In chronic implantation, the assurance of a secure position for the external electrode is facilitated by the associated wound healing process. Unlike our study, Wiegner (2016) and Fischer (2015) opted for an external reference point positioned on the animal's neck. Due to the nature of our acute experimental setup and the reutilization of implants, which prevented wound healing and a stable positioning, we employed the neighboring electrode as a reference point. This measure was implemented to prevent the CI from becoming loose or dislodging.

4.2.1.2 Reuse of CIs

We adjusted the chronic implantation procedure for our acute experiment by reusing the implants. Pre-implantation, a microscope was used to evaluate the reused implants for any exterior breaking points or silicon damage. Without any visible damage, the electrode wire may have been subject to lesions when force was applied during implantation. Nevertheless, we consistently observed the electrical artifact during the stimulation, so this confirms that the electrical current was being delivered to the brain.

Reuse of the implants also required that the implant was not designed to be fixated permanently. During our recordings, the bulla was not closed, and the wire was directed through muscle and skin tissue toward the back of the animal, where the implant connector was fixed with loose skin sutures. Fischer (2015) and Wiegner (2016) permanently fixed the implant connector on the skull using dental cement and drills. They guided the electrode array, touching the bone beneath the skin and muscle tissue directly to the bulla. After the CI implantation, both researchers closed the bulla with skin and muscle sutures. Using drills to fix the connector can cause brain damage or infection (via non-autoclaved screws).

In chronic implantation, such damage or infection can in turn impact the experimental outcome. In our acute experiments, by contrast, infections would not have interfered with the experiment. Though attaching the connector to the skull would have been optimal, the need to reuse the implants led us to make a less secure fit on the back of the animal.

4.2.1.3 CI Implantation

In humans, it has been shown that CI implantation can cause insertion trauma (Eshraghi et al., 2003; Martins et al., 2015) and misplacement of the CI within the scala vestibuli (Adunka & Buchman, 2007; Aschendorff et al., 2007).

In our study, misplacement or destruction of the cochlea—especially damage to the BM and the SGNs—would have had a significant impact on the results. Our aim was to stimulate the cochlea's high-frequency, i.e., basal region. Hence, a wire breakthrough to other cochlea compartments and resulting stimulation of the low-frequency regions was unwanted. Therefore, a stop marker on the implant itself, which limited further implantation, was used to prevent any harm to the cochlea. Indeed, our Technovit® 9100 histological sections did not reveal any such damage.

The experimental design we used was shown to be both safe and efficient in acute CI implantation using Mongolian gerbils.

4.2.1.4 CI Stimulation

As previously observed and evidenced in the literature (Israel & Burchiel, 2004) the morphology of the AP varies during extracellular recordings, exhibiting first either a positive and/or a negative potential based on the position of the recording electrode. The depolarization at the soma should manifest as a negative potential at the electrode, leading to an initial phase of the AP waveform being negative, succeeded by a subsequent positive component. When an electrode is in proximity to an isolated axon, the recorded AP displays a distinct pattern, characterized by a positive potential followed by a negative potential.

The initial negative phase of the AP was observable in both our electrical and acoustic recordings. This characteristic has consistently been identified in the majority of acoustically recorded APs based on the experiential knowledge accumulated in our laboratory over time. Therefore, the negative potential of the MNTB AP (Figure 13 d) recorded during electrical stimulation aligns with the shape of other recorded APs during acoustic stimulation (Figure 11 b, d), indicating that the waveform reflects the AP recorded from a different electrode position.

However, the waveform of the electrically recorded APs differed from acoustically recorded APs in terms of the pre-potentials (Figure 11, Figure 13) as they were obscured by artifact and therefore not discernible in the electrically generated AP waveform under CI stimulation. Thus, we had to rely on the electrode tracing and the marking of the recording side with HRP as evidence that cells in the AVCN and MNTB were recorded.

In contrast to our research, Stange-Marten et al. (2017) successfully identified pre-potentials in the recorded MNTB cells. Their study involved the direct electrical stimulation of cells, particularly the GBCs in the AVCN, using a 16-channel tungsten electrode microwire array (Omnetics-based electrodes, Tucker-Davies Technology). Subsequently, they conducted extracellular single-cell recordings of principal cells in the MNTB. They analyzed the duration from the peak of the stimulation artifact to the peak of the pre-potential to establish the latency of axonal action potential propagation.

Unlike the approach taken by Stange-Marten et al. (2017), in our study, we utilized the most apical electrode in the CI to stimulate the auditory nerve, as opposed to employing a 16-channel array as described above. In contrast to their use of a 16-channel array, our choice required more power for stimulation, consequently leading to the generation of larger artifacts. Moreover, our research focused on the timing and precision of electrically generated APs, not on latency. Consequently, the identification of pre-potentials was not a critical aspect of our study. Due to the adoption of different methods and objectives in both studies and the

significant artifact in our data, which prevented the detection of pre-potentials in the waveform, direct comparisons became unfeasible. Furthermore, since we implanted the CI in the basal turn of the cochlea to stimulate the auditory nerve, subsequently relaying information to cells in the AVCN and MNTB, including the endbulb of Held and the calyx of Held, there is no evidence to suggest that the cell activity as recorded is a result of direct electrical stimulation rather than the synaptic pathway.

4.2.2 Histology and its Shortcomings

The purpose of the Technovit® 9100 histology was to locate the placement of the implanted CI and, at the same time, to perform immunohistochemical staining on the same slice. As described in chapter 2.13, this method was picked because it was superior to other histological methods, including those using paraffin and resin. Paraffin-embedded hard materials such as electrode arrays cannot be sliced, while the high temperature needed for resin embedding denatures the protein and prevents immunohistochemistry (Merchant et al., 2006). Studies have shown that immunohistochemical staining and slicing of the tissue is, in principle, possible with the implants in place (Areid et al., 2021; Shahramian et al., 2020). However, our study was specifically based on data recently published by Bako et al. (2015) on Technovit® 9100 in relation to guinea pig and mouse cochlea, and the authors had demonstrated that Technovit® 9100 led to highly preserved morphology and immunogenicity.

Despite its promising attributes, we encountered several issues while using Technovit® 9100. Firstly, during polymerization the axis of the cochlea tilted, resulting in off-center slices. Since Technovit® 9100 polymerizes at low temperatures (-2°C to -20°C) without oxygen (Willbold & Witte, 2010), a vacuum was applied to the specimen at room temperature to remove the remaining oxygen. However, this step resulted in slight movements and tilting of the central axis (the mid-modiolar axis). Additionally, the advanced polymerization prevented repositioning of the cochlea.

Our protocol also differed from other studies in that we were not able to apply controlled vacuum pressures at 4°C to -4°C. Instead, we used pre-cooled Teflon embedding molds at room temperature. This temperature and vacuum pressure divergence may have caused the leftover bubbles to tilt the main axis of the cochlea as they attempted to reach the top of the solution. Other studies using controlled vacuums and regulated temperatures encountered decent results. For example, Shahramian et al. (2020) applied 200 to 400 mbar at -4°C for 30 minutes; Willbold and Witte (2010) evacuated the tissue in the pre-infiltration and infiltration step at 600 mbar at 4°C for 10 minutes.

In further studies, it is important to analyze whether temperature and vacuum pressure levels have an effect on the central axis rotation.

Secondly, in addition to tilting of the axis, the polymerization process varied during the protocol. Some samples demonstrated incomplete polymerization at the suggested temperature and time. According to the manual for Technovit® 9100, the polymerization process should be completed at -2°C to 20°C after 24 hours, while Bako et al. (2015) have reported that polymerization in their study took four days at -12°C.

After the first incomplete polymerization results, therefore, we decided to prolong the polymerization time to 7–14 days and to try different temperatures. However, even after the prolongation, some samples showed incomplete polymerization and had to be withdrawn from further steps. The cause for this incomplete polymerization was not detected. As mentioned above, Technovit® 9100 polymerizes without oxygen and at low temperatures. It is therefore possible that remaining oxygen and/or the ambient temperature may have caused incomplete polymerization. To rule out the second possibility, another series of tests would be necessary to analyze the influence of temperature on polymerization.

The second part of the research did not succeed in detecting the position of the implanted CI. The basal turn not being infiltrated could have been the result of incomplete polymerization and remaining bubbles. Consequently, the CI was not attached to the rest of the tissue and dropped out of the basal turn during slicing. Aside from more complete polymerization, tissue growth around the electrode during chronic implantation might improve attachment and prevent bubbles from covering the basal turn.

Since our protocol was based on Bako et al. (2015), we decalcified the cochlea. This created a different stiffness for the cochlea than that of the electrode array and the Technovit® 9100. In chronic experiments, the differing stiffness of different parts of the tissue could affect the slicing process and the quality of the preserved morphology. It should also be noted that, according to the manufacturer, no decalcification of the tissue is necessary. Additional research aligns with the manufacturer's guidelines, asserting that decalcification is not required (Areid et al., 2021; Shahramian et al., 2020; Willbold & Witte, 2010).

Ultimately, decalcification had no impact on our preserved morphology since the electrode array dropped out of the cochlea during slicing. Future studies should include testing to see if decalcification is inevitable.

While Bako et al. (2015) observed that the integrity of the Reissner's membrane was maintained, and O'Malley et al. (2009) found the best preservation in celloidin sections, we sometimes detected disrupted membrane integrity. Preserving the tissue depends not only on

the histological protocol but also on the researcher's slicing skills. In our case, an inexperienced student carried out the slicing. Hence, in future studies, a focus should be set on developing these skills to prevent rupture.

Neglecting the deplastification steps for the Giemsa and HE staining maintained the slices, but did not enhance the quality of the staining. Deplastification is detrimental to immunohistochemical labeling (Bako et al., 2015). Even though our slices were not tested for immunohistochemical labeling, marking the SGNs remains one of the original goals. Hence, it is preferred to modify the protocol instead of removing the deplastification part.

In order to avoid similar issues in future studies, extra caution and consideration should be paid to the polymerization steps, such as temperature, pressure, and oxygen retrieval. Additionally, sections should be preserved, despite deplastification taking place.

4.2.3 Electrophysiological Data

The forthcoming sections 4.2.3.1-4.2.3.4 cover the discussion of the physiological data acquired through extracellular acoustical and electrical recordings.

4.2.3.1 Yield of the Experiments

The acoustic dataset contained recordings of 18 cells located in the MNTB from 10 different animals. Additionally, the dataset included recordings from 22 BCs, collected from 13 animals. This means that, on average, 1.8 cells were obtained per recording session in the MNTB, while 1.7 cells were obtained in the AVCN. Over the course of the study, a greater number of cells were gathered; however, they were not included in the dataset as they were not recorded at 30 dB above the threshold.

Regarding the electrical recordings, the AVCN dataset comprised recordings from 11 cells, acquired from eight animals, resulting in an average of 1.4 cells per animal. By contrast, the MNTB dataset included recordings from nine cells obtained from seven animals, averaging 1.3 cells per animal. The yield of electrical recordings was slightly lower than that of the acoustic recordings. This difference can be attributed to the challenging nature of the recordings, as only after the recording sessions could histological sections confirm if the recordings were indeed obtained from the AVCN or the MNTB.

4.2.3.2 Acoustic Stimulated Cells

We have demonstrated that MNTB cells display a slight tendency for higher responsiveness than the bushy cells of the AVCN for smaller ICIs (≤ 4 ms). With larger (ICIs

> 4ms), this tendency changed, with the BCs now found to have a higher tendency of spiking at every click. However, the cells of both nuclei demonstrated mostly similar responsiveness.

These findings agree with previous reports, which state that the response properties of SBCs are very similar to those of GBCs and MNTB neurons (Joris & Yin, 1998). Another study investigating the anatomy and physiology of the cells in the MNTB has found that the responses of cells of the MNTB were similar to those of GBCs (Smith et al., 1998). Like GBCs, phase-locking of the cells in the MNTB was improved at lower CFs compared with the auditory nerve. Above 1 kHz, the spiking of the MNTB cells showed primary-like-with-notch responses resembling the PSTH of many GBCs.

Our results show that the spike timing of the cells in the MNTB and the BC was comparable. Comparing pre- and postsynaptic activity in the MNTB, Kopp-Scheinpflug et al. (2003) have found that phase locking is greater in postsynaptic than in presynaptic conditions, but only up to sound frequencies of 1 kHz. However, the CF of our recorded cells was mainly above 1 kHz (median CF MNTB: 15, median CF BC: 16.4), and so cannot be directly compared to these earlier findings.

4.2.3.3 Electrical Stimulated Cells

We found comparable responsiveness to both electrical and acoustic stimulation in the AVCN and MNTB. There was a tendency towards a higher response rate (close to the maximum of six per trial) for electrically stimulated bushy cells at ICIs of 5 ms, 4 ms, and 3 ms, as well as for MNTB cells at ICIs of 5 ms, 4 ms, 3 ms, and 2 ms. Our findings at ICIs of 5 ms, 4 ms, and 3 ms (200 pps, 250 pps, 333 pps) for the AVCN and at ICIs of 5 ms, 4 ms, 3 ms, and 2 ms (200 pps, 250 pps, 333 pps, 500 pps) for the MNTB are similar to observations in the ventral cochlear nucleus (VCN) and auditory nerve.

Babalian et al. (2003) examined the discharge patterns from in vitro isolated whole brain preparations in the VCN to electrical stimulation. The investigators found that the cells in the VCN have a high discharge synchronization at low stimulation rates (200–300 pps) (Babalian et al., 2003). Observations of the auditory nerve demonstrate higher response rates and entrainment during electrical stimulation than in acoustic stimulation. At low frequencies (< 800 Hz), auditory nerve spikes show unnatural entrainment, spiking once per stimulus cycle (Hartmann et al., 1984; Javel & Shepherd, 2000; Litvak et al., 2001; van den Honert & Stypulkowski, 1987).

At high stimulation rates, however, Babalian et al. (2003) show that many cells in the VCN exhibit discharge patterns comparable to natural sound stimuli. They have hypothesized

on the basis of their findings that high stimulation rates produce more physiologically meaningful discharge patterns. On the contrary, our BCs demonstrated decreasing spike rates at higher stimulation rates. However, our data was generated by in vivo electrophysiological recordings, whereas Babalian et al. (2003) used in vitro isolated whole brain preparations. Therefore, their findings cannot capture the complete auditory organ system's complexity and cannot fully be extrapolated to our results.

Dynes and Delgutte (1992) and Hartmann and Klinke (1990) were able to demonstrate that the auditory nerve follows electrical pulse trains at rates above 1,000 pps. However, phase locking and fidelity are shown to degrade at high stimulation rates (above 400 pps) (Shepherd & Javel, 1997). At 1,000 pps, responses vary between strong and weak (Wilson et al., 1997).

We found similar results in the MNTB. The AP recorded from the cells in the MNTB at ICI = 2 ms varied, with some cells responding to almost every click and others almost not at all. We can only make assumptions about the physiological data at an ICI of 1 ms (1,000 pps), because stimulation artifacts prevented data analysis. With the MTNB exhibiting this alternation between strong and weak responses at ICI = 2 ms, we assume that the response behavior would be similar at 1,000 pps.

4.2.3.4 Jitter during Electrical Stimulation

Consistent with earlier research by Hartmann et al. (1984) and van den Honert and Stypulkowski (1987), our electrical stimulation showed greater precision relative to acoustic stimulation. As previously reported by Kiang and Moxon (1972), electrically stimulated fibers generate PSTH with short latencies and less temporal dispersion compared with acoustic stimulation. What factors might explain the enhanced precision observed in electrical stimulation?

The neural responses to acoustic and electrical stimuli differ from each other. In the normal-hearing ear, the BM traveling wave generates a low-frequency (LF) latency, which arises from the delayed mechanical response of the BM (Ruggero & Temchin, 2007). In addition, the BM acts as a gain-control amplifier, boosting low-level sounds and compressing high-level sounds (Gregan et al., 2011). The mechanical response of the BM in intact ears leads to a more extensive dynamic range (Rhode, 1971; Sachs & Abbas, 1974; Yates et al., 1992). However, the electrically stimulated auditory nerve has a dynamic range of only 1.5–6 dB (Kiang & Moxon, 1972), as opposed to the acoustic dynamic range of 30 dB (Abbas & Miller, 2004).

An important distinction between acoustic and electrical stimulation pertains to the absence of hair cells and synapses in the deaf ear, which leads to minimal or no spontaneous activity of the auditory nerve (Hartmann & Klinke, 1990). This is because no transmitters are released into the synaptic cleft. By contrast, the spontaneous discharge rate of the auditory nerve fibers in an intact auditory system can range from 0 to 80 spikes per second (Liberman, 1978). The absence of BM latency, hair cells, and synapses may account for the heightened precision found in the auditory nerve and in our data.

Our findings suggest that the precision observed in the auditory nerve during electrical stimulation (as previously reported by Hartmann et al. (1984) and van den Honert and Stypulkowski (1987)) is maintained at the level of the cochlear nucleus and the MNTB, despite the involvement of multiple synapses. This suggests that the initial high precision achieved in the early stages of the auditory pathway remains unimpaired and may even be improved. At low acoustic stimulation rates, it has been shown that the SBCs, and especially the GBCs, demonstrate higher entrainment and phase locking compared with the auditory nerve (Joris, Carney, et al., 1994; Joris, Smith, et al., 1994). Joris et al. (1994) could not detect such differences at higher stimulation rates. It has been hypothesized that this behavior correlates with the number of synaptic inputs from the auditory nerve. Compared with SBCs, GBCs receive more auditory-nerve input via smaller synapses (Liberman, 1991; Spirou et al., 2005), known as the modified endbulbs of Held (Smith & Rhode, 1987). In contrast, auditory nerve inputs converge onto the SBCs via few large synapses, called the endbulbs of Held (Sento & Ryugo, 1989).

The convergence of multiple auditory nerve inputs onto GBCs results in increased entrainment and phase locking, as well as a decrease in jitter (Burkitt & Clark, 1999; Kuhlmann et al., 2002; Rhode & Smith, 1986; Rothman et al., 1993; Xu-Friedman & Regehr, 2005). While low acoustic stimulation rates have been shown to increase the entrainment and phase locking of SBCs and GBCs, we believe that the precision achieved through electrical stimulation of the auditory nerve is further enhanced at the level of the cochlear nucleus. This is likely because electrical stimulation presumably activates every auditory nerve synapse at the SBCs and GBCs, producing many subthreshold inputs that coincide and reduce the jitter.

4.2.4 Model

Our LSO model illustrates how the hyper-precise electrical input from the AVCN and MNTB contributes to ITD sensitivity with a pronounced lateralization effect, suggesting that coincidental detection of excitatory and inhibitory inputs remains functional.

The sensitivity to ITDs observed in our electrical brainstem model diverges from that found in normal-hearing animals. By contrast, a few studies propose that ITDs in the IC remain consistent between acoustic and electrical stimulation. Notably, Rosskothen-Kuhl et al. (2021) and Vollmer (2018) are the sole examples that illustrate the similarity of ITDs in the IC under both stimulation modalities. Rosskothen-Kuhl et al. (2021) demonstrated comparable electrical behavioral ITDs in the IC to those in normal-hearing rats, employing neonatally deafened rats with bilateral implants in adulthood. Vollmer (2018), meanwhile, implanted CIs in the round window of intact hearing gerbils and recorded in the IC, revealing analogous ITD discrimination thresholds for electric and acoustic stimuli.

Despite these findings, it is important to note that Rosskothen-Kuhl et al. (2021) conducted their study in rats, which likely employ the LSO for envelope ITD detection, while Vollmer (2018) implanted CIs in the round window. Despite Vollmer's (2018) assertion that electrophonic stimulation did not occur during the procedure, the potential for this stimulation remains high, given the absence of cochlear damage and preserved hearing in the animals. This type of stimulation and implantation markedly differs from conventional forms of CI implantation.

Conversely, Smith and Delgutte (2007), Hancock et al. (2010), and Chung et al. (2019) reported differences in ITD sensitivity between electrical and acoustical stimulation scenarios. When comparing ITD sensitivity in the brainstem and the IC, it is crucial to consider that the cells in the IC, receive converging projections from MSO and LSO cells and many other auditory nuclei (Grothe et al., 2010). This adds another layer of complexity, making it harder to understand ITD processing mechanisms in the IC on a broader scale.

In summary, more studies support the idea that ITDs in the IC vary between acoustic and electrical stimulation scenarios. Therefore, the differences observed in our electrical LSO model, leading to a pronounced lateralization effect, align with the broader evidence in this regard.

This, in turn raises the question of what could be the underlying cause of this phenomenon. The LSO integrates the hyper-precise input in an all-or-nothing manner, potentially due to strong inhibition from the MNTB. Activation of all modified endbulbs of Held through electrical stimulation could create coincidence-subthreshold input on the GBCs, potentially leading to increased precision that is then transmitted to the LSO. As a consequence, the inhibitory input from the MNTB might be stronger than the input from the SBCs because the SBCs receive less auditory nerve input than the GBCs (Liberman, 1991; Spirou et al., 2005).

Alternatively, or additionally, the lateralization effect may also arise from changes in the timing between excitatory and inhibitory inputs. Beiderbeck et al. (2018) demonstrate that inhibition controls the spiking of the LSO with microsecond precision in high-frequency click trains, whereby the timing of the inhibition and excitation either suppresses or facilitates spiking. Since the relative timing between input signals can be significantly altered during electrical stimulation, the specific role of inhibition in ITD processing might be strongly affected. However, the facilitatory effect of inhibition was not incorporated into our LSO model and thus was not captured in our binaural simulations.

Overall, the model adequately replicates the physiologically recorded data. However, one of its limitations is the absence of brainstem nuclei and synapses, such as the cochlear nucleus and MNTB. Instead of receiving synaptic input from SBCs and MNTB, the LSO model directly receives input from the auditory nerve.

To compensate for this discrepancy, we adjusted the intensities of ipsilateral and contralateral inputs (60 dB contra, 50 dB ipsi) to mimic the response properties of MNTB and cochlear nucleus cells as determined through our in vivo gerbil recordings However, it is important to note that, at low acoustic stimulation rates, SBCs and GBCs exhibit greater entrainment and phase locking than the auditory nerve (Joris, Carney, et al., 1994; Joris, Smith, et al., 1994). This likely relates to the number of synaptic inputs.

Considering the significance of jitter in ITD sensitivity, it would be interesting to incorporate such parameters into the model to investigate how the activation of multiple inputs during electrical stimulation might enhance the precision of jitter and whether electrical stimulation activates more inputs than acoustic stimulation does.

4.3 Does Jitter Influence ITD Detection?

We discovered that the level of jitter significantly influences the shape of electrical rate ITD functions. By adjusting the jitter input of the electrical LSO model to match physiological acoustic levels, we managed to restore the dynamic ITD range. Consequently, the model implies that physiological jitter levels play a critical role in defining the temporal width of the integration window between excitatory and inhibitory inputs.

Consistent with this concept, Myoga et al. (2014) illustrated that jitter can increase inhibition-driven shifts of excitatory postsynaptic potential peaks in the MSO, which shape excitatory timing. Their study shows that the introduction of jitter degrades spike timing without interfering with the efficiency of inhibition-enforced EPSP peak shifts (Myoga et al.,

2014). Although these findings were derived from the MSO low-frequency range, it reinforces the significance of jitter in shaping ITD sensitivity.

Our results may also contribute to recent findings on jittering the interpulse intervals to improve ITD sensitivity. According to Laback and Majdak (2008), this mechanism operates by resetting the adaptation process with each randomization of the pulse. They suggest that binaural adaptation during ongoing high stimulation results in compromised ITD detection. Additionally, their findings demonstrate that binaural jitter could enhance ITD sensitivity at higher stimulation rates (≥ 800 pps) (Laback & Majdak, 2008). The concept of binaural adaptation was first described by Hafter and Dye (1983). Increasing the envelope modulation rate of high-frequency carriers has been observed to induce binaural adaptation, reducing ITD sensitivity in individuals with normal hearing (Hafter & Dye, 1983). This adaptation leads to scenarios where the onset of a sound contributes significantly to ITD detection, while the ongoing signal contributes minimally (Saberi, 1996; Stecker & Hafter, 2002).

CI recipients exhibit a similar reduction in ITD sensitivity when exposed to high rates of unmodulated pulse trains. One potential explanation for the phenomenon of binaural adaptation observed during electrical stimulation is that it could be attributed to the atypical neuronal response evoked by electrical stimulation, characterized by a high degree of phase locking and synchronization across fibers (Dynes & Delgutte, 1992; Hartmann et al., 1984; Litvak et al., 2001; Wilson et al., 1997). Additionally, it has been hypothesized that the latency difference between electrical and acoustic stimulation due to the mechanical properties of the BM is responsible for poor ITD detection (Joris et al., 2006).

In a subsequent study, Hancock et al. (2012) conducted recordings from neurons in the IC of anesthetized cats. Their findings reveal an enhanced sensitivity to ITDs when higher stimulation rates are applied, which was achieved by implementing short inter-pulse intervals (SIPIs) (Hancock et al., 2012). The researchers observed that introducing jitter leads to an increase in firing activity in half of the neurons. Notably, the tuning of ITDs in these conditions becomes comparable to the tuning observed at lower stimulation rates.

Srinivasan et al. (2020) have conducted experiments involving the introduction of jittering in amplitude-modulated high-rate pulse trains. The results illustrate that the insertion of short SIPIs leads to an improvement in ITD sensitivity. Together, these studies provide evidence that incorporating jitter into pulse trains can affect behavioral ITD sensitivity, which could potentially be used reduce binaural adaptation.

It is important to note that our own findings may not be directly comparable. Discrepancies have possibly arisen from the brief duration of our stimulation click trains,

which may not have been long enough to initiate the adaptation process. Consequently, our data contradicts the earlier findings, indicating that the diminished spatial sensitivity in the LSO does not appear to result from binaural adaptation. Instead, in our research, it appears to be attributable to the exceptionally precise binaural input originating from the AVCN and MNTB. This precision leads to highly narrowed ITD range in the LSO.

Therefore, it is imperative to investigate longer stimulation conditions to ascertain whether binaural adaptation occurs in the superior olivary complex during electrical stimulation, as well as its potential impact on ITD detection. Additionally, studying the influence of synchronization between the two ears during jittering effects should be examined through synchronized and unsynchronized conditions.

While our data differs from the previous findings of Hancock et al. (2012), Laback and Majdak (2008), and Srinivasan et al. (2020) regarding binaural adaptation, both our results and theirs provide evidence supporting the idea that incorporating jitter into electrical input enhances the physiological neural representation of temporal information.

4.4 Myelination Specialization and its Implication for ITD Detection

As highlighted in section 1.9.2, myelination has been demonstrated to play a crucial role for ITD processing in the MSO (Ford et al., 2015; Stange-Marten et al., 2017). To elaborate, the fibers of low-frequency-tuned GBCs involved in ITD processing show shorter internode length and thicker axonal diameters when contrasted with high-frequency GBCs. However, differences extend beyond the distinction between high and low-frequency GBC axons; there is also a divergence between inhibitory GBCs and excitatory SBCs. Notably, the axons of GBCs that innervate the MNTB exhibit larger axonal diameters compared with those SBC axons responsible for conveying excitatory signals to the MSO, as reported by Ford et al. (2015). Besides higher precision (lower jitter), this configuration also results in faster conduction velocities, leading to the faster arrival of contralateral inhibitory signals in the MSO in comparison with the contralateral excitatory input from SBCs (Brand et al., 2002; Roberts et al., 2013).

Our research reveals precise jitter across all ICIs during electrical stimulation. No distinctions were observed in terms of firing precision between low-frequency (larger ICIs) and high-frequency (smaller ICIs) in our study. These results prompt us to reconsider the extent to which myelination plays a crucial role in ITD detection and precise jitter. This raises questions about the generalizability of the findings put forth by Stange-Marten et al. (2017)

and Ford et al. (2015), considering that their conclusions primarily pertained to MSO cells, while our study is centered around high-frequency LSO cells.

However, it is important to highlight that, in the study conducted by Stange-Marten et al. (2017), they not only identified low-frequency cells with consistent synaptic delays but also identified certain high-frequency cells that exhibited stable synaptic delay. Therefore, it is plausible that the myelination specialization observed in GBCs may not be limited solely to cells connected to the MSO, but could also be present in GBCs that contribute to other nuclei, such as the LSO.

In the LSO, high-frequency cells can detect envelope ITDs. Therefore, it is possible that GBC cells responsible for innervating the MNTB and transmitting this information to high-frequency LSO cells that detect envelope ITDs may also exhibit myelination specialization similar to that found in low-frequency GBC cells. However, this consideration remains unexplored. Additionally, our research does not differentiate between electrically stimulated SBCs and GBCs, meaning that our data encompasses both cell types. Consequently, it is possible that the precise electrical jitter observed across all frequencies is influenced by the inclusion of both cell types.

If myelination specialization is not needed for constant jitter, it could imply that factors such as electrical input and differences between acoustic and electrical hearing (e.g., absence of hair cells, no spontaneous activity, and no traveling wave along the BM) might influence jitter and ITD detection.

4.5 LSO versus MSO as the Main ITD Detector During CI-Based Stimulation

In order to preserve the experience-dependent mechanism responsible for refining input strength and timing, the animals involved in our experiments possessed fully developed hearing capabilities before the study. Moreover, no degenerative effects were noted beforehand.

By contrast, individuals who receive CIs often undergo extended periods of deafness, which can lead to various complications due to the inactivity of the auditory system. For example, researchers have demonstrated reduced ITD sensitivity in the IC (Hancock et al., 2010) and auditory cortex (Tillein et al., 2010) in congenitally deaf animals. However, if a CI is implanted during a critical early period, it can compensate for functional deficits in the auditory cortex that result from congenital deafness (Kral & Sharma, 2012).

On the other hand, Buck et al. (2021) and Rosskothen-Kuhl et al. (2021) propose that poor ITD detection in humans is independent of hearing experience during development, as

the ITD threshold of neonatally deafened rats was comparable to that of rats with normal hearing. These findings suggest that certain aspects of auditory development are not influenced by auditory experience. This leads to the inference that the LSO may serve as the primary ITD detector during CI stimulation. This proposition is supported by the fact that, in contrast to the MSO, the LSO's excitatory and inhibitory tuning curves are already aligned at the onset of hearing (Sanes & Rubel, 1988). Moreover, the developmental changes in inhibitory projections to the LSO are finalized before the onset of hearing (Kim & Kandler, 2003).

Conversely, the ITD sensitivity of the MSO undergoes developmental maturation after hearing onset and is dependent on auditory experience (Seidl & Grothe, 2005). Thus, the findings of Buck et al. (2021) and Rosskothen-Kuhl et al. (2021) align with our hypothesis, which is that the LSO, rather than the MSO, plays a primary role in CI-based ITD detection.

The data obtained by Buck et al. (2021) and Rosskothen-Kuhl et al. (2021) were derived from rats, an animal model with high-frequency hearing in which ITD detection in the MSO can be neglected. Therefore, it is presumed in this case that the envelope ITDs of the CIs are processed in the LSO and subsequently transferred to the midbrain. While this observation provides further support for our hypothesis that the LSO serves as the primary ITD detector during CI-based stimulation, the experimental data acquired by Buck et al. (2021) in the rat midbrain does not allow for an accurate determination of whether the collected data originates from the LSO or MSO.

In general, two types of ITD sensitivity can be identified: the through type and the peak type. The predominant view is that MSO neurons exhibit peak-type ITD sensitivity, resulting from the binaural coincidence of excitation, while LSO neurons exhibit through-type ITD sensitivity, arising from the coincidence of excitation and inhibition (Batra et al., 1997; Yin & Kuwada, 1983). Various studies assessing ITD sensitivity in the superior olivary complex (SOC) provide evidence for the existence of neurons with peak-type characteristics in the MSO and neurons with through-type characteristics in the LSO (Batra et al., 1997; Spitzer & Semple, 1993; Tollin & Yin, 2005).

To classify these ITD functions, best interaural phase differences (IPDs) are plotted against stimulus frequencies to calculate the characteristic phase (CP) (Yin & Kuwada, 1983). LSO cells typically exhibit a CP of ±0.5, indicating through-type ITD sensitivity, while MSO cells demonstrate a CP close to 0, signifying peak-type ITD sensitivity. Through-type ITD sensitivity is characterized by a specific ITD evoking the minimum response independent of

frequency, whereas peak-type ITD sensitivity generates the maximum response (peak) at a specific ITD regardless of frequency (Siveke, 2007).

However, LSO cells may also display peak-type ITD sensitivity, depending on the strength of the excitatory or inhibitory input, as perfect through-type ITD functions with a CP of 0.5 only occur when excitation and inhibition are maximally out of phase (Tollin & Yin, 2005). Furthermore, in addition to peak-type and through-type, intermediate-types with a CP between 0 and 0.5 have also been identified (Fitzpatrick & Kuwada, 2001; Pecka et al., 2007). Given that inhibition, rather than just excitatory inputs (EE), is involved in ITD sensitivity within the MSO, it becomes apparent that numerous non-zero CPs are observed within the MSO (Grothe et al., 2010; Pecka & Encke, 2020). At the midbrain level, the existing evidence suggests that the convergence of inputs from brainstem neurons may contribute to the emergence of intermediate-type ITD sensitivity (Cai et al., 1998; Fitzpatrick et al., 2002; Fitzpatrick & Kuwada, 2001; Kuwada & Yin, 1983). However, certain studies have observed the presence of intermediate-type ITD sensitivity even at the level of the superior olivary complex (SOC) (Batra et al., 1997; Spitzer & Semple, 1993).

Therefore, especially at the midbrain level, where different types of ITD inputs, including peak, through, and intermediate, converge, determining the source of ITD information (LSO or MSO) becomes challenging. Studies employing electrical stimulation, such as those conducted by Tillein et al. (2010) and Hancock et al. (2010), which demonstrated the presence of both peak-type and through-type ITD functions, or investigations by Smith and Delgutte (2007, 2008) and Vollmer (2018) reporting peak-type responses, do not establish a conclusive link between the origin of the ITD input and the ITD sensitivity types. Moreover, these studies did not differentiate ITD types based on the CP, given that CPs cannot be computed with electrical stimulation. This limitation makes it challenging to establish a clear differentiation between types during this form of stimulation. Consequently, discerning between the various types of ITD sensitivity and determining the ITD origin (LSO, MSO) solely based on the ITD type is rendered impossible.

As a result, recording electrical signals in the midbrain will not provide a definitive solution to whether the LSO or MSO is primarily utilized for ITD detection by CI patients.

In summary, considering the developmental disparities between MSO and LSO, where the LSO matures before the onset of hearing, along with the findings presented by Buck et al. (2021) and Rosskothen-Kuhl et al. (2021), and taking into account the technical limitations associated with CI implantation that primarily target the high frequencies of the cochlea, there is strong indication that the LSO plays a significant role as the primary ITD detector during

CI-based stimulation. However, to comprehensively address this question, it is imperative to obtain electrophysiological recordings from both the MSO and LSO. An outline of the proposed research required for this is presented in the concluding chapter that follows.

5 Conclusion

Our study indicates that electrical stimulation triggers exceptionally precise spiking in the AVCN and MNTB. As a result, the binaural comparators face different timing patterns compared to acoustic stimulation. Nevertheless, our LSO model anticipates that this heightened precision maintains ITD sensitivity in the LSO, resulting in a steep rate modulation. However, this modulation, represented by the slope of the function, was confined to a narrower range of ITDs compared to acoustic ITDs. Adjusting the electrical jitter level of excitatory and inhibitory LSO inputs to more closely mimic acoustic recordings restored a broader dynamic ITD range and expanded the range of distinguishable ITDs, highlighting the importance of jitter levels. It is hoped our findings can improve CI stimulation strategies, as well as help to enhance ITD coding in CI patients.

5.1 Limitation of my Study

A limitation of the study is the necessity to model the ITD coding of the LSO due to the inability to conduct bilateral extracellular electrical stimulated recordings in the LSO. While the model effectively reproduces physiologically recorded data, it lacks brainstem nuclei and synapses, such as the cochlear nucleus, MNTB, and the endbulb of Held and calyx of Held. Instead of receiving synaptic input from SBCs and MNTB, the LSO model directly receives input from the auditory nerve. The different synaptic inputs play a crucial role in influencing the spiking pattern of the AVCN and MNTB, thereby impacting subsequent nuclei like the LSO. As ITD coding in the LSO is directly influenced by inhibition and excitation, even minor timing deviations can alter the LSO's ITD detection. Incorporating the MNTB and AVCN stages, along with their synapses, into the LSO model would be valuable.

Although we posit that the LSO serves as the primary ITD detector during CI-based stimulation, we cannot fully address this question due to the absence of extracellular recordings from the LSO or MSO. Additionally, our hypotheses remain incompletely resolved as we employed acutely deafened animals, neglecting any long-term effects on the auditory system. It would be intriguing to conduct similar recordings in congenitally deaf animals to explore whether auditory deprivation affects ITD detection and if, even under such

conditions, the LSO remains the primary ITD detector during CI-based stimulation. The concluding chapter provides a framework for the proposed research needed for this endeavor.

5.2 Outlook

Given the constraints of the study, I propose an experimental framework for future research, which is outlined in this concluding chapter.

This proposed research would involve: (1) conducting in vivo extracellular recordings with extended click durations and incorporating these results into the model; (2) integrating additional parameters into the model and carrying out in vivo extracellular recordings in the mice; (3) performing bilateral in vivo extracellular recordings; and (4) conducting bilateral in vivo extracellular recordings involving congenitally deaf animals. These are considered in more detail as follows:

5.2.1 In vivo Extracellular Recordings with Extended Click Durations

First, I intend to replicate our experiments with extended click durations. The purpose is to examine whether binaural adaptation influences both jitter and ITD processing, in accordance with propositions by Hancock et al. (2012), Laback and Majdak (2008), and Srinivasan et al. (2020). During this first phase, the testing of ITD processing with the model becomes essential, as the extracellular acoustic and electrical in vivo recordings will be carried out in the AVCN and MNTB.

5.2.2 In Vivo Extracellular Recordings in the Mice

The next experimental paradigm would center on animals with varying hearing ranges, such as mice and gerbils, integrating additional factors into the model. Our research findings demonstrate that the precise transmission of information from the AVCN and MNTB to the LSO generates a distinct lateralization effect. Hence, it would be intriguing to introduce the GBC myelination specialization of gerbils into the model to observe its impact on jitter.

Furthermore, it would be of interest to conduct experiments in mice, which lack myelination specialization and have a high frequency hearing range. In mice, ITD detection likely occurs in the LSO, while the MSO can be disregarded (see chapter 4.1). The aim is to investigate whether the pronounced lateralization effect found in our model also manifests in non-specialized ITD-detector animals, such as mice. Initially, we would replicate the experiments and perform extracellular recordings in the AVCN and MNTB of mice. These

findings would subsequently be integrated into the model. Finally, it would be especially interesting to verify if the model's findings hold true for both gerbils and mice.

5.2.3 Bilateral in Vivo Extracellular Recordings

The next step would involve conducting bilateral electrical extracellular single-cell recordings, not limited to the LSO but also encompassing the MSO. The goal is to validate our hypothesis that the LSO primarily functions as the ITD detector during CI-based stimulation. To gain fundamental insights into ITD processing in both the MSO and LSO, an initial step would involve establishing bilateral CI implantation in gerbils and conducting extracellular single-cell recordings under anesthesia.

5.2.4 Bilateral in Vivo Extracellular Recordings Involving Congenitally Deaf Animals

The investigation would then assess the impact of developmental alterations in the auditory system on ITD processing within the LSO. Our argument hinges on the completion of inhibitory projections to the LSO before hearing onset, indicating the LSO's primary role in CI-based stimulation. By contrast, the MSO undergoes developmental maturation after hearing onset and relies on auditory experience. Consequently, alongside the aforementioned study, we plan to explore whether congenital deafness influences cue reweighting, particularly concerning the animals' reliance on envelope ITD cues. To execute this part of the study, animals that are congenitally deaf will undergo immediate implantation, followed by regular CI stimulation. Subsequent recordings in the LSO and MSO will shed light on whether these animals predominantly utilize envelope ITDs or ILDs for sound source detection.

5.3 Summary

As indicated and subsequently confirmed by our results, the parts of the auditory system stimulated electrically, including the auditory nerve, the AVCN, and the MNTB, demonstrate enhanced temporal precision compared with cells stimulated acoustically. In theory, this heightened precision should lead to improved ITD detection during CI stimulation for hearing-impaired subjects in comparison with normal-hearing listeners. However, as outlined in chapter 1.10, this is not the case, and CI patients still lag behind individuals with normal hearing in this respect.

Our findings reveal that electrical stimulation induces hyper-precise spiking in the AVCN and MNTB. Consequently, the binaural comparators must handle significantly different timing patterns compared with acoustic stimulation. However, our model predicts

that this hyper-precision does not diminish ITD sensitivity in the LSO. Instead, it generates a steep ITD sensitivity, resulting in a pronounced lateralization effect. These modeling predictions align with recent behavioral and neuronal data in rats (Rosskothen-Kuhl et al., 2021), as well as localization data from human CI patients (Laback et al., 2015).

Future studies involving CI patients could provide insights into the lateralization effect proposed by our LSO model. By testing ITD sensitivity in very fine steps, it should be possible to identify a region on the tuning curve where patients can distinguish small deviations in ITD, corresponding to the slope range of the LSO ITD curves.

The enhanced coding capacity for ITD, following the adaptation of electrical jitter to acoustic hearing, underscores the importance of jitter in ITD sensitivity. Future CI stimulation strategies should therefore focus on exploiting the LSO pathway by improving envelope ITD detection in the LSO using jitter values that mimic acoustic conditions. This approach may potentially lead to stimulation strategies that enable CI patients to attain comparable ITD abilities in localizing sound sources.

6 Bibliography

Abbas, P. J., & Miller, C. A. (2004). Biophysics and Physiology. In A. N. and F. R. R. Zeng Fan-Gang and Popper (Ed.), *Cochlear Implants: Auditory Prostheses and Electric Hearing*. Springer New York. https://doi.org/10.1007/978-0-387-22585-2_5

Adunka, O. F., & Buchman, C. A. (2007). Scala tympani cochleostomy I: results of a survey. *The Laryngoscope*, *117*(12), 2187–2194. https://doi.org/10.1097/MLG.0B013E3181453A6C

Aescht, E., Büchl-Zimmermann, S., Burmester, A., Dänhardt-Pfeiffer, S., Desel, C., Hamers, C., Jach, G., Kässens, M., Makovitzky, J., Mulisch, M., Nixdorf-Bergweiler, B., Pütz, D., Riedelsheimer, B., van den Boom, F., Wegerhoff, R., & Welsch, U. (2010). Romeis Mikroskopische Technik. In *Romeis Mikroskopische Technik*. Spektrum Akademischer Verlag. https://doi.org/10.1007/978-3-8274-2254-5

Agterberg, M. J. H., Snik, A. F. M., Hol, M. K. S., Van Wanrooij, M. M., & Van Opstal, A. J. (2012). Contribution of monaural and binaural cues to sound localization in listeners with acquired unilateral conductive hearing loss: improved directional hearing with a bone-conduction device. *Hearing Research*, *286*(1–2), 9–18. https://doi.org/10.1016/J.HEARES.2012.02.012

Areid, N., Willberg, J., Kangasniemi, I., & Närhi, T. O. (2021). Organotypic in vitro block culture model to investigate tissue-implant interface. An experimental study on pig mandible. *Journal of Materials Science: Materials in Medicine*, *32*(11), 1–10. https://doi.org/10.1007/S10856-021-06608-5/FIGURES/5

Arnott, R. H., Wallace, M. N., Shackleton, T. M., & Palmer, A. R. (2004). Onset Neurones in the Anteroventral Cochlear Nucleus Project to the Dorsal Cochlear Nucleus. *JARO: Journal of the Association for Research in Otolaryngology*, *5*(2), 153. https://doi.org/10.1007/S10162-003-4036-8

Aronoff, J. M., Yoon, Y., Freed, D. J., Vermiglio, A. J., Pal, I., & Soli, S. D. (2010). The use of interaural time and level difference cues by bilateral cochlear implant users. *The Journal of the Acoustical Society of America*, *127*(3), EL87. https://doi.org/10.1121/1.3298451

Aschendorff, A., Kromeier, J., Klenzner, T., & Laszig, R. (2007). Quality control after insertion of the nucleus contour and contour advance electrode in adults. *Ear and Hearing*, *28*(2 Suppl). https://doi.org/10.1097/AUD.0B013E318031542E

Ashida, G., Kretzberg, J., & Tollin, D. J. (2016). Roles for Coincidence Detection in Coding Amplitude-Modulated Sounds. *PLoS Computational Biology*, *12*(6). https://doi.org/10.1371/JOURNAL.PCBI.1004997

Babalian, A. L., Ryugo, D. K., & Rouiller, E. M. (2003). Discharge properties of identified cochlear nucleus neurons and auditory nerve fibers in response to repetitive electrical stimulation of the auditory nerve. *Experimental Brain Research*, *153*(4), 452–460. https://doi.org/10.1007/s00221-003-1619-x

Baker, C. A., Montey, K. L., Pongstaporn, T., & Ryugo, D. K. (2010). Postnatal development of the endbulb of held in congenitally deaf cats. *Frontiers in Neuroanatomy*, *4*. https://doi.org/10.3389/FNANA.2010.00019

Bako, P., Bassiouni, M., Eckhard, A., Gerlinger, I., Frick, C., Löwenheim, H., & Müller, M. (2015). Methyl methacrylate embedding to study the morphology and immunohistochemistry of adult guinea pig and mouse cochleae. *Journal of Neuroscience Methods*, *254*, 86–93. https://doi.org/10.1016/J.JNEUMETH.2015.07.017

Batra, R., Kuwada, S., & Fitzpatrick, D. C. (1997). Sensitivity to interaural temporal disparities of low- and high-frequency neurons in the superior olivary complex. I. Heterogeneity of responses. *Journal of Neurophysiology*, *78*(3), 1222–1236. https://doi.org/10.1152/JN.1997.78.3.1222

Bear, Mark. F., Connors, Barry. W., & Paradiso, M. A. (2007). The Auditory and Vestibular Systems. In Lupash Emily, Dilernia Betsy, Connolly Elizabeth, & Williams C. Paula (Eds.), *Neuroscience: Exploring the Brain* (Third Edition, pp. 343–384). Lippincott Wiliams & Wilkins.

Beiderbeck, B., Myoga, M. H., Müller, N. I. C., Callan, A. R., Friauf, E., Grothe, B., & Pecka, M. (2018). Precisely timed inhibition facilitates action potential firing for spatial coding in the auditory brainstem. *Nature Communications*, *9*(1). https://doi.org/10.1038/S41467-018-04210-Y

Bellis, T. J., & Bellis, J. D. (2015). Central auditory processing disorders in children and adults. In *Handbook of Clinical Neurology* (Vol. 129). Elsevier B.V. https://doi.org/10.1016/B978-0-444-62630-1.00030-5

Bernstein, L. R., & Trahiotis, C. (2002). Enhancing sensitivity to interaural delays at high frequencies by using "transposed stimuli." *The Journal of the Acoustical Society of America*, *112*(3 Pt 1), 1026–1036. https://doi.org/10.1121/1.1497620

Blackburn, C. C., & Sachs, M. B. (1989). Classification of unit types in the anteroventral cochlear nucleus: PST histograms and regularity analysis. *Journal of Neurophysiology*, *62*(6), 1303–1329. https://doi.org/10.1152/JN.1989.62.6.1303

Boyd, P. J. (2011). Potential benefits from deeply inserted cochlear implant electrodes. *Ear and Hearing*, *32*(4), 411–427. https://doi.org/10.1097/AUD.0B013E3182064BDA

Brand, A., Behrend, O., Marquardt, T., McAlpine, D., & Grothe, B. (2002). Precise inhibition is essential for microsecond interaural time difference coding. *Nature*, *417*(6888), 543–547. https://doi.org/10.1038/417543A

Bruce, I. C., Erfani, Y., & Zilany, M. S. A. (2018). A phenomenological model of the synapse between the inner hair cell and auditory nerve: Implications of limited neurotransmitter release sites. *Hearing Research*, *360*, 40–54. https://doi.org/10.1016/j.heares.2017.12.016

Brughera, A., Dunai, L., & Hartmann, W. M. (2013). Human interaural time difference thresholds for sine tones: The high-frequency limit. *The Journal of the Acoustical Society of America*, *133*(5), 2839. https://doi.org/10.1121/1.4795778

Brunso-Bechtold, J. K., Thompson, G. C., & Masterton, R. B. (1981). HRP study of the organization of auditory afferents ascending to central nucleus of inferior colliculus in cat. *The Journal of Comparative Neurology*, *197*(4), 705–722. https://doi.org/10.1002/CNE.901970410

Buck, A. N., Rosskothen-Kuhl, N., & Schnupp, J. W. (2021). Sensitivity to interaural time differences in the inferior colliculus of cochlear implanted rats with or without hearing experience. *Hearing Research*, *408*. https://doi.org/10.1016/J.HEARES.2021.108305

Burkitt, A. N., & Clark, G. M. (1999). Analysis of Integrate-and-Fire Neurons: Synchronization of Synaptic Input and Spike Output. *Neural Computation*, *11*(4), 871–901. https://doi.org/10.1162/089976699300016485

Cai, H., Carney, L. H., & Colburn, H. S. (1998). A model for binaural response properties of inferior colliculus neurons. I. A model with interaural time difference-sensitive excitatory and inhibitory inputs. *The Journal of the Acoustical Society of America*, *103*(1), 475–493. https://doi.org/10.1121/1.421100

Canfarotta, M. W., Dillon, M. T., Brown, K. D., Pillsbury, H. C., Dedmon, M. M., & O'Connell, B. P. (2021). Incidence of Complete Insertion in Cochlear Implant Recipients of Long Lateral Wall Arrays. *Otolaryngology - Head and Neck Surgery (United States)*, *165*(4), 571–577. https://doi.org/10.1177/0194599820987456

Cant, N. B., & Morest, D. K. (1979). Organization of the neurons in the anterior division of the anteroventral cochlear nucleus of the cat. Light-microscopic observations. *Neuroscience*, *4*(12), 1909–1923. https://doi.org/10.1016/0306-4522(79)90065-4

Carr, C. E., & Konishi, M. (1988). Axonal delay lines for time measurement in the owl's brainstem. *Proceedings of the National Academy of Sciences of the United States of America*, *85*(21), 8311–8315. https://doi.org/10.1073/PNAS.85.21.8311

Cederholm, J. M. E., Froud, K. E., Wong, A. C. Y., Ko, M., Ryan, A. F., & Housley, G. D. (2012). Differential actions of isoflurane and ketamine-based anaesthetics on cochlear function in the mouse. *Hearing Research*, *292*(1–2), 71–79. https://doi.org/10.1016/J.HEARES.2012.08.010

Chizh, B. A. (2007). Low dose ketamine: a therapeutic and research tool to explore N-methyl-D-aspartate (NMDA) receptor-mediated plasticity in pain pathways. *Journal of Psychopharmacology (Oxford, England)*, *21*(3), 259–271. https://doi.org/10.1177/0269881105062484

Chung, Y., Buechel, B. D., Sunwoo, W., Wagner, J. D., & Delgutte, B. (2019). Neural ITD Sensitivity and Temporal Coding with Cochlear Implants in an Animal Model of Early-Onset Deafness. *Journal of the Association for Research in Otolaryngology : JARO*, *20*(1), 37–56. https://doi.org/10.1007/s10162-018-00708-w

Chung, Y., Hancock, K. E., & Delgutte, B. (2016). Neural Coding of Interaural Time Differences with Bilateral Cochlear Implants in Unanesthetized Rabbits. *The Journal of Neuroscience : The Official Journal of the Society for Neuroscience*, *36*(20), 5520–5531. https://doi.org/10.1523/JNEUROSCI.3795-15.2016

Cisneros, J. C., Brito, R. de, Martins, G. S. de, Candido, N., Ferraz, R., & Bento, R. (2017). Evaluation of the microgrinding procedure for the microscopic analysis of temporal bones. *Cochlear Implants International*, *18*(2), 106–115. https://doi.org/10.1080/14670100.2016.1265190

Claussen, A. D., Quevedo, R. V., Mostaert, B., Kirk, J. R., Dueck, W. F., & Hansen, M. R. (2019). A mouse model of cochlear implantation with chronic electric stimulation. *PLoS ONE*, *14*(4). https://doi.org/10.1371/JOURNAL.PONE.0215407

Couchman, K., Grothe, B., & Felmy, F. (2010). Medial Superior Olivary Neurons Receive Surprisingly Few Excitatory and Inhibitory Inputs with Balanced Strength and Short-Term Dynamics. *The Journal of Neuroscience*, *30*(50), 17111. https://doi.org/10.1523/JNEUROSCI.1760-10.2010

Croghan, N. B. H., Duran, S. I., & Smith, Z. M. (2017). Re-examining the relationship between number of cochlear implant channels and maximal speech intelligibilitya). *The Journal of the Acoustical Society of America*, *142*(6), EL537. https://doi.org/10.1121/1.5016044

Dazert, S., Thomas, J. P., Loth, A., Zahnert, T., & Stöver, T. (2020). Cochlear Implantation: Diagnosis, Indications, and Auditory Rehabilitation Results. *Deutsches Ärzteblatt International*, *117*(41), 690. https://doi.org/10.3238/ARZTEBL.2020.0690

Dhanasingh, A., & Hochmair, I. (2021). Signal processing & audio processors. *Acta Oto-Laryngologica*, *141*(sup1), 106–134. https://doi.org/10.1080/00016489.2021.1888504

Dietz, M., Wang, L., Greenberg, D., & McAlpine, D. (2016). Sensitivity to Interaural Time Differences Conveyed in the Stimulus Envelope: Estimating Inputs of Binaural Neurons Through the Temporal Analysis of Spike Trains. *JARO: Journal of the Association for Research in Otolaryngology*, *17*(4), 313. https://doi.org/10.1007/S10162-016-0573-9

Dondzillo, A., Thompson, J. A., & Klug, A. (2016). Recurrent Inhibition to the Medial Nucleus of the Trapezoid Body in the Mongolian Gerbil (Meriones Unguiculatus). *PloS One*, *11*(8), e0160241. https://doi.org/10.1371/JOURNAL.PONE.0160241

Doucet, J. R., & Ryugo, D. K. (2006). Structural and functional classes of multipolar cells in the ventral cochlear nucleus. *The Anatomical Record Part A: Discoveries in Molecular, Cellular, and Evolutionary Biology*, *288A*(4), 331–344. https://doi.org/10.1002/AR.A.20294

Draguhn, A. (2023). Membranpotenzial und Signalübertragung in Zellverbänden. In H.-C. Pape, A. Kurtz, S. Silbernagl, R. Klinke, & B. Brenner (Eds.), *Physiologie* (10th ed., pp. 91–139). Thieme . https://doi.org/10.1055/F-0002-0003-B000000639

Dynes, S. B. C., & Delgutte, B. (1992). Phase-locking of auditory-nerve discharges to sinusoidal electric stimulation of the cochlea. *Hearing Research*, *58*(1), 79–90. https://doi.org/10.1016/0378-5955(92)90011-B

Eshraghi, A. A., Yang, N. W., & Balkany, T. J. (2003). Comparative study of cochlear damage with three perimodiolar electrode designs. *The Laryngoscope*, *113*(3), 415–419. https://doi.org/10.1097/00005537-200303000-00005

Finlayson, P. G., & Caspary, D. M. (1991). Low-frequency neurons in the lateral superior olive exhibit phase-sensitive binaural inhibition. *Journal of Neurophysiology*, *65*(3), 598–605. https://doi.org/10.1152/JN.1991.65.3.598

Fischer, J. (2015). *Elektrophysiologische Studien, Impedanzmessungen und Histologie bei PTFEP-beschichteten Cochlea-Implantaten am Meerschweinchen-Modell* [Ludwig - Maximilians - Universität München]. https://doi.org/10.5282/edoc.18529

Fischer, T., Schmid, C., Kompis, M., Mantokoudis, G., Caversaccio, M., & Wimmer, W. (2021). Effects of temporal fine structure preservation on spatial hearing in bilateral cochlear implant users. *The Journal of the Acoustical Society of America*, *150*(2), 673–686. https://doi.org/10.1121/10.0005732

Fischl, M. J., Burger, R. M., Schmidt-Pauly, M., Alexandrova, O., Sinclair, J. L., Grothe, B., Forsythe, I. D., & Kopp-Scheinpflug, C. (2016). Physiology and anatomy of neurons in the medial superior olive of the mouse. *Journal of Neurophysiology*, *116*(6), 2676. https://doi.org/10.1152/JN.00523.2016

Fitzpatrick, D. C., & Kuwada, S. (2001). Tuning to interaural time differences across frequency. *The Journal of Neuroscience : The Official Journal of the Society for Neuroscience*, *21*(13), 4844–4851. https://doi.org/10.1523/JNEUROSCI.21-13-04844.2001

Fitzpatrick, D. C., Kuwada, S., & Batra, R. (2002). Transformations in processing interaural time differences between the superior olivary complex and inferior colliculus: Beyond the Jeffress model. *Hearing Research*, *168*(1–2), 79–89. https://doi.org/10.1016/S0378-5955(02)00359-3

Ford, M. C., Alexandrova, O., Cossell, L., Stange-Marten, A., Sinclair, J., Kopp-Scheinpflug, C., Pecka, M., Attwell, D., & Grothe, B. (2015). Tuning of Ranvier node and internode properties in myelinated axons to adjust action potential timing. *Nature Communications*, *6*. https://doi.org/10.1038/ncomms9073

Franzen, D. L., Gleiss, S. A., Kellner, C. J., Kladisios, N., & Felmy, F. (2020). Activity-Dependent Calcium Signaling in Neurons of the Medial Superior Olive during Late Postnatal Development. *The Journal of Neuroscience : The Official Journal of the Society for Neuroscience*, *40*(8), 1689–1700. https://doi.org/10.1523/JNEUROSCI.1545-19.2020

Fredelake, S., & Hohmann, V. (2012). Factors affecting predicted speech intelligibility with cochlear implants in an auditory model for electrical stimulation. *Hearing Research*, *287*(1–2), 76–90. https://doi.org/10.1016/J.HEARES.2012.03.005

Friauf, E., & Ostwald, J. (1988). Divergent projections of physiologically characterized rat ventral cochlear nucleus neurons as shown by intra-axonal injection of horseradish peroxidase. *Experimental Brain Research* , *73*(2), 263–284. https://doi.org/10.1007/BF00248219

Frölich, M. A., Banks, C., & Ness, T. J. (2017). The Effect of Sedation on Cortical Activation: A Randomized Study Comparing the Effects of Sedation With Midazolam, Propofol, and Dexmedetomidine on Auditory Processing. *Anesthesia and Analgesia*, *124*(5), 1603–1610. https://doi.org/10.1213/ANE.0000000000002021

Gao, M., Rejaei, D., & Liu, H. (2016). Ketamine use in current clinical practice. *Acta Pharmacologica Sinica*, *37*(7), 865. https://doi.org/10.1038/APS.2016.5

Geiger, J. (2019). Hören und Sprechen: Kommunikation des Menschen. In H.-C. Pape, A. Kurtz, & S. Silbernagl (Eds.), *Physiologie* (9th ed., pp. 784–807). Georg Thieme Verlag. https://doi.org/10.1055/B-006-163285

Gillespie, L. N., Clark, G. M., Bartlett, P. F., & Marzella, P. L. (2003). BDNF-induced survival of auditory neurons in vivo: Cessation of treatment leads to accelerated loss of survival effects. *Journal of Neuroscience Research*, *71*(6), 785–790. https://doi.org/10.1002/JNR.10542

Gleiss, H., Encke, J., Lingner, A., Jennings, T. R., Brosel, S., Kunz, L., Grothe, B., & Pecka, M. (2019). Cooperative population coding facilitates efficient sound-source separability by adaptation to input statistics. *PLoS Biology*, *17*(7). https://doi.org/10.1371/JOURNAL.PBIO.3000150

Glendenning, K. K., Baker, B. N., Hutson, K. A., & Masterton, R. B. (1992). Acoustic chiasm V: inhibition and excitation in the ipsilateral and contralateral projections of LSO. *The Journal of Comparative Neurology*, *319*(1), 100–122. https://doi.org/10.1002/CNE.903190110

Grantham, D. W., Ashmead, D. H., Ricketts, T. A., Haynes, D. S., & Labadie, R. F. (2008). Interaural time and level difference thresholds for acoustically presented signals in post-lingually deafened adults fitted with bilateral cochlear implants using CIS+ processing. *Ear and Hearing*, *29*(1), 33–44. https://doi.org/10.1097/AUD.0B013E31815D636F

Gregan, M. J., Nelson, P. B., & J. Oxenham, A. (2011). Behavioral estimates of basilar-membrane compression: additivity of forward masking in noise-masked normal-hearing listeners. *The Journal of the Acoustical Society of America*, *130*(5), 2835–2844. https://doi.org/10.1121/1.3643817

Grothe, B., & Pecka, M. (2014). The natural history of sound localization in mammals-a story of neuronal inhibition. *Frontiers in Neural Circuits*, *8*(OCT). https://doi.org/10.3389/fncir.2014.00116

Grothe, B., Pecka, M., & McAlpine, D. (2010). Mechanisms of sound localization in mammals. *Physiological Reviews*, *90*(3), 983–1012. https://doi.org/10.1152/physrev.00026.2009

Guinan, J. J., & Li, R. Y. S. (1990). Signal processing in brainstem auditory neurons which receive giant endings (calyces of Held) in the medial nucleus of the trapezoid body of the cat. *Hearing Research*, *49*(1–3), 321–334. https://doi.org/10.1016/0378-5955(90)90111-2

Hafter, E. R., & Dye, R. H. (1983). Detection of interaural differences of time in trains of high-frequency clicks as a function of interclick interval and number. *The Journal of the Acoustical Society of America*, *73*(2), 644–651. https://doi.org/10.1121/1.388956

Hamacher, V. (2004). *Signalverarbeitungsmodelle des elektrisch stimulierten Gehörs* (P. Vary, Ed.; Issue 17). IND, RWTH Aachen.

Hancock, K. E., Chung, Y., Delgutte, B., & Hancock, K. E. (2012). Neural ITD coding with bilateral cochlear implants: effect of binaurally coherent jitter. *J Neurophysiol*, *108*, 714–728. https://doi.org/10.1152/jn.00269.2012.-Poor

Hancock, K. E., Noel, V., Ryugo, D. K., & Delgutte, B. (2010). Neural coding of interaural time differences with bilateral cochlear implants: Effects of congenital deafness. *Journal of Neuroscience*, *30*(42), 14068–14079. https://doi.org/10.1523/JNEUROSCI.3213-10.2010

Harrison, J. M., & Irving, R. (1965). The anterior ventral cochlear nucleus. *The Journal of Comparative Neurology*, *124*(1), 15–41. https://doi.org/10.1002/CNE.901240103

Harrison, J. M., & Irving, R. (1966). The organization of the posterior ventral cochlear nucleus in the rat. *The Journal of Comparative Neurology*, *126*(3), 391–401. https://doi.org/10.1002/CNE.901260303

Hartmann, R., & Klinke, R. (1990a). Impulse patterns of auditory nerve fibres to extra- and intracochlear electrical stimulation. *Acta Oto-Laryngologica, Supplement*, *109*(469), 128–134. https://doi.org/10.1080/00016489.1990.12088419

Hartmann, R., & Klinke, R. (1990b). Response Characteristics of Nerve Fibers to Patterned Electrical Stimulation. In J. M. Miller & F. A. Spelman (Eds.), *Cochlear Implants: Models of the Electrically Stimulated Ear* (pp. 135–160). Springer New York. https://doi.org/10.1007/978-1-4612-3256-8_10

Hartmann, R., Topp, G., & Klinke, R. (1984). Discharge patterns of cat primary auditory fibers with electrical stimulation of the cochlea. *Hearing Research*, *13*(1), 47–62. https://doi.org/10.1016/0378-5955(84)90094-7

Heil, P., & Peterson, A. J. (2015). Basic response properties of auditory nerve fibers: a review. *Cell and Tissue Research*, *361*(1), 129–158. https://doi.org/10.1007/S00441-015-2177-9

Held, H. (1893). Die centrale Gehörleitung. *Archiv Für Anatomie Und Physiologie / Anatomische Abteilung*, 201–248. http://publikationen.ub.uni-frankfurt.de/opus4/frontdoor/index/index/docId/21039

Henkel, C. K., & Spangler, K. M. (1983). Organization of the efferent projections of the medial superior olivary nucleus in the cat as revealed by HRP and autoradiographic tracing methods. *The Journal of Comparative Neurology*, *221*(4), 416–428. https://doi.org/10.1002/CNE.902210405

Hinojosa, R., & Nelson, E. G. (2011). Cochlear nucleus neuron analysis in individuals with presbycusis. *The Laryngoscope*, *121*(12), 2641–2648. https://doi.org/10.1002/LARY.22383

Hu, H., Klug, J., & Dietz, M. (2022). Simulation of ITD-Dependent Single-Neuron Responses Under Electrical Stimulation and with Amplitude-Modulated Acoustic Stimuli. *Journal of the Association for Research in Otolaryngology : JARO*. https://doi.org/10.1007/s10162-021-00823-1

Huth, M. E., Ricci, A. J., & Cheng, A. G. (2011). Mechanisms of Aminoglycoside Ototoxicity and Targets of Hair Cell Protection. *International Journal of Otolaryngology*, *2011*, 1–19. https://doi.org/10.1155/2011/937861

Israel, Z., & Burchiel, K. J. (2004). 2 Principles of Extracellular Single-Unit Recording. In *Microelectrode Recording in Movement Disorder Surgery*. Thieme Verlag. https://doi.org/10.1055/B-0034-56092

Javel, E., & Shepherd, R. K. (2000). Electrical stimulation of the auditory nerve. III. Response initiation sites and temporal fine structure. *Hearing Research*, *140*(1–2), 45–76. https://doi.org/10.1016/S0378-5955(99)00186-0

Jeffress, L. A. (1948). A place theory of sound localization. *Journal of Comparative and Physiological Psychology*, *41*(1), 35–39. https://doi.org/10.1037/H0061495

Johnson, S. L., Safieddine, S., Mustapha, M., & Marcotti, W. (2019). *Hair Cell Afferent Synapses: Function and Dysfunction*. https://doi.org/10.1101/cshperspect.a033175

Joris, P. X., Carney, L. H., Smith, P. H., & Yin, T. C. T. (1994). Enhancement of neural synchronization in the anteroventral cochlear nucleus. I. Responses to tones at the characteristic frequency. *Journal of Neurophysiology*, *71*(3), 1022–1036. https://doi.org/10.1152/JN.1994.71.3.1022

Joris, P. X., Smith, P. H., & Yin, T. C. T. (1994). Enhancement of neural synchronization in the anteroventral cochlear nucleus. II. Responses in the tuning curve tail. *Journal of Neurophysiology*, *71*(3), 1037–1051. https://doi.org/10.1152/JN.1994.71.3.1037

Joris, P. X., van de Sande, B., Louage, D. H., & van der Heijden, M. (2006). Binaural and cochlear disparities. *Proceedings of the National Academy of Sciences of the United States of America*, *103*(34), 12917. https://doi.org/10.1073/PNAS.0601396103

Joris, P. X., & Yin, T. C. T. (1998). Envelope coding in the lateral superior olive. III. Comparison with afferent pathways. *Journal of Neurophysiology*, *79*(1), 253–269. https://doi.org/10.1152/JN.1998.79.1.253

Kacelnik, O., Nodal, F. R., Parsons, C. H., & King, A. J. (2006). Training-induced plasticity of auditory localization in adult mammals. *PLoS Biology*, *4*(4), 627–638. https://doi.org/10.1371/JOURNAL.PBIO.0040071

Kapfer, C., Seidl, A. H., Schweizer, H., & Grothe, B. (2002). Experience-dependent refinement of inhibitory inputs to auditory coincidence-detector neurons. *Nature Neuroscience 2002 5:3*, *5*(3), 247–253. https://doi.org/10.1038/nn810

Keating, P., Dahmen, J. C., & King, A. J. (2013). Context-Specific Reweighting of Auditory Spatial Cues following Altered Experience during Development. *Current Biology*, *23*(14), 1291. https://doi.org/10.1016/J.CUB.2013.05.045

Kiang, N. Y. S., & Moxon, E. C. (1972). Physiological considerations in artificial stimulation of the inner ear. *The Annals of Otology, Rhinology, and Laryngology*, *81*(5), 714–730. https://doi.org/10.1177/000348947208100513

Kiefer, J., von Ilberg, C., Rupprecht, V., Hubner-Egner, J., & Knecht, R. (2000). Optimized speech understanding with the continuous interleaved sampling speech coding strategy in patients with cochlear implants: effect of variations in stimulation rate and number of channels. *The Annals of Otology, Rhinology, and Laryngology*, *109*(11), 1009–1020. https://doi.org/10.1177/000348940010901105

Kim, G., & Kandler, K. (2003). Elimination and strengthening of glycinergic/GABAergic connections during tonotopic map formation. *Nature Neuroscience*, *6*(3), 282–290. https://doi.org/10.1038/nn1015

Klug, J., Schmors, L., Ashida, G., & Dietz, M. (2020). Neural rate difference model can account for lateralization of high-frequency stimuli. *Citation: The Journal of the Acoustical Society of America*, *148*, 678. https://doi.org/10.1121/10.0001602

Kohrman, D. C., Wan, G., Cassinotti, L., & Corfas, G. (2020). *Hidden Hearing Loss: A Disorder with Multiple Etiologies and Mechanisms*. https://doi.org/10.1101/cshperspect.a035493

Kopp-Scheinpflug, C., Dehmel, S., Tolnai, S., Dietz, B., Milenkovic, I., & Rübsamen, R. (2008). Glycine-mediated changes of onset reliability at a mammalian central synapse. *Neuroscience*, *157*(2), 432–445. https://doi.org/10.1016/J.NEUROSCIENCE.2008.08.068

Kopp-Scheinpflug, C., & Forsythe, I. D. (2018). Integration of Synaptic and Intrinsic Conductances Shapes Microcircuits in the Superior Olivary Complex. In D. L. Oliver, N. B. Cant, R. R. Fay, & A. N. Popper (Eds.), *The Mammalian Auditory Pathways: Synaptic Organization and Microcircuits* (pp. 101–126). Springer International Publishing. https://doi.org/10.1007/978-3-319-71798-2_5

Kopp-Scheinpflug, C., Lippe, W. R., Dörrscheidt, G. J., & Rübsamen, R. (2003). The medial nucleus of the trapezoid body in the gerbil is more than a relay: comparison of pre- and postsynaptic activity. *Journal of the Association for Research in Otolaryngology : JARO*, *4*(1), 1–23. https://doi.org/10.1007/S10162-002-2010-5

Kral, A. (2017). Pathophysiologie des Hörverlusts: Klassifikation und Therapieoptionen. *Hno*, *65*(4), 290–297. https://doi.org/10.1007/s00106-016-0183-1

Kral, A., & Sharma, A. (2012). Developmental neuroplasticity after cochlear implantation. *Trends in Neurosciences*, *35*(2), 111–122. https://doi.org/10.1016/j.tins.2011.09.004

Kranzer, K., Elamin, W. F., Cox, H., Seddon, J. A., Ford, N., & Drobniewski, F. (2015). A systematic review and meta-analysis of the efficacy and safety of N-acetylcysteine in preventing aminoglycoside-induced ototoxicity: Implications for the treatment of multidrug-resistant TB. *Thorax*, *70*(11), 1070–1077. https://doi.org/10.1136/thoraxjnl-2015-207245

Kuhlmann, L., Burkitt, A. N., Paolini, A., & Clark, G. M. (2002). Summation of Spatiotemporal Input Patterns in Leaky Integrate-and-Fire Neurons: Application to Neurons in the Cochlear Nucleus Receiving Converging Auditory Nerve Fiber Input. *Journal of Computational Neuroscience*, *12*(1), 55–73. https://doi.org/10.1023/A:1014994113776

Kumpik, D. P., Kacelnik, O., & King, A. J. (2010). Adaptive reweighting of auditory localization cues in response to chronic unilateral earplugging in humans. *The Journal of Neuroscience : The Official Journal of the Society for Neuroscience*, *30*(14), 4883–4894. https://doi.org/10.1523/JNEUROSCI.5488-09.2010

Kuwabara, N., DiCaprio, R. A., & Zook, J. M. (1991). Afferents to the medial nucleus of the trapezoid body and their collateral projections. *The Journal of Comparative Neurology*, *314*(4), 684–706. https://doi.org/10.1002/CNE.903140405

Kuwada, S., & Yin, T. C. T. (1983). Binaural interaction in low-frequency neurons in inferior colliculus of the cat. I. Effects of long interaural delays, intensity, and repetition rate on interaural delay function. *Journal of Neurophysiology*, *50*(4), 981–999. https://doi.org/10.1152/JN.1983.50.4.981

Laback, B., Egger, K., & Majdak, P. (2015). Perception and coding of interaural time differences with bilateral cochlear implants. *Hearing Research*, *322*, 138–150. https://doi.org/10.1016/J.HEARES.2014.10.004

Laback, B., & Majdak, P. (2008). Binaural jitter improves interaural time-difference sensitivity of cochlear implantees at high pulse rates. *Proceedings of the National Academy of Sciences of the United States of America*, *105*(2), 814–817. https://doi.org/10.1073/PNAS.0709199105

Liberman, M. C. (1978). Auditory-nerve response from cats raised in a low-noise chamber. *The Journal of the Acoustical Society of America*, *63*(2), 442–455. https://doi.org/10.1121/1.381736

Liberman, M. C. (1991). Central projections of auditory-nerve fibers of differing spontaneous rate. I. Anteroventral cochlear nucleus. *Journal of Comparative Neurology*, *313*(2), 240–258. https://doi.org/10.1002/CNE.903130205

Litvak, L., Delgutte, B., & Eddington, D. (2001). Auditory nerve fiber responses to electric stimulation: Modulated and unmodulated pulse trains. *The Journal of the Acoustical Society of America*, *110*(1), 368–379. https://doi.org/10.1121/1.1375140

Lo, E. H., Sun, G. H., & Steinberg, G. K. (1991). Effects of NMDA and calcium channel antagonists on regional cerebral blood flow. *Neuroscience Letters*, *131*(1), 17–20. https://doi.org/10.1016/0304-3940(91)90327-P

Loizou, P. C., Poroy, O., & Dorman, M. (2000). The effect of parametric variations of cochlear implant processors on speech understanding. *The Journal of the Acoustical Society of America*, *108*(2), 790–802. https://doi.org/10.1121/1.429612

Macpherson, E. A., & Middlebrooks, J. C. (2002). Listener weighting of cues for lateral angle: The duplex theory of sound localization revisited. *The Journal of the Acoustical Society of America*, *111*(5), 2219. https://doi.org/10.1121/1.1471898

Magnusson, A. K., Park, T. J., Pecka, M., Grothe, B., & Koch, U. (2008). Retrograde GABA signaling adjusts sound localization by balancing excitation and inhibition in the brainstem. *Neuron*, *59*(1), 125–137. https://doi.org/10.1016/J.NEURON.2008.05.011

Maki, K., & Furukawa, S. (2005). Acoustical cues for sound localization by the Mongolian gerbil, Meriones unguiculatus. *The Journal of the Acoustical Society of America*, *118*(2), 872. https://doi.org/10.1121/1.1944647

Malmierca, M. S., & Ryugo, D. K. (2012). Chapter 24 - Auditory System. In C. Watson, G. Paxinos, & L. Puelles (Eds.), *The Mouse Nervous System* (pp. 607–645). Academic Press. https://doi.org/https://doi.org/10.1016/B978-0-12-369497-3.10024-X

Martins, G. D. S. Q., Neto, R. V. B., Tsuji, R. K., Gebrim, E. M. M. S., & Bento, R. F. (2015). Evaluation of Intracochlear Trauma Caused by Insertion of Cochlear Implant Electrode Arrays through Different Quadrants of the Round Window. *BioMed Research International*, *2015*. https://doi.org/10.1155/2015/236364

Masterton, B., & Heffner, H. (1998). Hearing in Glires: Domestic rabbit, cotton rat, feral house mouse, and kangaroo rat. *The Journal of the Acoustical Society of America*, *68*(6), 1584. https://doi.org/10.1121/1.385213

McFadden, S. L., Walsh, E. J., & McGee, J. (1996). Onset and development of auditory brainstem responses in the Mongolian gerbil (Meriones unguiculatus). *Hearing Research*, *100*(1–2), 68–79. https://doi.org/10.1016/0378-5955(96)00108-6

MEDEL Audio Processor SONNET 2 Cochlear Implant SYNCHRONY 2. (n.d.). *MEDEL Audio Processor SONNET 2 Cochlear Implant SYNCHRONY 2*. Retrieved January 5, 2024, from https://www.medel.com/hearing-solutions/cochlear-implants/synchrony2

MEDEL Cochlear Implants Synchrony 2. (n.d.). *MEDEL Cochlear Implants Synchrony 2*. Retrieved January 5, 2024, from https://www.medel.com/hearing-solutions/cochlear-implants

Mehanna, A. M., Gamaleldin, O. A., & Fathalla, M. F. (2019). The misplaced cochlear implant electrode array. *International Journal of Pediatric Otorhinolaryngology*, *117*, 96–104. https://doi.org/10.1016/J.IJPORL.2018.11.027

Merchant, S. N., Burgess, B., O'Malley, J., Jones, D., & Adams, J. C. (2006). Polyester Wax: A New Embedding Medium for the Histopathologic Study of Human Temporal Bones. *The Laryngoscope*, *116*(2), 245–249. https://doi.org/10.1097/01.MLG.0000192171.85406.47

Mills, J. H., Schmiedt, R. A., & Kulish, L. F. (1990). Age-related changes in auditory potentials of Mongolian gerbil. *Hearing Research*, *46*(3), 201–210. https://doi.org/10.1016/0378-5955(90)90002-7

Moon, I. J., & Hong, S. H. (2014). What is temporal fine structure and why is it important? *Korean Journal of Audiology*, *18*(1), 1–7. https://doi.org/10.7874/KJA.2014.18.1.1

Müller, M., Hu, H., Dietz, M., Beiderbeck, B., Ferreiro, D. N., & Pecka, M. (2023). Temporal hyper-precision of brainstem neurons alters spatial sensitivity of binaural auditory processing with cochlear implants. *Frontiers in Neuroscience*, *16*. https://doi.org/10.3389/fnins.2022.1021541

Myoga, M. H., Lehnert, S., Leibold, C., Felmy, F., & Grothe, B. (2014). Glycinergic inhibition tunes coincidence detection in the auditory brainstem. *Nature Communications*, *5*. https://doi.org/10.1038/ncomms4790

Nelken, I., & Young, E. D. (1994). Two separate inhibitory mechanisms shape the responses of dorsal cochlear nucleus type IV units to narrowband and wideband stimuli. *Journal of Neurophysiology*, *71*(6), 2446–2462. https://doi.org/10.1152/JN.1994.71.6.2446

Newton, V. E. (1983). Sound localisation in children with a severe unilateral hearing loss. *Audiology : Official Organ of the International Society of Audiology*, *22*(2), 189–198. https://doi.org/10.3109/00206098309072782

Oertel, D., Bal, R., Gardner, S. M., Smith, P. H., & Joris, P. X. (2000). Detection of synchrony in the activity of auditory nerve fibers by octopus cells of the mammalian cochlear nucleus. *Proceedings of the National Academy of Sciences of the United States of America*, *97*(22), 11773. https://doi.org/10.1073/PNAS.97.22.11773

Olkkola, K. T., & Ahonen, J. (2008). Midazolam and other benzodiazepines. *Handbook of Experimental Pharmacology*, *182*(182), 335–360. https://doi.org/10.1007/978-3-540-74806-9_16

O'Malley, J. T., Merchant, S. N., Burgess, B. J., Jones, D. D., & Adams, J. C. (2009). Effects of fixative and embedding medium on morphology and immunostaining of the cochlea. *Audiology & Neuro-Otology*, *14*(2), 78–87. https://doi.org/10.1159/000158536

Ono, M., Bishop, D. C., & Oliver, D. L. (2020). Neuronal sensitivity to the interaural time difference of the sound envelope in the mouse inferior colliculus. *Hearing Research*, *385*. https://doi.org/10.1016/J.HEARES.2019.107844

Osen, K. K. (1969). Cytoarchitecture of the cochlear nuclei in the cat. *The Journal of Comparative Neurology*, *136*(4), 453–483. https://doi.org/10.1002/CNE.901360407

Ostapoff, E. -Michael, Feng, J. J., & Morest, D. K. (1994). A physiological and structural study of neuron types in the cochlear nucleus. II. Neuron types and their structural correlation with response properties. *Journal of Comparative Neurology*, *346*(1), 19–42. https://doi.org/10.1002/cne.903460103

Park, T. J., Grothe, B., Pollak, G. D., Schuller, G., & Koch, U. (1995). Neural Delays Shape Selectivity to Interaural Intensity Differences in the Lateral Superior Olive. *The Journal of Neuroscience*, *16*(20), 6554–6566.

Park, T. J., Grothe, B., Pollak, G. D., Schuller, G., & Koch, U. (1996). Neural delays shape selectivity to interaural intensity differences in the lateral superior olive. *The Journal of Neuroscience : The Official Journal of the Society for Neuroscience*, *16*(20), 6554–6566. https://doi.org/10.1523/JNEUROSCI.16-20-06554.1996

Pecka, M., Brand, A., Behrend, O., & Grothe, B. (2008). Interaural Time Difference Processing in the Mammalian Medial Superior Olive: The Role of Glycinergic Inhibition. *The Journal of Neuroscience*, *28*(27), 6914. https://doi.org/10.1523/JNEUROSCI.1660-08.2008

Pecka, M., & Encke, J. (2020). 2.36 - Coding of Spatial Information. In B. Fritzsch (Ed.), *The Senses: A Comprehensive Reference (Second Edition)* (Second Edition, pp. 713–731). Elsevier. https://doi.org/https://doi.org/10.1016/B978-0-12-809324-5.24243-0

Pecka, M., Siveke, I., Grothe, B., & Lesica, N. A. (2010). Enhancement of ITD coding within the initial stages of the auditory pathway. *Journal of Neurophysiology*, *103*(1), 38–46. https://doi.org/10.1152/jn.00628.2009

Pecka, M., Zahn, T. P., Saunier-Rebori, B., Siveke, I., Felmy, F., Wiegrebe, L., Klug, A., Pollak, G. D., & Grothe, B. (2007). Inhibiting the Inhibition: A Neuronal Network for Sound Localization in Reverberant Environments. *The Journal of Neuroscience*, *27*(7), 1782. https://doi.org/10.1523/JNEUROSCI.5335-06.2007

Pfeiffer, R. R. (1966). Classification of response patterns of spike discharges for units in the cochlear nucleus: Tone-burst stimulation. *Experimental Brain Research*, *1*(3), 220–235. https://doi.org/10.1007/BF00234343

Pollak, G. D. (2012). Circuits for processing dynamic interaural intensity disparities in the inferior colliculus. *Hearing Research*, *288*(1–2), 47–57. https://doi.org/10.1016/J.HEARES.2012.01.011

Purves D, Augustine GJ, & Fitzpatrick D, et al. (2001). *Figure 13.4 The cochlea, viewed face-on (upper left) and in cross section (subsequent panels).* Neuroscience. 2nd Edition. Sunderland (MA): Sinauer Associates. https://www.ncbi.nlm.nih.gov/books/NBK10946/figure/A895/

Ramos-Miguel, A., Ramos-Macías, A., Artiles, J. V., & Zaballos, M. T. P. (2015). The Effect of Reference Electrode Position in Cochlear Implants. *The Journal of International Advanced Otology*, *11*(3), 222–228. https://doi.org/10.5152/IAO.2015.1746

Reiß, M., Reiß, G., Plontke, S. K., Leuwer, R., & Waldfahrer, F. (2021). Ohr – Anatomie und physiologische Grundlagen. In *Facharztwissen HNO-Heilkunde* (Issue 1, pp. 243–266). Springer, Berlin, Heidelberg. https://doi.org/10.1007/978-3-662-58178-0_19

Rhode, W. S. (1971). Observations of the vibration of the basilar membrane in squirrel monkeys using the Mössbauer technique. *The Journal of the Acoustical Society of America*, *49*(4), 1218–1231. https://doi.org/10.1121/1.1912485

Rhode, W. S. (2008). Response patterns to sound associated with labeled globular/bushy cells in cat. *Neuroscience*, *154*(1), 87–98. https://doi.org/10.1016/J.NEUROSCIENCE.2008.03.013

Rhode, W. S., Oertel, D., & Smith, P. H. (1983). Physiological response properties of cells labeled intracellularly with horseradish peroxidase in cat ventral cochlear nucleus. *Journal of Comparative Neurology*, *213*(4), 448–463. https://doi.org/10.1002/cne.902130408

Rhode, W. S., & Smith, P. H. (1986). Encoding timing and intensity in the ventral cochlear nucleus of the cat. *Journal of Neurophysiology*, *56*(2), 261–286. https://doi.org/10.1152/JN.1986.56.2.261

Ricketts, T. A., & Kan, A. (2021). Binaural Hearing with Devices. In R. Y. Litovsky, M. J. Goupell, R. R. Fay, & A. N. Popper (Eds.), *Binaural Hearing: With 93 Illustrations* (pp. 385–417). Springer International Publishing. https://doi.org/10.1007/978-3-030-57100-9_13

Risoud, M., Bonne, N. X., Fourdrinier, M., Hubert, T., & Vincent, C. (2016). Technical note for post-auricular route surgery in Mongolian gerbil. *Hearing Research*, *337*, 65–69. https://doi.org/10.1016/J.HEARES.2016.05.010

Roberts, M. T., Seeman, S. C., & Golding, N. L. (2013). A mechanistic understanding of the role of feedforward inhibition in the mammalian sound localization circuitry. *Neuron*, *78*(5), 923. https://doi.org/10.1016/J.NEURON.2013.04.022

Rosen, S. (1992). Temporal information in speech: acoustic, auditory and linguistic aspects. *Philosophical Transactions of the Royal Society of London. Series B: Biological Sciences*, *336*(1278), 367–373. https://doi.org/10.1098/RSTB.1992.0070

Rosowski, J. J., & Graybeal, A. (1991). What did Morganucodon hear? *Zoological Journal of the Linnean Society*, *101*(2), 131–168. https://doi.org/10.1111/J.1096-3642.1991.TB00890.X

Rosskothen-Kuhl, N., Buck, A. N., Li, K., & Schnupp, J. W. (2021). Microsecond interaural time difference discrimination restored by cochlear implants after neonatal deafness. *ELife*, *10*, 1–22. https://doi.org/10.7554/eLife.59300

Rothman, J. S., Young, E. D., & Manis, P. B. (1993). Convergence of auditory nerve fibers onto bushy cells in the ventral cochlear nucleus: Implications of a computational model. *Journal of Neurophysiology*, *70*(6), 2562–2583. https://doi.org/10.1152/JN.1993.70.6.2562

Rubio, M. E. (2018). Microcircuits of the Ventral Cochlear Nucleus. In D. L. Oliver, N. B. Cant, R. R. Fay, & A. N. Popper (Eds.), *The Mammalian Auditory Pathways: Synaptic Organization and Microcircuits* (pp. 41–71). Springer International Publishing. https://doi.org/10.1007/978-3-319-71798-2_3

Ruddell, C. L. (1967). Hydroxyethyl methacrylate combined with polyethylene glycol 400 and water; and embedding medium for routine 1-2 micron sectioning. *Stain Technology*, *42*(3), 119–123. https://doi.org/10.3109/10520296709114993

Ruebhausen, M. R., Brozoski, T. J., & Bauer, C. A. (2012). A comparison of the effects of isoflurane and ketamine anesthesia on auditory brainstem response (ABR) thresholds in rats. *Hearing Research*, *287*(1–2), 25–29. https://doi.org/10.1016/J.HEARES.2012.04.005

Ruggero, M. A., & Temchin, A. N. (2007). Similarity of Traveling-Wave Delays in the Hearing Organs of Humans and Other Tetrapods. *JARO: Journal of the Association for Research in Otolaryngology*, *8*(2), 153. https://doi.org/10.1007/S10162-007-0081-Z

Ryan, A. (1998). Hearing sensitivity of the mongolian gerbil, Meriones unguiculatis. *The Journal of the Acoustical Society of America*, *59*(5), 1222. https://doi.org/10.1121/1.380961

Ryugo, D. K., & May, S. K. (1993). The projections of intracellularly labeled auditory nerve fibers to the dorsal cochlear nucleus of cats. *Journal of Comparative Neurology*, *329*(1), 20–35. https://doi.org/10.1002/cne.903290103

Saberi, K. (1996). Observer weighting of interaural delays in filtered impulses. *Perception & Psychophysics*, *58*(7), 1037–1046. https://doi.org/10.3758/BF03206831

Sachs, M. B., & Abbas, P. J. (1974). Rate versus level functions for auditory-nerve fibers in cats: tone-burst stimuli. *The Journal of the Acoustical Society of America*, *56*(6), 1835–1847. https://doi.org/10.1121/1.1903521

Sakitt, B. (1973). Indices of Discriminability. *Nature 1973 241:5385*, *241*(5385), 133–134. https://doi.org/10.1038/241133a0

Sanchez, J. T., Ghelani, S., & Otto-Meyer, S. (2015). From development to disease: Diverse functions of NMDA-type glutamate receptors in the lower auditory pathway. *Neuroscience*, *285*, 248–259. https://doi.org/10.1016/J.NEUROSCIENCE.2014.11.027

Sanes, D. H., & Bao, S. (2009). Tuning up the developing auditory CNS. *Current Opinion in Neurobiology*, *19*(2), 188–199. https://doi.org/10.1016/J.CONB.2009.05.014

Sanes, D. H., & Rubel, E. W. (1988). The ontogeny of inhibition and excitation in the gerbil lateral superior olive. *Journal of Neuroscience*, *8*(2), 682–700. https://doi.org/10.1523/JNEUROSCI.08-02-00682.1988

Sato, M., Baumhoff, P., & Kral, A. (2016). Cochlear Implant Stimulation of a Hearing Ear Generates Separate Electrophonic and Electroneural Responses. *The Journal of Neuroscience : The Official Journal of the Society for Neuroscience*, *36*(1), 54–64. https://doi.org/10.1523/JNEUROSCI.2968-15.2016

Sato, M., Baumhoff, P., Tillein, J., & Kral, A. (2017). Physiological Mechanisms in Combined Electric-Acoustic Stimulation. *Otology & Neurotology : Official Publication of the American Otological Society, American Neurotology Society and European Academy of Otology and Neurotology*, *38*(8), 215–223. https://doi.org/10.1097/MAO.0000000000001428

Scheper, V., Paasche, G., Miller, J. M., Warnecke, A., Berkingali, N., Lenarz, T., & Stöver, T. (2009). Effects of delayed treatment with combined GDNF and continuous electrical stimulation on spiral ganglion cell survival in deafened guinea pigs. *Journal of Neuroscience Research*, *87*(6), 1389–1399. https://doi.org/10.1002/JNR.21964

Seidl, A. H., & Grothe, B. (2005). Development of sound localization mechanisms in the Mongolian gerbil is shaped by early acoustic experience. *Journal of Neurophysiology*, *94*(2), 1028–1036. https://doi.org/10.1152/JN.01143.2004

Sento, S., & Ryugo, D. K. (1989). Endbulbs of held and spherical bushy cells in cats: Morphological correlates with physiological properties. *Journal of Comparative Neurology*, *280*(4), 553–562. https://doi.org/10.1002/CNE.902800406

Shahramian, K., Gasik, M., Kangasniemi, I., Walboomers, X. F., Willberg, J., Abdulmajeed, A., & Närhi, T. (2020). Zirconia implants with improved attachment to the gingival tissue. *Journal of Periodontology*, *91*(9), 1213–1224. https://doi.org/10.1002/JPER.19-0323

Shepherd, R. K., & Hardie, N. A. (2001). Deafness-induced changes in the auditory pathway: implications for cochlear implants. *Audiology & Neuro-Otology*, *6*(6), 305–318. https://doi.org/10.1159/000046843

Shepherd, R. K., & Javel, E. (1997). Electrical stimulation of the auditory nerve. I. Correlation of physiological responses with cochlear status. *Hearing Research*, *108*(1–2), 112–144. https://doi.org/10.1016/S0378-5955(97)00046-4

Shu Hui Wu, & Kelly, J. B. (1992). Binaural interaction in the lateral superior olive: time difference sensitivity studied in mouse brain slice. *Journal of Neurophysiology*, *68*(4), 1151–1159. https://doi.org/10.1152/JN.1992.68.4.1151

Siveke, I. (2007). *Novel approaches for the investigation of sound localization in mammals*. https://doi.org/10.5282/EDOC.7791

Smith, D. I., & Mills, J. H. (1989). Anesthesia effects: auditory brain-stem response. *Electroencephalography and Clinical Neurophysiology*, *72*(5), 422–428. https://doi.org/10.1016/0013-4694(89)90047-3

Smith, P. H., Joris, P. X., Carney, L. H., & Yin, T. C. T. (1991). Projections of physiologically characterized globular bushy cell axons from the cochlear nucleus of the cat. *The Journal of Comparative Neurology*, *304*(3), 387–407. https://doi.org/10.1002/CNE.903040305

Smith, P. H., Joris, P. X., & Yin, T. C. T. (1998). Anatomy and physiology of principal cells of the medial nucleus of the trapezoid body (MNTB) of the cat. *Journal of Neurophysiology*, *79*(6), 3127–3142. https://doi.org/10.1152/JN.1998.79.6.3127

Smith, P. H., & Rhode, W. S. (1987). Characterization of HRP-labeled globular bushy cells in the cat anteroventral cochlear nucleus. *Journal of Comparative Neurology*, *266*(3), 360–375. https://doi.org/10.1002/CNE.902660305

Smith, R. L., & Zwislocki, J. J. (1975). Short-term adaptation and incremental responses of single auditory-nerve fibers. *Biological Cybernetics* , *17*(3), 169–182. https://doi.org/10.1007/BF00364166

Smith, Z. M., & Delgutte, B. (2007). Sensitivity to interaural time differences in the inferior colliculus with bilateral cochlear implants. *The Journal of Neuroscience : The Official Journal of the Society for Neuroscience*, *27*(25), 6740–6750. https://doi.org/10.1523/JNEUROSCI.0052-07.2007

Soken, H., Robinson, B. K., Goodman, S. S., Abbas, P. J., Hansen, M. R., & Kopelovich, J. C. (2013). Mouse Cochleostomy: A Minimally Invasive Dorsal Approach for Modeling Cochlear Implantation. *The Laryngoscope*, *123*(12), E109. https://doi.org/10.1002/LARY.24174

Spirou, G. A., Brownell, W. E., & Zidanic, M. (1990). Recordings from cat trapezoid body and HRP labeling of globular bushy cell axons. *Journal of Neurophysiology*, *63*(5), 1169–1190. https://doi.org/10.1152/JN.1990.63.5.1169

Spirou, G. A., Rager, J., & Manis, P. B. (2005). Convergence of auditory-nerve fiber projections onto globular bushy cells. *Neuroscience*, *136*(3), 843–863. https://doi.org/10.1016/J.NEUROSCIENCE.2005.08.068

Spitzer, M. W., & Semple, M. N. (1993). Responses of inferior colliculus neurons to time-varying interaural phase disparity: effects of shifting the locus of virtual motion. *Journal of Neurophysiology*, *69*(4), 1245–1263. https://doi.org/10.1152/JN.1993.69.4.1245

Srinivasan, S., Laback, B., Majdak, P., & Arnoldner, C. (2020). Improving Interaural Time Difference Sensitivity Using Short Inter-pulse Intervals with Amplitude-Modulated Pulse Trains in Bilateral Cochlear Implants. *JARO - Journal of the Association for Research in Otolaryngology*, *120*, 105–120. https://doi.org/10.1007/s10162-020-00743-6

Stahl, S. M. (2013). Mechanism of action of ketamine. *CNS Spectrums*, *18*(4), 171–174. https://doi.org/10.1017/S109285291300045X

Stange, A., Myoga, M. H., Lingner, A., Ford, M. C., Alexandrova, O., Felmy, F., Pecka, M., Siveke, I., & Grothe, B. (2013). Adaptation in sound localization: from GABA(B) receptor-mediated synaptic modulation to perception. *Nature Neuroscience*, *16*(12), 1840–1847. https://doi.org/10.1038/nn.3548

Stange-Marten, A., Nabel, A. L., Sinclair, J. L., Fischl, M., Alexandrova, O., Wohlfrom, H., Kopp-Scheinpflug, C., Pecka, M., & Grothe, B. (2017). Input timing for spatial processing is precisely tuned via constant synaptic delays and myelination patterns in the auditory brainstem. *Proceedings of the National Academy of Sciences of the United States of America*, *114*(24), 4851–4858. https://doi.org/10.1073/PNAS.1702290114

Stecker, G. C., & Hafter, E. R. (2002). Temporal weighting in sound localization. *The Journal of the Acoustical Society of America*, *112*(3 Pt 1), 1046–1057. https://doi.org/10.1121/1.1497366

Stöver, T., Issing, P., Graurock, G., Erfurt, P., ElBeltagy, Y., Paasche, G., & Lenarz, T. (2005). Evaluation of the Advance Off-Stylet insertion technique and the cochlear insertion tool in temporal bones. *Otology and Neurotology*, *26*(6), 1161–1170. https://doi.org/10.1097/01.MAO.0000179527.17285.85

Ter-Mikaelian, M., Sanes, D. H., & Semple, M. N. (2007). Transformation of Temporal Properties between Auditory Midbrain and Cortex in the Awake Mongolian Gerbil. *The Journal of Neuroscience*, *27*(23), 6091. https://doi.org/10.1523/JNEUROSCI.4848-06.2007

Thavam, S., & Dietz, M. (2019). Smallest perceivable interaural time differences. *The Journal of the Acoustical Society of America*, *145*(1), 458. https://doi.org/10.1121/1.5087566

Tian, S. Y., Zou, L., Quan, X., Zhang, Y., Xue, F. S., & Ye, T. H. (2010). Effect of midazolam on memory: a study of process dissociation procedure and functional magnetic resonance imaging. *Anaesthesia*, *65*(6), 586–594. https://doi.org/10.1111/J.1365-2044.2010.06343.X

Tillein, J., Hubka, P., & Kral, A. (2016). Monaural Congenital Deafness Affects Aural Dominance and Degrades Binaural Processing. *Cerebral Cortex* , *26*(4), 1762–1777. https://doi.org/10.1093/CERCOR/BHV351

Tillein, J., Hubka, P., Syed, E., Hartmann, R., Engel, A. K., & Kral, A. (2010). Cortical representation of interaural time difference in congenital deafness. *Cerebral Cortex* , *20*(2), 492–506. https://doi.org/10.1093/CERCOR/BHP222

Tollin, D. J., & Yin, T. C. T. (2002). The coding of spatial location by single units in the lateral superior olive of the cat. II. The determinants of spatial receptive fields in azimuth. *The Journal of Neuroscience : The Official Journal of the Society for Neuroscience*, *22*(4), 1468–1479. https://doi.org/10.1523/JNEUROSCI.22-04-01468.2002

Tollin, D. J., & Yin, T. C. T. (2005). Interaural phase and level difference sensitivity in low-frequency neurons in the lateral superior olive. *The Journal of Neuroscience : The Official Journal of the Society for Neuroscience*, *25*(46), 10648–10657. https://doi.org/10.1523/JNEUROSCI.1609-05.2005

Tolnai, S., Englitz, B., Kopp-Scheinpflug, C., Dehmel, S., Jost, J., & Rübsamen, R. (2008). Dynamic coupling of excitatory and inhibitory responses in the medial nucleus of the trapezoid body. *The European Journal of Neuroscience*, *27*(12), 3191–3204. https://doi.org/10.1111/J.1460-9568.2008.06292.X

Trattner, B., Gravot, C. M., Grothe, B., & Kunz, L. (2013). Metabolic Maturation of Auditory Neurones in the Superior Olivary Complex. *PLoS ONE*, *8*(6), 67351. https://doi.org/10.1371/JOURNAL.PONE.0067351

Typlt, M., Englitz, B., Sonntag, M., Dehmel, S., Kopp-Scheinpflug, C., & Ruebsamen, R. (2012). Multidimensional characterization and differentiation of neurons in the anteroventral cochlear nucleus. *PLoS ONE*, *7*(1). https://doi.org/10.1371/journal.pone.0029965

van den Honert, C., & Stypulkowski, P. H. (1987). Temporal response patterns of single auditory nerve fibers elicited by periodic electrical stimuli. *Hearing Research*, *29*(2–3), 207–222. https://doi.org/10.1016/0378-5955(87)90168-7

van Hoesel, R., Böhm, M., Pesch, J., Vandali, A., Battmer, R. D., & Lenarz, T. (2008). Binaural speech unmasking and localization in noise with bilateral cochlear implants using envelope and fine-timing based strategies. *The Journal of the Acoustical Society of America*, *123*(4), 2249–2263. https://doi.org/10.1121/1.2875229

Verschooten, E., Shamma, S., Oxenham, A. J., Moore, B. C. J., Joris, P. X., Heinz, M. G., & Plack, C. J. (2019). The upper frequency limit for the use of phase locking to code temporal fine structure in humans: A compilation of viewpoints. *Hearing Research*, *377*, 109–121. https://doi.org/10.1016/J.HEARES.2019.03.011

Vollmer, M. (2018). Neural Processing of Acoustic and Electric Interaural Time Differences in Normal-Hearing Gerbils. *The Journal of Neuroscience : The Official Journal of the Society for Neuroscience*, *38*(31), 6949–6966. https://doi.org/10.1523/JNEUROSCI.3328-17.2018

Whitlon, D. S., Szakaly, R., & Greiner, M. A. (2001). Cryoembedding and sectioning of cochleas for immunocytochemistry and in situ hybridization. *Brain Research Protocols*, *6*(3), 159–166. https://doi.org/10.1016/S1385-299X(00)00048-9

Wiegner, A. (2016). *Auswirkungen der gepaarten Stimulation des Hörnerven und des Nervus vagus auf die spektrale Plastizität im auditorischen Kortex der mongolischen Wüstenrennmaus*. https://opus.bibliothek.uni-wuerzburg.de/frontdoor/index/index/docId/13588

Wightman, F. L., & Kistler, D. J. (1998). The dominant role of low-frequency interaural time differences in sound localization. *The Journal of the Acoustical Society of America*, *91*(3), 1648. https://doi.org/10.1121/1.402445

Willbold, E., & Witte, F. (2010). Histology and research at the hard tissue–implant interface using Technovit 9100 New embedding technique. *Acta Biomaterialia*, *6*(11), 4447–4455. https://doi.org/10.1016/J.ACTBIO.2010.06.022

Wilson, B. S., Finley, C. C., Lawson, D. T., Wolford, R. D., Eddington, D. K., & Rabinowitz, W. M. (1991). Better speech recognition with cochlear implants. *Nature*, *352*(6332), 236–238. https://doi.org/10.1038/352236a0

Wilson, B. S., Finley, C. C., Lawson, D. T., & Zerbi, M. (1997). Temporal representations with cochlear implants. *American Journal of Otology*, *18*(6 SUPPL.), 30–34.

World Health Organization. (2021). *World Report on Hearing - Executive Summary*. World Health Organization . https://www.who.int/publications/i/item/9789240021570

Xu-Friedman, M. A., & Regehr, W. G. (2005). Dynamic-clamp analysis of the effects of convergence on spike timing. I. Many synaptic inputs. *Journal of Neurophysiology*, *94*(4), 2512–2525. https://doi.org/10.1152/JN.01307.2004

Yamashita, S., & Okada, Y. (2014). Heat-induced Antigen Retrieval in Conventionally Processed Epon-embedded Specimens: Procedures and Mechanisms. *The Journal of Histochemistry and Cytochemistry : Official Journal of the Histochemistry Society*, *62*(8), 584–597. https://doi.org/10.1369/0022155414537899

Yang, R., Davies, C. M., Archer, C. W., Richards, & R. G., & Richards, R. G. (2003). Immunohistochemistry of matrix markers in Technovit 9100 New-embedded undecalcified bone sections. *European Cells and Materials*, *6*, 57–71. https://doi.org/10.22203/eCM.v006a06

Yao, H., Ooboshi, H., Ibayashi, S., Uchimura, H., & Fujishima, M. (1993). Cerebral blood flow and ischemia-induced neurotransmitter release in the striatum of aged spontaneously hypertensive rats. *Stroke*, *24*(4), 577–580. https://doi.org/10.1161/01.STR.24.4.577

Yates, G. K., Johnstone, B. M., Patuzzi, R. B., & Robertson, D. (1992). Mechanical preprocessing in the mammalian cochlea. *Trends in Neurosciences*, *15*(2), 57–61. https://doi.org/10.1016/0166-2236(92)90027-6

Yin, T. C. T., & Kuwada, S. (1983). Binaural interaction in low-frequency neurons in inferior colliculus of the cat. III. Effects of changing frequency. *Journal of Neurophysiology*, *50*(4), 1020–1042. https://doi.org/10.1152/JN.1983.50.4.1020

Zahnert, T. (2011). Differenzialdiagnose der schwerhörigkeit. *Deutsches Arzteblatt*, *108*(25), 433–444. https://doi.org/10.3238/ARZTEBL.2011.0433

Zeng, F.-G. (2022). Celebrating the one millionth cochlear implant. *JASA Express Letters*, *2*(7). https://doi.org/10.1121/10.0012825

Zilany, M. S. A., Bruce, I. C., & Carney, L. H. (2014). Updated parameters and expanded simulation options for a model of the auditory periphery. *The Journal of the Acoustical Society of America*, *135*(1), 283–286. https://doi.org/10.1121/1.4837815

Zilany, M. S. A., Bruce, I. C., Nelson, P. C., & Carney, L. H. (2009). A phenomenological model of the synapse between the inner hair cell and auditory nerve: long-term adaptation with power-law dynamics. *The Journal of the Acoustical Society of America*, *126*(5), 2390–2412. https://doi.org/10.1121/1.3238250

7 List of Figures

8 List of Tables

9 Glossary

µs microseconds

A1 primary auditory cortex

AN auditory nerve

AP action potential

APs action potentials

AVCN anterior ventral part of the cochlear nucleus

BC bushy cells

BM basilar membrane

Ca^{2+} calcium

CI cochlear implant

CIs cochlear implants

CP characteristic phase

dB SPL sound pressure level, measured in decibels

DCN dorsal cochlear nucleus

DNLL dorsal nucleus of the lateral lemniscus

EDTA ethylenediaminetetraacetic-acid

EE excitatory-excitatory input

EI excitatory–inhibitory

EPSP excitatory postsynaptic potential

ETS epoxy tissue stain

GABA Gamma-Aminobutyric Acid

GBC globular bushy cell

HE hematoxylin-eosin

IC inferior colliculus

ICI inter click interval

IHC inner hair cells

ILD interaural level difference

IPSP inhibitory postsynaptic potential

ITD interaural time difference

kHz kilohertz

LNTB lateral nucleus of the trapezoid body

LSO lateral superior olive

MGB medial geniculate body

MMF medetomidine, midazolam, and fentanyl

MNTB medical nucleus of the trapezoid body

MSO medial superior olive

NaCl sodium chloride

NMDA N-methyl-D-aspartate receptors

OHC outer hair cell

PP Pre-Potential

pps pulses per second

PSTH peri stimulus time histogram

PVCN posterior ventral part of the cochlear nuclei

SBC spherical bushy cells

SGN spiral ganglion neuron

SGNs spiral ganglion neurons

SIPIs short inter-pulse intervals

SOC superior olivary complex

TFS temporal fine structure

UV ultraviolet light

VCN ventral cochlear nucleus

10 Acknowledgement

Firstly, I express my gratitude to my supervisor and mentor, PD. Dr. Michael Pecka. I appreciate your introduction to the lab and the field of neuroscience. Your guidance and support, particularly during the challenging final stages when I doubted the possibility of completion, proved invaluable. Whether it was learning ephys techniques, conducting data analysis, or composing my thesis, your unwavering assistance was a constant source of reliability. Thank you for your support and belief in my abilities.

I extend my thanks to Prof. Grothe for providing me with the opportunity to work in the lab and for his continuous support throughout my Ph.D. Your insightful input during TAC meetings has been instrumental in my academic journey. Despite initial doubts about the relevance of this experience for a veterinarian, I am grateful for the wealth of knowledge and experience gained over the years. This scientific exposure has undoubtedly made me a better veterinarian.

A heartfelt thank you to all members of my TAC – PD. Dr. Conny-Kopp Scheinpflug, Dr. Jochen Tillein, and Dr. Susanne Braun. Your suggestions and insightful discussions have been immensely beneficial.

I appreciate the GSN for its consistent support and flexibility, offering valuable workshops and retreats.

Barbara, our shared experiments were always enjoyable. Your dedication and determination to complete your thesis in a short timeframe served as an inspiration, motivating me to work harder. As they say, hard work pays off (HWPO).

Special thanks to Hilde, Olga, and Karin for their assistance in the histology lab with my slicings and stainings. Hilde, our conversations about various aspects of life were always a pleasure.

Over the years, I formed new friendships beyond the field of veterinary medicine. I am delighted to have met Eli, Ella, Sara, Alex, Delwen, Alisha, Dardo, Franzi, Mihai, Nicola, Shreya, Steffi, Dani, and Magda. Our breaks in the mensa and our engaging conversations on diverse topics enriched my experience.

Foremost, I want to express my gratitude to Philipp. Your unwavering support throughout these years has been immeasurable. From taking care of our dogs to handling household chores while I was engrossed in writing or experiments, your constant presence was a pillar of strength. Words cannot adequately convey the love and support I have received from you throughout my Ph.D. Thank you sincerely.

Lastly, heartfelt thanks to my mum and dad. Your consistent support, from looking after the dogs to preparing meals, and your positive encouragement, even in moments of self-doubt, have been indispensable.

11 List of Publications

Presented publications in this thesis:

Publication 1:
Müller, M., Hu, H., Dietz, M., Beiderbeck, B., Ferreiro, D. N., & Pecka, M. (2023). Temporal hyper-precision of brainstem neurons alters spatial sensitivity of binaural auditory processing with cochlear implants. *Frontiers in neuroscience*, *16*, 1021541. https://doi.org/10.3389/fnins.2022.1021541

12 Declaration of Author Contribution

Publication 1: (Müller et al., 2023) 'Temporal hyper-precision of brainstem neurons alters spatial sensitivity of binaural auditory processing with cochlear implants.'

Michaela Müller, Hongmei Hu, Mathias Dietz, Barbara Beiderbeck, Dardo N. Ferreiro and Michael Pecka.

The study was conceived by MP, who also designed the physiological experiments and wrote the initial manuscript draft. BB conducted the LSO recordings. MM and BB designed the CI stimulation, while HH and MD were involved in model generation. MM performed CI implantations and recorded extracellular activity in the AVCN and MNTB. HH presented the model results. DNF and MM analyzed the results, and MP and DNF collaborated on designing and generating the figures. HH and MM made contributions to the figures.

My contribution to this publication in detail:

I was responsible for designing and executing the CI stimulation and cochlear implantations, carrying out histology, ABR recordings, deafening procedures, and extracellular in vivo recordings in the AVCN and MNTB. Following this, I conducted the analysis of the results and played a role in creating the figures as well as in commenting the manuscript.

_____

(Date, Signature 1st supervisor)

_____

(Date, Signature first author Michaela Müller)

13 Affidavit

Hiermit versichere ich an Eides statt, dass ich die vorliegende Dissertation “Comparison of single cell spike rate and timing in response to cochlear implant and acoustic stimulation“ selbstständig angefertigt habe, mich außer der angegebenen keiner weiteren Hilfsmittel bedient und alle Erkenntnisse, die aus dem Schrifttum ganz oder annähernd übernommen sind, als solche kenntlich gemacht und nach ihrer Herkunft unter Bezeichnung der Fundstelle einzeln nachgewiesen habe.

I hereby confirm that the dissertation “Comparison of single cell spike rate and timing in response to cochlear implant and acoustic stimulation” is the result of my own work and that I have only used sources or materials listed and specified in the dissertation.

München, den 28. Januar, 2024
Munich, January 28, 2024

_____
Michaela Müller